面向多任务动态场景的雷达与干扰空时协同波束联合优化方法(中文/English)

廖晓容[①] 孙国皓[*①②] 钟苏川[①] 余显祥[③] 李 明[④]

[①](四川大学空天科学与工程学院 成都 610207)

[②](机器人卫星四川省重点实验室 成都 610207)

[③](电子科技大学信息与通信工程学院 成都 611731)

[④](电子科技大学长三角研究院(衢州) 衢州 324003)

摘要：现代雷达对抗形势复杂多变，体系与体系的作战已成为基本特点，而体系整体性能关乎着战场的主动权乃至最终的胜负。通过优化体系中雷达与干扰波束资源可以提升整体性能，获得在空间、时间域优效的低截获探测性能，然而空时域协同波束联合优化是一个复杂多参数耦合的非凸问题。该文针对空时域多任务动态场景，建立了以雷达探测性能为优化目标，以干扰性能以及能量限制为约束条件的优化模型。为求解该模型，该文提出了基于迭代优化的空时协同波束联合设计方法，即以雷达发射、接收、多干扰机发射波束交替迭代优化。其中，针对多干扰机协同优化的不定矩阵二次约束二次规划(QCQP)问题，该文基于可行点追踪-连续凸逼近(FPP-SCA)算法，在SCA算法的基础上，通过引入松弛变量与惩罚项，保证算法在合理松弛度下的可行性，解决了矩阵不定情况下难以获得可行解的问题。仿真表明，在一定的干扰机能量约束下，该文所提方法在保证雷达高性能探测目标且不受干扰情况下，同时实现了多干扰机在空时域干扰对方每个平台以掩护我方雷达探测的效果；相比传统算法，在动态场景中基于FPP-SCA算法的协同干扰具有更优效果。

关键词：雷达与干扰资源；空时波束联合优化；多参数耦合非凸问题；迭代优化；可行点追踪-连续凸逼近(FPP-SCA)

中图分类号：TN974 **文献标识码**：A **文章编号**：2095-283X(2024)03-0613-16

DOI: 10.12000/JR23243

引用格式：廖晓容, 孙国皓, 钟苏川, 等. 面向多任务动态场景的雷达与干扰空时协同波束联合优化方法[J]. 雷达学报(中英文), 2024, 13(3): 613–628. doi: 10.12000/JR23243.

Reference format: LIAO Xiaorong, SUN Guohao, ZHONG Suchuan, *et al*. Joint optimization of radar and jammer space-time cooperative beamforming for a multitasking dynamic scene[J]. *Journal of Radars*, 2024, 13(3): 613–628. doi: 10.12000/JR23243.

Joint Optimization of Radar and Jammer Space-time Cooperative Beamforming for a Multitasking Dynamic Scene (in English)

LIAO Xiaorong[①] SUN Guohao[*①②] ZHONG Suchuan[①]
YU Xianxiang[③] LI Ming[④]

[①](*School of Aeronautics and Astronautics, Sichuan University, Chengdu* 610207, *China*)

[②](*Sichuan Provincial Key Laboratory of Robotics Satellites, Chengdu* 610207, *China*)

[③](*School of Information and Communication Engineering, University of Electronic Science and Technology of China, Chengdu* 611731, *China*)

收稿日期：2023-12-25；改回日期：2024-03-22；网络出版：2024-04-23

*通信作者： 孙国皓 sghsjw2005@126.com *Corresponding Author: SUN Guohao, sghsjw2005@126.com

基金项目：国家自然科学基金(62201371)，四川省自然科学基金(2022NSFSC1952)，衢州市大科创项目(2022D013)

Foundation Items: The National Natural Science Foundation of China (62201371), Sichuan Provincial Natural Science Foundation (2022NSFSC1952), Municipal Government of Quzhou (2022D013)

责任主编：易伟 Corresponding Editor: YI Wei

©The Author(s) 2024. This is an open access article under the CC-BY 4.0 License (https://creativecommons.org/licenses/by/4.0/)

④(*Yangtze Delta Region Institute* (*Quzhou*), *University of Electronic Science and Technology of China*, *Quzhou* 324003, *China*)

Abstract: The modern radar confrontation situation is complex and changeable, and inter-system combat has become a basic feature. The overall system performance affects the initiative on the battlefield and even the final victory or defeat. By optimizing the beam resources of radar and jammers in a system, the overall performance can be improved, and the effective low-intercept detection effect can be obtained in the spatial and temporal domains. However, joint optimization of cooperative beamforming in the spatial and temporal domains is a nonconvex problem with complex multiparameter coupling. In this paper, an optimization model is established for a multitasking dynamic scene in the spatial and temporal domains. Radar detection performance is the optimization goal, while the interference performance and energy limitation of jammers are the constraints. To solve the model, a joint design method of space-time cooperative beamforming based on iterative optimization was proposed; that is, iterative optimization of radar transmitting, receiving, and multiple jammers transmitting beamforming vectors was alternately optimized. To solve the Quadratically Constrained Quadratic Programs (QCQP) problem with indefinite matrices for multijammer collaborative optimization, this paper is based on the Feasible Point Pursuit Successive Convex Approximation (FPP-SCA) algorithm. In other words, on the basis of the SCA algorithm, algorithm feasibility is ensured through reasonable relaxation by introducing relaxation variables and a penalty term, which solves the difficulty of obtaining a feasible solution when a problem contains indefinite matrices. Simulation results show that under the constraint of certain jammer energy, the proposed method achieves the effect of multiple jammers interfering with each enemy platform in the spatial and temporal domains to cover our radar detection. This effect is achieved while ensuring high-performance radar detection of the target without interference. Compared with traditional algorithms, the collaborative interference based on the FPP-SCA algorithm exhibits a better performance in the dynamic scene.

Key words: Radar and jammer resources; Space-time beamforming joint optimization; Multiparameter coupling nonconvex problem; Iterative optimization; Feasible Point Pursuit Successive Convex Approximation (FPP-SCA)

1 引言

雷达是对抗体系中目标信息获取的重要装备，如果它遭到破坏，不仅会使信息来源受阻，也会严重影响系统对抗效能；而主动发射干扰可以通过辐射或散射电磁波扰乱对方平台的正常工作，使其不能正确地获取我方雷达信息[1]。因此，雷达与干扰组网协同可以在保证目标探测性能的条件下，达到降低雷达信号被截获概率的目的。将雷达与多个干扰机组网，联合分配各平台的时间、功率、波束指向等，可达到在空间、时间域内我方雷达的更优探测性能和对方侦察探测平台难以发现我方雷达信号的效果，避免了传统探测平台单独作用和一对一干扰方式在时间、空间、功率等方面的局限性。然而，虽然干扰机具有灵巧低成本的优势，但其资源十分有限。因此，如何将波束资源合理分配以获得最优干扰效果，是动态场景资源优化中不可或缺的问题。

资源分配问题遵循系统资源最小化或任务性能最优准则，本文探讨的主要是后者，即用尽资源来实现性能的最优化[2]。近年来，雷达组网中的资源分配问题一直受到广泛关注，且在这一领域涌现了很多优秀的研究成果[3–21]。文献[3]提出了波束分配与驻留时间联合优化算法以实现资源的分配，在保证跟踪精度的前提下，最小化总波束驻留时间，并采用两步法求解；不过该方法针对的是单个雷达的目标跟踪任务，不涉及多平台间的资源联合分配。在此基础上，文献[7]针对组网雷达多目标跟踪场景，考虑目标威胁度和跟踪精度下界，基于迭代下降搜索法求解了最大化相关效用函数的优化问题。同样针对多目标跟踪资源分配问题，文献[8]考虑了雷达系统与通信基站共享同一工作频段的情况，研究了组网雷达功率时间联合优化分配模型。面向雷达波束与功率联合分配问题，文献[9]针对性能最优跟踪准则，给出了一种基于指数效用函数的全局目标函数设计方案，文献[10]利用基于效益成本比(Benefit-Cost Ratio, BCR)的局部搜索将该问题转化为凸问题求解。在协同干扰资源分配方面，文献[11]通过优化多干扰机波束和发射功率，降低组网雷达系统对目标的检测概率以实现多目标突防；文献[12]考虑干扰资源有限情况下的干扰波束和功率分配问

题，建立并求解了基于改进遗传算法的干扰资源分配模型。然而上述方法主要是对目标跟踪或协同干扰单一任务，不涉及多任务下的资源分配；并且对波束资源的优化分配是通过遍历波束指向矩阵中的二元变量对其赋值1或0，未达到波束权矢量级别的连续优化效果。

除上述基于启发式算法的研究外，基于深度强化学习(Deep Reinforcement Learning, DRL)和博弈论的资源分配方法也用于组网资源分配优化中。其中，DRL算法通过智能体与环境交互来学习状态到动作的最优映射策略。针对目标探测环境下的雷达资源分配问题，文献[13]将组网雷达作为智能体，在传统的深度强化学习算法中加入领域知识以辅助奖励机制的设置，提高了策略网络收敛性和收敛速度。针对伴随压制干扰下组网雷达功率分配问题，文献[18]将干扰机和雷达分别映射为两个智能体，由近端策略优化(Proximal Policy Optimization, PPO)策略网络生成雷达功率分配向量，并设计混合策略网络同时生成干扰机智能体的波束选择和功率分配动作，最后进行交替训练以学习两个智能体的策略网络参数。然而，DRL需要大量的数据训练，在多任务对抗中，无法提前获取足够的环境数据以供智能体学习；并且由于场景的复杂化，策略网络难以收敛。另一方面，基于博弈论的方法是在一定的约束条件下，双方都选择满足自身最大化收益的策略行为。针对杂波环境中的目标探测问题，文献[19]在满足每个目标一定的检测准则前提下，优化每个雷达的波束资源分配，使传输功率最小化；文献[20]对多基地分布式MIMO雷达组网的功率分配进行了纳什均衡(Nash Equilibrium, NE)分析，建立了信干噪比约束下的极小化发射功率优化模型，并且将凸优化和博弈论方法结合以求解。另外，文献[21]综述了雷达在进行目标探测和干扰抑制时所使用的策略，包括功率分配博弈、目标干扰博弈、编码方式博弈、波形设计博弈、目标检测和跟踪博弈等。然而上述博弈论方法下的优化模型仅含1～2个耦合度较低的优化变量，在多任务场景下，由于优化变量增多且变量间的耦合度高、难以分离，求解难度大大增加。

因此，本文针对空时域多任务场景，联合优化雷达与干扰机波束资源的分配问题，并取得了良好的低截获探测效果。其难点主要体现为：一是在复杂约束条件下，多平台的同时作用和多任务的联合优化导致优化模型是一个多参数耦合的非凸问题；二是波束与能量资源分配涉及了空间域和时间域的协同优化，使模型更为复杂，而传统半正定松弛(Semi-Definite Relaxation, SDR)算法随着模型的复杂度增加不再适用[22]。针对以上难点，本文主要工作及创新点包括：

(1) 针对雷达探测收发波束、干扰协同波束优化的多优化任务动态场景，提出了基于迭代优化的空时协同波束联合设计方法，解决了空时域干扰效果、干扰能量为约束的多参数耦合问题；

(2) 本文将优化对象精确到空时域波束权矢量，实现了雷达与干扰波束能量在不同时刻和不同方向上的灵活分配；

(3) 针对多干扰机协同优化的不定矩阵二次约束二次规划(Quadratically Constrained Quadratic Programs, QCQP)非凸优化问题，本文基于可行点追踪-连续凸逼近(Feasible Point Pursuit Successive Convex Approximation, FPP-SCA)算法[22]，解决了传统算法在矩阵不定时难以获得可行解的问题；相比SDR和连续凸逼近(Successive Convex Approximation, SCA)算法，基于FPP-SCA算法的协同干扰具有更优效果。

2　面向多任务动态场景的雷达与干扰波束资源联合优化问题模型

本节首先介绍雷达与干扰协同对抗动态场景，然后针对该场景建立问题模型，最后详细阐述模型中的目标函数和约束条件。

2.1　雷达与干扰场景及参数

考虑多任务动态场景：我方雷达执行探测目标的任务，此时对方L部探测雷达、K个侦察平台对我方雷达进行探测和侦察。其中，对方雷达通过发射电磁波照射我方雷达并接收回波，可获取我方雷达至电磁波发射点的距离、径向速度、方位、高度等信息。侦察平台呈平面部署，具有宽频带、大视场特点。对方雷达可“主动”探测我方雷达，侦察平台虽是“被动”接收，但其隐蔽性高、作用距离远。对方将地面侦察平台与空中探测雷达相结合以获取我方雷达信息，给我方造成了不可小觑的威胁。因此，我方N部干扰机协同干扰对方平台，以掩护我方雷达，如图1所示。

本文假设对方各平台的参数(如位置、载频、波束权矢量、噪声功率等)已知，其中雷达参数可通过电子侦察系统识别和分析得到[23–25]；目标和对方雷达的运动路线短时间内可预测[26,27]；侦察平台可采用卫星侦察、红外侦察等方法获取其信息。目前，在陆地目标侦察监视方面已有大量的高分辨率成像侦察卫星[28]以及红外侦察告警装备[29]。地杂波可通过相应杂波抑制方法克服[30]。为达到频域掩护

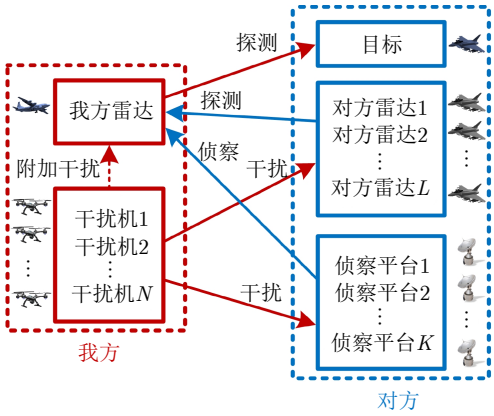

图 1 多任务场景示意图

Fig. 1 Schematic diagram of the multitask scene

效果，干扰机平台采用我方雷达相同频段。根据对方侦察平台任务需求，设其对我方雷达频段展开侦收，并指向我方雷达所在方向。同时，假设对方雷达与我方平台有频段重叠区域。为描述信号收发方向，引入θ_{12}表示以平台1为参考点，平台2的方向与平台1的天线阵列法线方向的夹角；为描述各个方向上收发波束的不同强度，引入$M\times 1$维发射波束权矢量$\boldsymbol{w}_{1\mathrm{t}}$和接收波束权矢量$\boldsymbol{w}_{1\mathrm{r}}$。其中，1, 2为任一平台的表示符号，干扰机表示为$n(n=1,2,\cdots,N)$、雷达为o、侦察机为$k(k=1,2,\cdots,K)$、对方雷达为$l(l=1,2,\cdots,L)$、目标为s。任一平台均包含M部呈等间距d排列的收发天线，故最多可同时发射或接收M个波束。考虑波束指向问题，本文引入$\boldsymbol{a}(\theta_{12})$, $\boldsymbol{b}(\theta_{12})$分别表示平台1针对平台2的发射和接收导向向量。另外，设本文中信号传输模型的两个通用形式为：$f(1,2,\tau)=\boldsymbol{w}_{1\mathrm{t}}^{\mathrm{H}}(\tau)\boldsymbol{a}\left(\theta_{12}(\tau)\right)$和$g(1,2,\tau)=\boldsymbol{w}_{1\mathrm{r}}^{\mathrm{H}}(\tau)\boldsymbol{b}\left(\theta_{12}(\tau)\right)$，分别表示$\tau$时刻平台1在平台2方向的发射和接收信号。$[\cdot]^{\mathrm{H}}$表示共轭转置运算。

2.2 雷达与干扰空时协同波束联合优化问题模型

为保证实时的目标探测与协同干扰效果，本文建立了以全时段最小的雷达探测信干噪比为优化目标、以侦察平台和对方雷达的干信比和每部干扰机总能量为约束条件的优化问题，模型框架见式(1)。

$$\max \text{ 全时段最小的}\frac{\text{雷达探测目标的回波信号功率}}{\text{雷达接收的干扰信号功率}+\text{接收端噪声功率}}$$
$$\text{s.t.}\begin{cases}\text{任意时刻满足：}\dfrac{\text{侦察平台接收的干扰信号功率}+\text{接收端噪声功率}}{\text{侦察平台接收的我方雷达信号功率}}\geq\text{阈值}\\ \text{任意时刻满足：}\dfrac{\text{对方雷达接收的干扰信号功率}+\text{接收端噪声功率}}{\text{对方雷达探测我方雷达的回波信号功率}}\geq\text{阈值}\\ \text{每部干扰机的全时段总能量}\leq\text{上限}\end{cases}\tag{1}$$

将全时段离散化为T个时刻，任意时刻表示为τ，即$\tau\in[1,T]$。以P表示有效信号功率，J表示干扰和噪声功率之和，则式(1)对应的问题模型如下：

$$\max_{\boldsymbol{w}_{\mathrm{or}}(\tau),\boldsymbol{w}_{\mathrm{ot}}(\tau),\boldsymbol{w}_{nt}(\tau)}\ \min_{\tau\in\{1,2,\cdots,T\}}\frac{P_o(\boldsymbol{w}_{\mathrm{or}}(\tau),\boldsymbol{w}_{\mathrm{ot}}(\tau))}{J_o(\boldsymbol{w}_{\mathrm{or}}(\tau),\boldsymbol{w}_{nt}(\tau))}$$
$$\text{s.t.}\begin{cases}\dfrac{J_k(\boldsymbol{w}_{nt}(\tau))}{P_k(\boldsymbol{w}_{\mathrm{ot}}(\tau))}\geq\gamma_k,\quad k=1,2,\cdots,K\\ \dfrac{J_l(\boldsymbol{w}_{nt}(\tau))}{P_l}\geq\gamma_l,\quad l=1,2,\cdots,L\\ \displaystyle\sum_{\tau=1}^{T}\|\boldsymbol{w}_{nt}(\tau)\|^2\leq\rho_n,\quad n=1,2,\cdots,N\end{cases}\tag{2}$$

其中，优化变量包括雷达发射波束权矢量$\boldsymbol{w}_{\mathrm{ot}}(\tau)$、雷达接收波束权矢量$\boldsymbol{w}_{\mathrm{or}}(\tau)$和干扰机发射波束权矢量$\boldsymbol{w}_{nt}(\tau)$。波束权矢量反映了各阵元上的能量分配，因此在其他参数一定的情况下，各平台的有效信号功率和干扰功率取决于待优化的波束权矢量，具体为：

(1) 雷达探测目标的回波信号功率$P_o(\boldsymbol{w}_{\mathrm{or}}(\tau),\boldsymbol{w}_{\mathrm{ot}}(\tau))$，由雷达发射、接收波束权矢量决定；

(2) 由于各干扰机与雷达信号在相同频段且与对方雷达有频段重叠，雷达会受到干扰机信号和对方雷达探测信号的影响，故雷达接收的干扰和噪声功率之和$J_o(\boldsymbol{w}_{\mathrm{or}}(\tau),\boldsymbol{w}_{nt}(\tau))$由干扰机发射、雷达接收波束权矢量决定；

(3) $J_k(\boldsymbol{w}_{nt}(\tau))$, $J_l(\boldsymbol{w}_{nt}(\tau))$分别表示侦察平台$k$和对方雷达$l$接收的干扰信号功率，由干扰机波束权矢量决定；

(4) $P_k(\boldsymbol{w}_{\mathrm{ot}}(\tau))$, P_l分别表示侦察平台k和对方雷达l接收的有效信号功率。由于侦察平台的目的是获取我方雷达信息，因此$P_k(\boldsymbol{w}_{\mathrm{ot}}(\tau))$由雷达发射波束权矢量决定；而对方雷达的有效信号功率是其探测我方雷达的回波功率，主要受其自身因素影响。

此外，γ_k, γ_l分别表示侦察平台k和对方雷达l被有效干扰的最小干信比阈值；ρ_n表示第n部干扰机的全时段功率上限；$\|\cdot\|^2$为向量范数运算。

可见，本文波束资源空时协同优化分配，就是在能量约束和保证干扰效果的前提下，寻找使目标探测性能最优的波束分配方案，即求解模型中的波束权矢量。接下来详细介绍上述模型的组成部分。

2.2.1 问题模型的目标函数

为评估雷达探测目标的性能，本文选用信干噪比作为量化指标。此处的信干噪比即我方雷达接收的有效信号功率与干扰和噪声功率之和的比值。有效信号功率即我方雷达探测目标的回波信号功率

$$P_o(\boldsymbol{w}_{\mathrm{or}}(\tau),\boldsymbol{w}_{\mathrm{ot}}(\tau))=|g(o,s,\tau)f(o,s,\tau)\Omega_1(\tau)|^2 \quad (3)$$

其中，$g(o,s,\tau)f(o,s,\tau)\Omega_1(\tau)=\boldsymbol{w}_{\mathrm{or}}^{\mathrm{H}}(\tau)\boldsymbol{b}(\theta_{\mathrm{os}}(\tau))\,\boldsymbol{w}_{\mathrm{ot}}^{\mathrm{H}}(\tau)\cdot\boldsymbol{a}(\theta_{\mathrm{os}}(\tau))\,\Omega_1(\tau)$，表示我方雷达探测目标的回波信号；符号$\Omega_i(\tau)\,(i=1,2,\cdots,7)$表示$\tau$时刻下不同传输信道的幅度常量，$\Omega_1(\tau)$主要与我方雷达到目标的距离、目标的雷达散射截面积(Radar Cross Section, RCS)有关。

另外，干扰和噪声功率之和表示为

$$\begin{aligned}&J_o(\boldsymbol{w}_{\mathrm{or}}(\tau),\boldsymbol{w}_{nt}(\tau))\\&=\underbrace{\sum_{n=1}^{N}|g(o,n,\tau)f(n,o,\tau)\Omega_2(\tau)|^2}_{\text{(I)}}\\&\quad+\underbrace{\sum_{l=1}^{L}|g(o,l,\tau)f(l,o,\tau)\Omega_3(\tau)|^2}_{\text{(II)}}+\underbrace{\sigma_n^2}_{\text{(III)}}\end{aligned}\quad (4)$$

式(4)可分为3部分，分别是：

(I) N部干扰机对我方雷达的干扰信号功率之和。干扰机在协同干扰对方平台的同时，在我方雷达方向的信号为$g(o,n,\tau)f(n,o,\tau)$，即$\boldsymbol{w}_{\mathrm{or}}^{\mathrm{H}}(\tau)\boldsymbol{b}\,(\theta_{on})\cdot\boldsymbol{w}_{nt}^{\mathrm{H}}(\tau)\boldsymbol{a}\,(\theta_{no})$；$\Omega_2(\tau)$与干扰机到我方雷达的距离平方成反比；

(II) 对方L部雷达的发射信号功率对我方雷达的总体干扰。对方雷达l在我方雷达所在方向的信号为$g(o,l,\tau)f(l,o,\tau)$，即$\boldsymbol{w}_{\mathrm{or}}^{\mathrm{H}}(\tau)\boldsymbol{b}\,(\theta_{ol}(\tau))\,\boldsymbol{w}_{\mathrm{lt}}^{\mathrm{H}}(\tau)\cdot\boldsymbol{a}\,(\theta_{lo}(\tau))$；$\Omega_3(\tau)$与对方雷达到我方雷达的距离平方成反比；

(III) 雷达接收端的噪声功率。

综上，本文模型目标函数为

$$\begin{aligned}&\mathrm{SINR}_o(\boldsymbol{w}_{\mathrm{or}}(\tau),\boldsymbol{w}_{\mathrm{ot}}(\tau),\boldsymbol{w}_{nt}(\tau))\\&=\frac{P_o(\boldsymbol{w}_{\mathrm{or}}(\tau),\boldsymbol{w}_{\mathrm{ot}}(\tau))}{J_o(\boldsymbol{w}_{\mathrm{or}}(\tau),\boldsymbol{w}_{nt}(\tau))}\end{aligned}\quad (5)$$

2.2.2 问题模型的约束条件

对方平台受到的干扰包括N部干扰机的协同干扰作用及其自身的噪声影响，故侦察平台k接收的总干扰信号功率为

$$J_k(\boldsymbol{w}_{nt}(\tau))=\sum_{n=1}^{N}|g(k,n,\tau)f(n,k,\tau)\Omega_4(\tau)|^2+\sigma_n^2 \quad (6)$$

其中，$g(k,n,\tau)f(n,k,\tau)$表示干扰机n对侦察平台k的干扰信号，即$\boldsymbol{w}_{\mathrm{kr}}^{\mathrm{H}}(\tau)\boldsymbol{b}(\theta_{kn}(\tau))\boldsymbol{w}_{nt}^{\mathrm{H}}(\tau)\boldsymbol{a}(\theta_{nk}(\tau))$；$\Omega_4(\tau)$与干扰机到侦察平台的距离平方成反比。由侦察平台$k$的任务需求可知，来自我方雷达的信号是其有效信号，则侦察平台k接收的有效信号功率为

$$\begin{aligned}P_k(\boldsymbol{w}_{\mathrm{ot}}(\tau))&=|g(k,o,\tau)f(o,k,\tau)\Omega_5(\tau)|^2\\&=\left|\boldsymbol{w}_{\mathrm{kr}}^{\mathrm{H}}(\tau)\boldsymbol{b}(\theta_{ko}(\tau))\boldsymbol{w}_{\mathrm{ot}}^{\mathrm{H}}(\tau)\right.\\&\quad\left.\cdot\boldsymbol{a}(\theta_{ok}(\tau))\Omega_5(\tau)\right|^2\end{aligned}\quad (7)$$

$\Omega_5(\tau)$与我方雷达到侦察平台的距离平方成反比。任意侦察平台都需要满足最小干信比约束条件，即

$$\frac{J_k(\boldsymbol{w}_{nt}(\tau))}{P_k(\boldsymbol{w}_{\mathrm{ot}}(\tau))}\geq\gamma_k,\ \ k=1,2,\cdots,K \quad (8)$$

类似地，对方雷达l 接收的总干扰信号功率为

$$J_l(\boldsymbol{w}_{nt}(\tau))=\sum_{n=1}^{N}|g(l,n,\tau)f(n,l,\tau)\Omega_6(\tau)|^2+\sigma_n^2 \quad (9)$$

其中，$g(l,n,\tau)f(n,l,\tau)$表示干扰机n干扰对方雷达l的信号，即$\boldsymbol{w}_{\mathrm{lr}}^{\mathrm{H}}(\tau)\boldsymbol{b}(\theta_{ln}(\tau))\boldsymbol{w}_{nt}^{\mathrm{H}}(\tau)\boldsymbol{a}(\theta_{nl}(\tau))$，$\Omega_6(\tau)$与干扰机到对方雷达的距离平方成反比。同理，对方雷达l 接收的有效信号功率为

$$\begin{aligned}P_l&=|g(l,o,\tau)f(l,o,\tau)\Omega_7(\tau)|^2\\&=\left|\boldsymbol{w}_{lr}^{\mathrm{H}}(\tau)\boldsymbol{b}(\theta_{lo}(\tau))\boldsymbol{w}_{lt}^{\mathrm{H}}(\tau)\boldsymbol{a}(\theta_{lo}(\tau))\Omega_7(\tau)\right|^2\end{aligned}\quad (10)$$

式(10)包括对方雷达l在我方雷达方向的发射信号$f(l,o,\tau)$、回波信号$g(l,o,\tau)$以及幅度常量$\Omega_7(\tau)$。同样，对方所有雷达需满足最小干信比约束

$$\frac{J_l(\boldsymbol{w}_{nt}(\tau))}{P_l}\geq\gamma_l,\ \ l=1,2,\cdots,L \quad (11)$$

另外，考虑每个干扰机的总能量约束，如式(12)所示。

$$\sum_{\tau=1}^{T}\|\boldsymbol{w}_{nt}(\tau)\|^2\leq\rho_n,\ \ n=1,2,\cdots,N \quad (12)$$

3 基于多参数迭代的空域波束优化算法

为便于说明，本节在$T=1$的特殊情况下详细介绍了所提算法的原理及用法，并在第4节推广至动态场景。

3.1 空域波束迭代优化算法总体框架

本节主要体现空间域上的优化，设式(2)中参数$T=1$，得式(13)问题模型。

$$\max_{\boldsymbol{w}_{ot},\boldsymbol{w}_{or},\boldsymbol{w}_{nt}} \frac{\left|\boldsymbol{w}_{or}^{\mathrm{H}}\boldsymbol{b}(\theta_{os})\boldsymbol{w}_{ot}^{\mathrm{H}}\boldsymbol{a}(\theta_{os})\Omega_1\right|^2}{\sum_{n=1}^{N}\left|\boldsymbol{w}_{or}^{\mathrm{H}}\boldsymbol{b}(\theta_{on})\boldsymbol{w}_{nt}^{\mathrm{H}}\boldsymbol{a}(\theta_{no})\Omega_2\right|^2+\sum_{l=1}^{L}\left|\boldsymbol{w}_{or}^{\mathrm{H}}\boldsymbol{b}(\theta_{ol})\boldsymbol{w}_{lt}^{\mathrm{H}}\boldsymbol{a}(\theta_{lo})\Omega_3\right|^2+\sigma_n^2}$$

$$\text{s.t.}\begin{cases}\dfrac{\sum_{n=1}^{N}\left|\boldsymbol{w}_{kr}^{\mathrm{H}}\boldsymbol{b}(\theta_{kn})\boldsymbol{w}_{nt}^{\mathrm{H}}\boldsymbol{a}(\theta_{nk})\Omega_4\right|^2+\sigma_n^2}{\left|\boldsymbol{w}_{kr}^{\mathrm{H}}\boldsymbol{b}(\theta_{ko})\boldsymbol{w}_{ot}^{\mathrm{H}}\boldsymbol{a}(\theta_{ok})\Omega_5\right|^2}\geq\gamma_k,\ k=1,2,\cdots,K\\ \dfrac{\sum_{n=1}^{N}\left|\boldsymbol{w}_{lr}^{\mathrm{H}}\boldsymbol{b}(\theta_{ln})\boldsymbol{w}_{nt}^{\mathrm{H}}\boldsymbol{a}(\theta_{nl})\Omega_6\right|^2+\sigma_n^2}{\left|\boldsymbol{w}_{lr}^{\mathrm{H}}\boldsymbol{b}(\theta_{lo})\boldsymbol{w}_{lt}^{\mathrm{H}}\boldsymbol{a}(\theta_{lo})\Omega_7\right|^2}\geq\gamma_l,\ l=1,2,\cdots,L\\ \left\|\boldsymbol{w}_{nt}\right\|^2\leq\rho_n,\ n=1,2,\cdots,N\end{cases} \tag{13}$$

该模型包含3个优化变量且约束较多，难以使用传统方法求解。因此，本文提出了一种基于迭代的波束资源联合优化算法，即分别将两个优化变量视为常量，据已知条件简化模型，再求解使目标函数最优的另一个变量，如此循环迭代，直到目标函数和变量收敛。算法总体框架如图2所示。

3.2 基于广义瑞利商的雷达接收波束权矢量优化方法

根据上述算法，在固定雷达发射波束权矢量$\boldsymbol{w}_{ot}$和干扰机发射波束权矢量$\boldsymbol{w}_{nt}$时，雷达接收波束权矢量$\boldsymbol{w}_{or}$为唯一的优化变量。由于式(13)约束不含$\boldsymbol{w}_{or}$，模型等价为

$$\max_{\boldsymbol{w}_{or}} \frac{\left|\boldsymbol{w}_{or}^{\mathrm{H}}\boldsymbol{b}(\theta_{os})\boldsymbol{w}_{ot}^{\mathrm{H}}\boldsymbol{a}(\theta_{os})\Omega_1\right|^2}{\sum_{n=1}^{N}\left|\boldsymbol{w}_{or}^{\mathrm{H}}\boldsymbol{b}(\theta_{on})\boldsymbol{w}_{nt}^{\mathrm{H}}\boldsymbol{a}(\theta_{no})\Omega_2\right|^2+\sum_{l=1}^{L}\left|\boldsymbol{w}_{or}^{\mathrm{H}}\boldsymbol{b}(\theta_{ol})\boldsymbol{w}_{lt}^{\mathrm{H}}\boldsymbol{a}(\theta_{lo})\Omega_3\right|^2+\sigma_n^2} \tag{14}$$

令M维向量$\boldsymbol{a}=\boldsymbol{b}(\theta_{os})\boldsymbol{w}_{ot}^{\mathrm{H}}\boldsymbol{a}(\theta_{os})\Omega_1$，$\boldsymbol{b}_n=\boldsymbol{b}(\theta_{on})\cdot\boldsymbol{w}_{nt}^{\mathrm{H}}\boldsymbol{a}(\theta_{no})\Omega_2$，$\boldsymbol{c}_l=\boldsymbol{b}(\theta_{ol})\boldsymbol{w}_{lt}^{\mathrm{H}}\boldsymbol{a}(\theta_{lo})\Omega_3$，式(14)简化为

$$\max_{\boldsymbol{w}_{or}} \frac{\boldsymbol{w}_{or}^{\mathrm{H}}\boldsymbol{a}\boldsymbol{a}^{\mathrm{H}}\boldsymbol{w}_{or}}{\sum_{n=1}^{N}\boldsymbol{w}_{or}^{\mathrm{H}}\boldsymbol{b}_n\boldsymbol{b}_n^{\mathrm{H}}\boldsymbol{w}_{or}+\sum_{l=1}^{L}\boldsymbol{w}_{or}^{\mathrm{H}}\boldsymbol{c}_l\boldsymbol{c}_l^{\mathrm{H}}\boldsymbol{w}_{or}+\sigma_n^2} \tag{15}$$

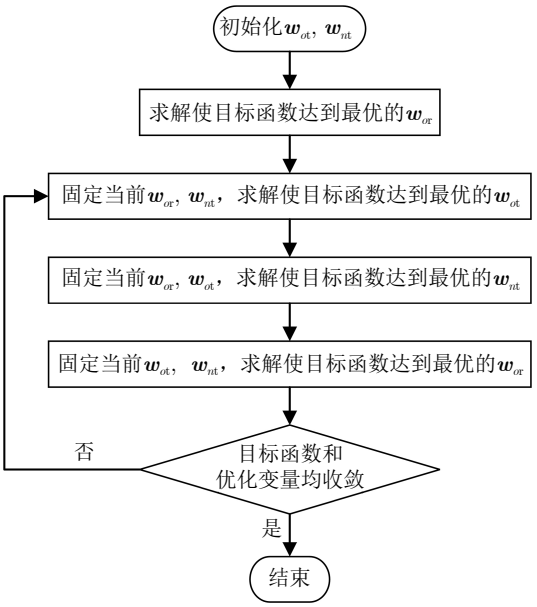

图 2 基于迭代的波束资源联合优化算法总体框架

Fig. 2 The overall framework of the joint optimization algorithm of beamforming resources based on iteration

其中，$\sigma_n^2=\boldsymbol{w}_{or}^{\mathrm{H}}\boldsymbol{I}\sigma_n^2\boldsymbol{w}_{or}/\left\|\boldsymbol{w}_{or}\right\|^2$，将雷达接收波束的功率归一化，即$\left\|\boldsymbol{w}_{or}\right\|^2=1$，则$\sigma_n^2=\boldsymbol{w}_{or}^{\mathrm{H}}\boldsymbol{I}\sigma_n^2\boldsymbol{w}_{or}$。令$\boldsymbol{A}=\boldsymbol{a}\boldsymbol{a}^{\mathrm{H}}$，$\boldsymbol{B}=\sum_{n=1}^{N}\boldsymbol{b}_n\boldsymbol{b}_n^{\mathrm{H}}+\sum_{l=1}^{L}\boldsymbol{c}_l\boldsymbol{c}_l+\boldsymbol{I}\sigma_n^2$，式(15)简化为

$$\max_{\boldsymbol{w}_{or}} \frac{\boldsymbol{w}_{or}^{\mathrm{H}}\boldsymbol{A}\boldsymbol{w}_{or}}{\boldsymbol{w}_{or}^{\mathrm{H}}\boldsymbol{B}\boldsymbol{w}_{or}} \tag{16}$$

其中，$\boldsymbol{A}$, $\boldsymbol{B}$均为Hermitian矩阵且$\boldsymbol{B}$正定，满足广义瑞利商条件，则式(16)最优解为[31]

$$\boldsymbol{w}_{or}^{*}=\lambda_{\max}\left(\boldsymbol{B}^{-1}\boldsymbol{A}\right) \tag{17}$$

其中，$\lambda_{\max}(\cdot)$表示矩阵最大特征值对应的特征向量。

3.3 基于半负定矩阵定义放缩的雷达发射波束权矢量优化方法

同理，将雷达接收波束权矢量$\boldsymbol{w}_{or}$和干扰机发射波束权矢量$\boldsymbol{w}_{nt}$视为常量时，式(13)可简化为

$$\max_{\boldsymbol{w}_{ot}} \left|\boldsymbol{w}_{or}^{\mathrm{H}}\boldsymbol{b}(\theta_{os})\boldsymbol{w}_{ot}^{\mathrm{H}}\boldsymbol{a}(\theta_{os})\Omega_1\right|^2$$

$$\text{s.t.}\ \frac{\sum_{n=1}^{N}\left|\boldsymbol{w}_{kr}^{\mathrm{H}}\boldsymbol{b}(\theta_{kn})\boldsymbol{w}_{nt}^{\mathrm{H}}\boldsymbol{a}(\theta_{nk})\Omega_4\right|^2+\sigma_n^2}{\left|\boldsymbol{w}_{kr}^{\mathrm{H}}\boldsymbol{b}(\theta_{ko})\boldsymbol{w}_{ot}^{\mathrm{H}}\boldsymbol{a}(\theta_{ok})\Omega_5\right|^2}\geq\gamma_k,\ k=1,2,\cdots,K \tag{18}$$

令常数

$\beta_k=\left(\sum_{n=1}^{N}\left|\boldsymbol{w}_{kr}^{\mathrm{H}}\boldsymbol{b}(\theta_{kn})\boldsymbol{w}_{nt}^{\mathrm{H}}\boldsymbol{a}(\theta_{nk})\Omega_4\right|^2+\sigma_n^2\right)/\gamma_k$，$M$维向量$\boldsymbol{d}=\boldsymbol{w}_{or}^{\mathrm{H}}\boldsymbol{b}(\theta_{os})\boldsymbol{a}(\theta_{os})\Omega_1$，$\boldsymbol{g}_k=\boldsymbol{w}_{kr}^{\mathrm{H}}\boldsymbol{b}(\theta_{ko})\cdot\boldsymbol{a}(\theta_{ok})\Omega_5$，得

$$\begin{aligned}&\max_{\boldsymbol{w}_{ot}}\ \left|\boldsymbol{w}_{ot}^{\mathrm{H}}\boldsymbol{d}\right|^2\\&\text{s.t.}\ \left|\boldsymbol{w}_{ot}^{\mathrm{H}}\boldsymbol{g}_k\right|^2\le\beta_k,\ \forall k\end{aligned}\tag{19}$$

令矩阵$\boldsymbol{D}=\boldsymbol{d}\boldsymbol{d}^{\mathrm{H}}$，$\boldsymbol{G}_k=\boldsymbol{g}_k\boldsymbol{g}_k^{\mathrm{H}}$，式(19)简化为

$$\begin{aligned}&\min_{\boldsymbol{w}_{ot}}\ \boldsymbol{w}_{ot}^{\mathrm{H}}(-\boldsymbol{D})\boldsymbol{w}_{ot}\\&\text{s.t.}\ \boldsymbol{w}_{ot}^{\mathrm{H}}\boldsymbol{G}_k\boldsymbol{w}_{ot}\le\beta_k,\ \forall k\end{aligned}\tag{20}$$

其中，$(-\boldsymbol{D})$为半负定Hermitian矩阵，因此对任意M维向量$\boldsymbol{z}$，有[19]

$$\boldsymbol{w}_{ot}^{\mathrm{H}}(-\boldsymbol{D})\boldsymbol{w}_{ot}\le2\mathrm{Re}\left\{\boldsymbol{z}^{\mathrm{H}}(-\boldsymbol{D})\boldsymbol{w}_{ot}\right\}-\boldsymbol{z}^{\mathrm{H}}(-\boldsymbol{D})\boldsymbol{z}\tag{21}$$

其中，$\mathrm{Re}\{\cdot\}$表示取实部运算。将优化变量$\boldsymbol{w}_{ot}$功率归一化，即$\|\boldsymbol{w}_{ot}\|^2=1$，优化问题最终等价为

$$\begin{aligned}&\min_{\boldsymbol{w}_{ot}}\ 2\mathrm{Re}\left\{\boldsymbol{z}^{\mathrm{H}}(-\boldsymbol{D})\boldsymbol{w}_{ot}\right\}-\boldsymbol{z}^{\mathrm{H}}(-\boldsymbol{D})\boldsymbol{z}\\&\text{s.t.}\ \boldsymbol{w}_{ot}^{\mathrm{H}}\boldsymbol{G}_k\boldsymbol{w}_{ot}\le\beta_k,\ \forall k\\&\quad\boldsymbol{w}_{ot}^{\mathrm{H}}\boldsymbol{w}_{ot}=1\end{aligned}\tag{22}$$

式(22)是一个凸优化问题，可直接求解。

3.4 基于FPP-SCA算法的干扰机发射波束权矢量优化方法

3.2节和3.3节分别介绍了优化雷达接收波束权矢量$\boldsymbol{w}_{or}$和雷达发射波束权矢量$\boldsymbol{w}_{ot}$的方法，本节继续阐述迭代优化算法的第3个重要步骤，即将干扰机发射波束权矢量$\boldsymbol{w}_{nt}$视作唯一变量的优化方法。式(13)所示模型可等价为

$$\begin{aligned}&\min_{\boldsymbol{w}_{nt}}\ \sum_{n=1}^{N}\left|\boldsymbol{w}_{or}^{\mathrm{H}}\boldsymbol{b}(\theta_{on})\boldsymbol{w}_{nt}^{\mathrm{H}}\boldsymbol{a}(\theta_{no})\Omega_2\right|^2\\&\text{s.t.}\begin{cases}\dfrac{\sum_{n=1}^{N}\left|\boldsymbol{w}_{kr}^{\mathrm{H}}\boldsymbol{b}(\theta_{kn})\boldsymbol{w}_{nt}^{\mathrm{H}}\boldsymbol{a}(\theta_{nk})\Omega_4\right|^2+\sigma_n^2}{\left|\boldsymbol{w}_{kr}^{\mathrm{H}}\boldsymbol{b}(\theta_{ko})\boldsymbol{w}_{ot}^{\mathrm{H}}\boldsymbol{a}(\theta_{ok})\Omega_5\right|^2}\ge\gamma_k,\ k=1,2,\cdots,K\\\dfrac{\sum_{n=1}^{N}\left|\boldsymbol{w}_{lr}^{\mathrm{H}}\boldsymbol{b}(\theta_{ln})\boldsymbol{w}_{nt}^{\mathrm{H}}\boldsymbol{a}(\theta_{nl})\Omega_6\right|^2+\sigma_n^2}{\left|\boldsymbol{w}_{lr}^{\mathrm{H}}\boldsymbol{b}(\theta_{lo})\boldsymbol{w}_{lt}^{\mathrm{H}}\boldsymbol{a}(\theta_{lo})\Omega_7\right|^2}\ge\gamma_l,\ l=1,2,\cdots,L\\\|\boldsymbol{w}_{nt}\|^2\le\rho_n,\ n=1,2,\cdots,N\end{cases}\end{aligned}\tag{23}$$

令向量$\boldsymbol{h}_n=\boldsymbol{w}_{or}^{\mathrm{H}}\boldsymbol{b}(\theta_{on})\boldsymbol{a}(\theta_{no})\Omega_2$，$\boldsymbol{p}_{nk}=\boldsymbol{w}_{kr}^{\mathrm{H}}\cdot\boldsymbol{b}(\theta_{kn})\boldsymbol{a}(\theta_{nk})\Omega_4$，$\boldsymbol{q}_{nl}=\boldsymbol{w}_{lr}^{\mathrm{H}}\boldsymbol{b}(\theta_{ln})\boldsymbol{a}(\theta_{nl})\Omega_6$，常量$\beta_k=\left|\boldsymbol{w}_{kr}^{\mathrm{H}}\boldsymbol{b}(\theta_{ko})\boldsymbol{w}_{ot}^{\mathrm{H}}\boldsymbol{a}(\theta_{ok})\Omega_5\right|^2\gamma_k-\sigma_n^2$，$\beta_l=\left|\boldsymbol{w}_{lr}^{\mathrm{H}}\boldsymbol{b}(\theta_{lo})\boldsymbol{w}_{lt}^{\mathrm{H}}\cdot\boldsymbol{a}(\theta_{lo})\Omega_7\right|^2\gamma_l-\sigma_n^2$，得

$$\begin{aligned}&\min_{\boldsymbol{w}_{nt}}\ \sum_{n=1}^{N}\left|\boldsymbol{w}_{nt}^{\mathrm{H}}\boldsymbol{h}_n\right|^2\\&\text{s.t.}\begin{cases}\sum_{n=1}^{N}\left|\boldsymbol{w}_{nt}^{\mathrm{H}}\boldsymbol{p}_{nk}\right|^2\ge\beta_k,\ k=1,2,\cdots,K\\\sum_{n=1}^{N}\left|\boldsymbol{w}_{nt}^{\mathrm{H}}\boldsymbol{q}_{nl}\right|^2\ge\beta_l,\ l=1,2,\cdots,L\\\|\boldsymbol{w}_{nt}\|^2\le\rho_n,\ n=1,2,\cdots,N\end{cases}\end{aligned}\tag{24}$$

令MN维向量$\boldsymbol{w}_{\mathrm{t}}=\left(\boldsymbol{w}_{1\mathrm{t}}^{\mathrm{T}}\ \ \boldsymbol{w}_{2\mathrm{t}}^{\mathrm{T}}\ \ \cdots\ \ \boldsymbol{w}_{N\mathrm{t}}^{\mathrm{T}}\right)^{\mathrm{T}}$，$MN$阶矩阵$\boldsymbol{H}=\mathrm{diag}(\boldsymbol{h}_1\boldsymbol{h}_1^{\mathrm{H}},\boldsymbol{h}_2\boldsymbol{h}_2^{\mathrm{H}},\cdots,\boldsymbol{h}_N\boldsymbol{h}_N^{\mathrm{H}})$，$\boldsymbol{P}_k=\mathrm{diag}(\boldsymbol{P}_{1k}\boldsymbol{P}_{1k}^{\mathrm{H}},\boldsymbol{P}_{2k}\boldsymbol{P}_{2k}^{\mathrm{H}},\cdots,\boldsymbol{P}_{Nk}\boldsymbol{P}_{Nk}^{\mathrm{H}})$，$\boldsymbol{Q}_l=\mathrm{diag}(\boldsymbol{q}_{1l}\boldsymbol{q}_{1l}^{\mathrm{H}},\boldsymbol{q}_{2l}\boldsymbol{q}_{2l}^{\mathrm{H}},\cdots,\boldsymbol{q}_{Nl}\boldsymbol{q}_{Nl}^{\mathrm{H}})$，设$MN$阶分块矩阵$\boldsymbol{R}_n$的对角线第$N$个位置为单位阵$\boldsymbol{I}$，其余位置为零矩阵$\boldsymbol{0}$，即：$\boldsymbol{R}_1=\mathrm{diag}(\boldsymbol{I},\boldsymbol{0},\cdots,\boldsymbol{0})$，$\boldsymbol{R}_2=\mathrm{diag}(\boldsymbol{0},\boldsymbol{I},\boldsymbol{0},\cdots,\boldsymbol{0})$，$\cdots$，$\boldsymbol{R}_N=\mathrm{diag}(\boldsymbol{0},\boldsymbol{0},\cdots,\boldsymbol{0},\boldsymbol{I})$，化简可得

$$\begin{aligned}&\min_{\boldsymbol{w}_{\mathrm{t}}}\ \boldsymbol{w}_{\mathrm{t}}^{\mathrm{H}}\boldsymbol{H}\boldsymbol{w}_{\mathrm{t}}\\&\text{s.t.}\begin{cases}\boldsymbol{w}_{\mathrm{t}}^{\mathrm{H}}(-\boldsymbol{P}_k)\boldsymbol{w}_{\mathrm{t}}\le-\beta_k,\ k=1,2,\cdots,K\\\boldsymbol{w}_{\mathrm{t}}^{\mathrm{H}}(-\boldsymbol{Q}_l)\boldsymbol{w}_{\mathrm{t}}\le-\beta_l,\ l=1,2,\cdots,L\\\boldsymbol{w}_{\mathrm{t}}^{\mathrm{H}}\boldsymbol{R}_n\boldsymbol{w}_{\mathrm{t}}\le\rho_n,\ n=1,2,\cdots,N\end{cases}\end{aligned}\tag{25}$$

其中，$\boldsymbol{H}$为半正定矩阵，但由于$(-\boldsymbol{P}_k)$和$(-\boldsymbol{Q}_l)$不满足正定或半正定条件，该问题是非凸的。为此，采用FPP-SCA算法求解[22]：先引入松弛惩罚s_m以确保问题的可行性、加入松弛量μ以平衡原目标函数和惩罚项，如式(26)；再进行可行点的追踪和逼近。具体流程如算法1所示。

$$\begin{aligned}&\min_{\boldsymbol{w}_{\mathrm{t}},\boldsymbol{s}}\ \boldsymbol{w}_{\mathrm{t}}^{\mathrm{H}}\boldsymbol{H}\boldsymbol{w}_{\mathrm{t}}+\mu\sum_{m=1}^{(K+L+N)}s_m\\&\text{s.t.}\begin{cases}\boldsymbol{w}_{\mathrm{t}}^{\mathrm{H}}(-\boldsymbol{P}_k)\boldsymbol{w}_{\mathrm{t}}\le-\beta_k+s_k,\ k=1,2,\cdots,K\\\boldsymbol{w}_{\mathrm{t}}^{\mathrm{H}}(-\boldsymbol{Q}_l)\boldsymbol{w}_{\mathrm{t}}\le-\beta_l+s_{K+l},\ l=1,2,\cdots,L\\\boldsymbol{w}_{\mathrm{t}}^{\mathrm{H}}\boldsymbol{R}_n\boldsymbol{w}_{\mathrm{t}}\le\rho_n+s_{K+L+n},\ n=1,2,\cdots,N\\s_m\ge0,\ m=1,2,\cdots,K+L+N\end{cases}\end{aligned}\tag{26}$$

综上所述，本节介绍了基于迭代的空域波束资源联合优化算法，如算法2所示。

算法 1 基于FFP-SCA算法的干扰机发射波束权矢量优化过程

Alg. 1 Optimization process of jammers' transmit beamforming vectors based on FFP-SCA algorithm

步骤1 初始化：

设迭代次数$q=0$，初始化M维向量$\boldsymbol{z}_0$；

步骤2 循环执行：

(1) 求解下式凸优化问题：

$$\min_{\boldsymbol{w}_{\mathrm{t}},\boldsymbol{s}} \ \boldsymbol{w}_{\mathrm{t}}^{\mathrm{H}}\boldsymbol{H}\boldsymbol{w}_{\mathrm{t}}+\mu\sum_{m=1}^{K+L+N}s_m$$

$$\text{s.t.}\begin{cases}2\mathrm{Re}\left\{\boldsymbol{z}_q^{\mathrm{H}}(-\boldsymbol{P}_k)\boldsymbol{w}_{\mathrm{t}}\right\}\le-\beta_k+\boldsymbol{z}_q^{\mathrm{H}}(-\boldsymbol{P}_k)\boldsymbol{z}_q+s_k,\ k=1,2,\cdots,K\\ 2\mathrm{Re}\left\{\boldsymbol{z}_q^{\mathrm{H}}(-\boldsymbol{Q}_l)\boldsymbol{w}_{\mathrm{t}}\right\}\le-\beta_l+\boldsymbol{z}_q^{\mathrm{H}}(-\boldsymbol{Q}_l)\boldsymbol{z}_q+s_{K+l},\ l=1,2,\cdots,L\\ \boldsymbol{w}_{\mathrm{t}}^{\mathrm{H}}\boldsymbol{R}_n\boldsymbol{w}_{\mathrm{t}}\le\rho_n+s_{K+L+n},\ n=1,2,\cdots,N\\ s_m\ge0,\ m=1,2,\cdots,K+L+N\end{cases}$$

得到当前最优解$\boldsymbol{w}_{\mathrm{t}}^{*}$；

(2) 将第q次得到的$\boldsymbol{w}_{\mathrm{t}}^{*}$赋值给$\boldsymbol{z}_{q+1}$；

(3) 令$q=q+1$；

直到目标函数收敛，循环结束。

算法 2 基于迭代的空域波束资源联合优化算法

Alg. 2 Joint optimization algorithm of beamforming resources based on iterative optimization in the spatial domain

步骤1 初始化：

设置场景数据(如平台位置、阵元个数、阵元间距等)，给定$\boldsymbol{w}_{\mathrm{ot}}$, $\boldsymbol{w}_{n\mathrm{t}}$初值；

步骤2 执行循环：

(1) 求解式(17)，得到当前最优解$\boldsymbol{w}_{\mathrm{or}}^{*}$：对矩阵$\boldsymbol{B}^{-1}\boldsymbol{A}$进行特征值分解，最大特征值对应的特征向量即所求$\boldsymbol{w}_{\mathrm{or}}^{*}$；

(2) 求解如式(22)所示的凸优化问题，得到当前最优解$\boldsymbol{w}_{ot}^{*}$；

(3) 根据算法1，得到当前最优$\boldsymbol{w}_{nt}^{*}$；

直到目标函数收敛和优化变量收敛，循环结束；

步骤3 输出结果：

最终波束权矢量$\boldsymbol{w}_{\mathrm{or}}^{*}$, $\boldsymbol{w}_{ot}^{*}$和$\boldsymbol{w}_{nt}^{*}$的值即为波束资源联合优化的最优结果。

4 面向动态场景的空时域波束联合优化算法

第3节以$T=1$的非动态场景为例，介绍了基于迭代的波束资源联合优化算法原理，本节将其推广到一般情况以求解式(2)动态场景模型。其中，雷达发射波束权矢量和接收波束权矢量的优化过程与前文如出一辙，仅维度从一维增加到了T维；干扰机发射波束权矢量也可化为式(25)所示形式，然后采用FPP-SCA算法求解。但由于动态场景中第3个约束的形式改变，求解干扰机发射波束权矢量的简化过程不再一致，下面作具体说明。

化简目标函数可得

$$\tilde{\boldsymbol{w}}_{\mathrm{t}}^{\mathrm{H}}\tilde{\boldsymbol{A}}\tilde{\boldsymbol{w}}_{\mathrm{t}} \tag{27}$$

其中，$\tilde{\boldsymbol{A}}=\mathrm{diag}(\tilde{\boldsymbol{A}}_1,\tilde{\boldsymbol{A}}_2,\cdots,\tilde{\boldsymbol{A}}_N)$，$\tilde{\boldsymbol{A}}$斜对角线上的各矩阵

$$\tilde{\boldsymbol{A}}_n=\begin{pmatrix}\tilde{\boldsymbol{a}}_n(1)\tilde{\boldsymbol{a}}_n^{\mathrm{H}}(1) & 0 & \cdots & 0\\ 0 & \tilde{\boldsymbol{a}}_n(2)\tilde{\boldsymbol{a}}_n^{\mathrm{H}}(2) & \cdots & 0\\ \vdots & \vdots & \ddots & \vdots\\ 0 & 0 & \cdots & \tilde{\boldsymbol{a}}_n(T)\tilde{\boldsymbol{a}}_n^{\mathrm{H}}(T)\end{pmatrix} \tag{28}$$

其中，$\tilde{\boldsymbol{a}}_n(\tau)=\boldsymbol{w}_{\mathrm{or}}^{\mathrm{H}}(\tau)\boldsymbol{b}\left(\theta_{on}\right)\boldsymbol{a}\left(\theta_{no}\right)\Omega_2(\tau)$，$\tilde{\boldsymbol{w}}_{\mathrm{t}}=\left(\tilde{\boldsymbol{w}}_{1\mathrm{t}}^{\mathrm{H}}\ \tilde{\boldsymbol{w}}_{2\mathrm{t}}^{\mathrm{H}}\cdots\tilde{\boldsymbol{w}}_{n\mathrm{t}}^{\mathrm{H}}\ \cdots\ \tilde{\boldsymbol{w}}_{N\mathrm{t}}^{\mathrm{H}}\right)^{\mathrm{H}}$，$\tilde{\boldsymbol{w}}_{n\mathrm{t}}=\left(\boldsymbol{w}_{n\mathrm{t}}^{\mathrm{H}}(1)\ \boldsymbol{w}_{n\mathrm{t}}^{\mathrm{H}}(2)\ \cdots\ \boldsymbol{w}_{n\mathrm{t}}^{\mathrm{H}}(T)\right)^{\mathrm{H}}$。

化简3个约束条件，分别得

$$\tilde{\boldsymbol{w}}_{\mathrm{t}}^{\mathrm{H}}\left(-\tilde{\boldsymbol{B}}_k(\tau)\right)\tilde{\boldsymbol{w}}_{\mathrm{t}}\leq-\tilde{\beta}_k(\tau),\ k=1,2,\cdots,K;\ \tau=1,2,\cdots,T \tag{29}$$

$$\tilde{\boldsymbol{w}}_{\mathrm{t}}^{\mathrm{H}}\left(-\tilde{\boldsymbol{C}}_l(\tau)\right)\tilde{\boldsymbol{w}}_{\mathrm{t}}\leq-\tilde{\beta}_l(\tau),\ l=1,2,\cdots,L;\ \tau=1,2,\cdots,T \tag{30}$$

$$\tilde{\boldsymbol{w}}_{\mathrm{t}}^{\mathrm{H}}\tilde{\boldsymbol{D}}_n\tilde{\boldsymbol{w}}_{\mathrm{t}}\leq\rho_n \tag{31}$$

式(29)和式(30)中，常量 $\tilde{\beta}_k(\tau)=\left|\boldsymbol{w}_{\mathrm{kr}}^{\mathrm{H}}(\tau)\boldsymbol{b}\left(\theta_{ko}(\tau)\right)\boldsymbol{w}_{\mathrm{ot}}^{\mathrm{H}}(\tau)\boldsymbol{a}\left(\theta_{ok}(\tau)\right)\Omega_5(\tau)\right|^2\gamma_k-\sigma_n^2$，$\tilde{\beta}_l(\tau)=\left|\boldsymbol{w}_{\mathrm{lr}}^{\mathrm{H}}(\tau)\cdot\boldsymbol{b}(\theta_{lo}(\tau))\boldsymbol{w}_{\mathrm{lt}}^{\mathrm{H}}(\tau)\boldsymbol{a}(\theta_{lo}(\tau))\Omega_7(\tau)\right|^2\gamma_l-\sigma_n^2$，$NMT$ 阶矩阵

$$\tilde{\boldsymbol{B}}_k(\tau)=\begin{pmatrix}\boldsymbol{I}_\tau^{\mathrm{H}}\tilde{\boldsymbol{b}}_{1k}(\tau)\tilde{\boldsymbol{b}}_{1k}^{\mathrm{H}}(\tau)\boldsymbol{I}_\tau & \boldsymbol{0} & \cdots & \boldsymbol{0}\\ \boldsymbol{0} & \boldsymbol{I}_\tau^{\mathrm{H}}\tilde{\boldsymbol{b}}_{2k}(\tau)\tilde{\boldsymbol{b}}_{2k}^{\mathrm{H}}(\tau)\boldsymbol{I}_\tau & \cdots & \boldsymbol{0}\\ \vdots & \vdots & \ddots & \vdots\\ \boldsymbol{0} & \boldsymbol{0} & \cdots & \boldsymbol{I}_\tau^{\mathrm{H}}\tilde{\boldsymbol{b}}_{Nk}(\tau)\tilde{\boldsymbol{b}}_{Nk}^{\mathrm{H}}(\tau)\boldsymbol{I}_\tau\end{pmatrix} \tag{32}$$

$$\tilde{\boldsymbol{C}}_l(\tau)=\begin{pmatrix}\boldsymbol{I}_\tau^{\mathrm{H}}\tilde{\boldsymbol{c}}_{1l}(\tau)\tilde{\boldsymbol{c}}_{1l}^{\mathrm{H}}(\tau)\boldsymbol{I}_\tau & \boldsymbol{0} & \cdots & \boldsymbol{0}\\ \boldsymbol{0} & \boldsymbol{I}_\tau^{\mathrm{H}}\tilde{\boldsymbol{c}}_{2l}(\tau)\tilde{\boldsymbol{c}}_{2l}^{\mathrm{H}}(\tau)\boldsymbol{I}_\tau & \cdots & \boldsymbol{0}\\ \vdots & \vdots & \ddots & \vdots\\ \boldsymbol{0} & \boldsymbol{0} & \cdots & \boldsymbol{I}_\tau^{\mathrm{H}}\tilde{\boldsymbol{c}}_{Nl}(\tau)\tilde{\boldsymbol{c}}_{Nl}^{\mathrm{H}}(\tau)\boldsymbol{I}_\tau\end{pmatrix} \tag{33}$$

式(32)中 $\tilde{\boldsymbol{b}}_{nk}(\tau)=\boldsymbol{w}_{\mathrm{kr}}^{\mathrm{H}}(\tau)\boldsymbol{b}\left(\theta_{kn}(\tau)\right)\boldsymbol{a}\left(\theta_{nk}(\tau)\right)\Omega_4(\tau)$，式(33)中 $\tilde{\boldsymbol{c}}_{nl}(\tau)=\boldsymbol{w}_{\mathrm{lr}}^{\mathrm{H}}(\tau)\boldsymbol{b}(\theta_{ln}(\tau))\boldsymbol{a}(\theta_{nl}(\tau))\Omega_6(\tau)$。$\boldsymbol{I}_\tau$ 表示 $M\times MT$ 维分块矩阵，其第 τ 个位置是 M 阶单位阵 $\boldsymbol{E}_M$，其余为零矩阵，即

$$\begin{cases}\boldsymbol{I}_1=\begin{pmatrix}\boldsymbol{E}_M & \boldsymbol{0} & \cdots & \boldsymbol{0}\end{pmatrix}\\ \boldsymbol{I}_2=\begin{pmatrix}\boldsymbol{0} & \boldsymbol{E}_M & \cdots & \boldsymbol{0}\end{pmatrix}\\ \quad\vdots\\ \boldsymbol{I}_T=\begin{pmatrix}\boldsymbol{0} & \boldsymbol{0} & \cdots & \boldsymbol{E}_M\end{pmatrix}\end{cases} \tag{34}$$

式(31)中 $\tilde{\boldsymbol{D}}_n$ 表示对角线第 n 个位置为 MT 阶单位阵 $\boldsymbol{E}_{MT}$、其余为 MT 阶零矩阵的 NMT 阶分块矩阵，即：$\tilde{\boldsymbol{D}}_1=\mathrm{diag}(\boldsymbol{E}_{MT},\boldsymbol{0},\cdots,\boldsymbol{0})$，$\tilde{\boldsymbol{D}}_2=\mathrm{diag}(\boldsymbol{0},\boldsymbol{E}_{MT},\boldsymbol{0},\cdots,\boldsymbol{0})$，$\cdots,\tilde{\boldsymbol{D}}_N=\mathrm{diag}(\boldsymbol{0},\cdots,\boldsymbol{0},\boldsymbol{E}_{MT})$。

于是最终优化问题等价为

$$\min_{\tilde{\boldsymbol{w}}_{\mathrm{t}}}\ \tilde{\boldsymbol{w}}_{\mathrm{t}}^{\mathrm{H}}\tilde{\boldsymbol{A}}\tilde{\boldsymbol{w}}_{\mathrm{t}}$$

$$\mathrm{s.t.}\begin{cases}\tilde{\boldsymbol{w}}_{\mathrm{t}}^{\mathrm{H}}\left(-\tilde{\boldsymbol{B}}_k(\tau)\right)\tilde{\boldsymbol{w}}_{\mathrm{t}}\leq-\tilde{\beta}_k(\tau),\ k=1,2,\cdots,K\\ \quad\tau=1,2,\cdots,T\\ \tilde{\boldsymbol{w}}_{\mathrm{t}}^{\mathrm{H}}\left(-\tilde{\boldsymbol{C}}_l(\tau)\right)\tilde{\boldsymbol{w}}_{\mathrm{t}}\leq-\tilde{\beta}_l(\tau),\ l=1,2,\cdots,L\\ \quad\tau=1,2,\cdots,T\\ \tilde{\boldsymbol{w}}_{\mathrm{t}}^{\mathrm{H}}\tilde{\boldsymbol{D}}_n\tilde{\boldsymbol{w}}_{\mathrm{t}}\leq\rho_n,\ n=1,2,\cdots,N\end{cases} \tag{35}$$

式(35)已与式(25)形式相同，可采用算法1求解。

综上，本文所提基于迭代的空时协同波束资源联合优化方法解决了多平台的波束资源空时域分配问题，如算法3所示。其中，凸问题基于原对偶内点法求解，算法整体复杂度为 $O\left((MNT+K+L)^{3.5}\right)$[22,32]。

5　仿真结果与分析

本节通过仿真实验，验证了本文所提基于迭代优化的空时协同波束联合优化方法的有效性。并且，将求解协同干扰波束权矢量的FPP-SCA算法与SDR[33]和SCA算法[34,35]进行比较，验证了FPP-SCA算法的更优效果。

5.1　仿真参数设置

假设我方协同飞行编队有一部探测雷达和 $N=3$ 部干扰机，对方有地面侦察平台 $K=2$ 个、机载探测雷达 $L=1$ 部以及我方雷达探测的一个目标，各平台相对地面的位置及运动路线如图3所示。

假设各平台阵元数 M=16，阵元间距 d 为半波长。机载火控雷达典型工作频段为 X 波段(8～12 Hz)，设本文机载平台信号载频 f_{c}=10 GHz，雷达和侦察

算法 3　基于迭代的空时协同波束资源联合优化方法

Alg. 3　Joint optimization method of space-time cooperative beamforming resources based on iterative optimization

步骤1　初始化：

设置场景数据(如平台运动轨迹、阵元个数、阵元间距等)，给定 $\boldsymbol{w}_{\mathrm{ot}}(\tau)$，$\boldsymbol{w}_{nt}(\tau)$ 初值。

步骤2　执行循环：

(1) 固定当前 $\boldsymbol{w}_{\mathrm{ot}}(\tau)$，$\boldsymbol{w}_{nt}(\tau)$，化简并求解式(2)，得到最优 $\boldsymbol{w}_{\mathrm{or}}^*(\tau)$；

(2) 固定当前 $\boldsymbol{w}_{\mathrm{or}}(\tau)$，$\boldsymbol{w}_{nt}(\tau)$，化简并求解式(2)，得到最优 $\boldsymbol{w}_{\mathrm{ot}}^*(\tau)$；

(3) 固定当前 $\boldsymbol{w}_{\mathrm{or}}(\tau)$，$\boldsymbol{w}_{\mathrm{ot}}(\tau)$，采用FPP-SCA算法求解式(35)，得到最优 $\boldsymbol{w}_{nt}^*(\tau)$；

直到目标函数和优化变量收敛，循环结束；

步骤3　输出结果：

当前波束权矢量 $\boldsymbol{w}_{\mathrm{or}}^*(\tau)$，$\boldsymbol{w}_{\mathrm{ot}}^*(\tau)$ 和 $\boldsymbol{w}_{nt}^*(\tau)$ 的值即为运动平台的波束资源联合优化最优结果。

平台接收端噪声功率σ_{n}^2=0 dB。应对不同雷达，干扰措施有效所需要的干信比不同，一般为几分贝到二十几分贝，故设对方平台被有效干扰的阈值γ=17 dB。设FPP-SCA算法中松弛量$\mu=2$。设波束角度约束为$(-\pi/2,\pi/2)$。为便于后续仿真与分析，以我方雷达为参考系，各平台位置及运动路线如图4所示。

本文方法将未来短时间内的波束资源预先分配，设$T=4$，各时刻的平台坐标如表1所示。

5.2 算法仿真效果

在雷达发射、接收、干扰机发射波束的联合优化过程中，本文问题模型的目标函数变化过程如图5所示。可见，在本文所提迭代优化方法下，每个时刻的目标函数都快速收敛，验证了该方法的可行性。如图5(a)所示，优化后各时刻雷达探测目标的信干噪比约为16.6 dB, 18.1 dB, 17.7 dB和18.0 dB，相比初始化状态(5.2 dB, 16.0 dB, 10.4 dB和10.7 dB)提升效果显著；理论上，跟踪时刻较多时仍可保证优化目标收敛，不妨设$T=8$，目标函数优化过程如图5(b)所示。

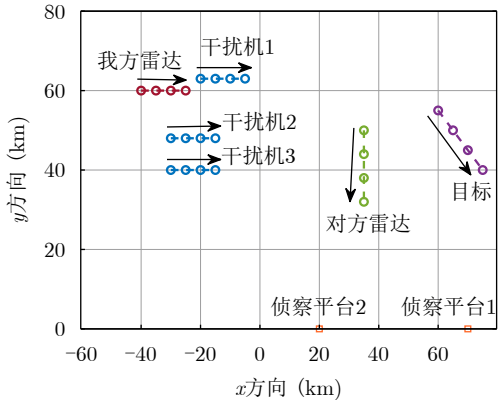

图 3 各平台相对地面的位置及运动路线

Fig. 3 The position and movement route of each platform relative to the ground

为进一步说明波束资源的联合优化分配效果，图6和图7给出了优化后我方平台在每个时刻各方向上的波束功率分配。其中图6是针对雷达平台的，由于目标相对于雷达一直往X轴正方向运动，图中雷达的发射、接收波束主瓣所在角度随时间推移也逐渐变大，准确指向目标方向；图7是针对干扰机平台的，可见，每部干扰机并不是固定干扰某一平台，而是根据场景情况调整为更优方案，且波束功率都分配在了对方雷达或侦察平台所在角度。

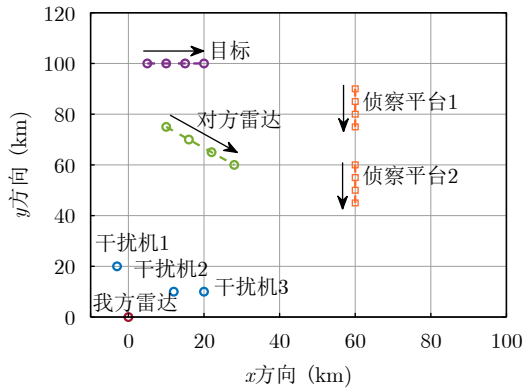

图 4 各平台相对雷达的位置及运动路线

Fig. 4 The position and movement route of each platform relative to the radar

表 1 各时刻的平台坐标(km)

Tab. 1 The coordinates of each platform at each time (km)

平台	$\tau=1$时刻	$\tau=2$时刻	$\tau=3$时刻	$\tau=4$时刻
目标	(5,100)	(10,100)	(15,100)	(20,100)
对方雷达	(10,75)	(16,70)	(22,65)	(28,60)
侦察平台1	(60,90)	(60,85)	(60,80)	(60,75)
侦察平台2	(60,60)	(60,55)	(60,50)	(60,45)
我方雷达	(0,0)			
干扰机1	(–3,20)			
干扰机2	(12,10)			
干扰机3	(20,10)			

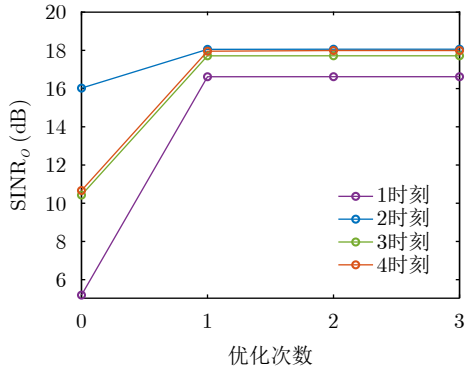

(a) T=4

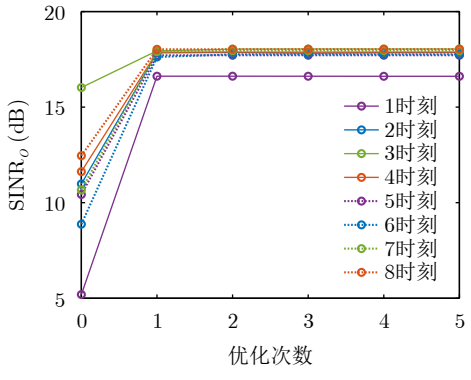

(b) T=8

图 5 各时刻的目标函数优化过程

Fig. 5 The optimization process of the objective function at each moment

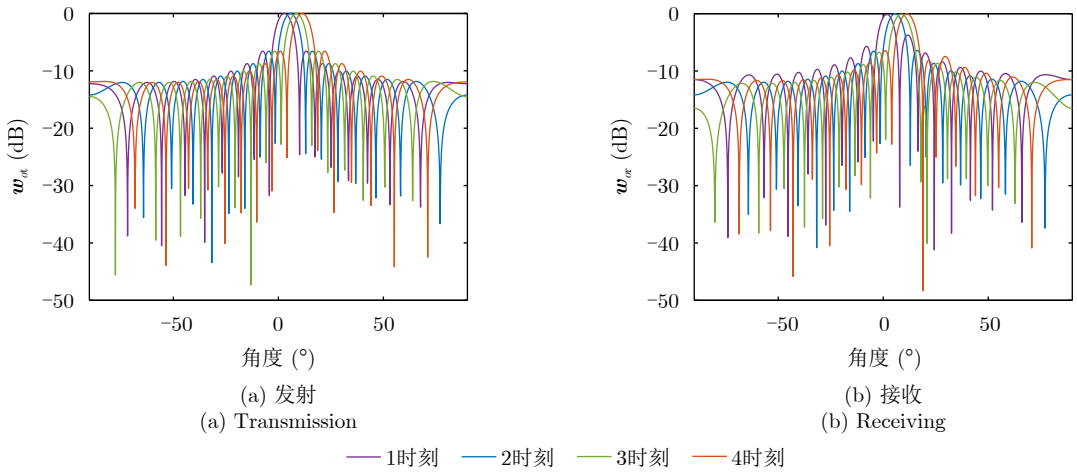

(a) 发射
(a) Transmission

(b) 接收
(b) Receiving

图 6 各时刻的雷达波束权矢量

Fig. 6 The beamforming vectors of radar at each moment

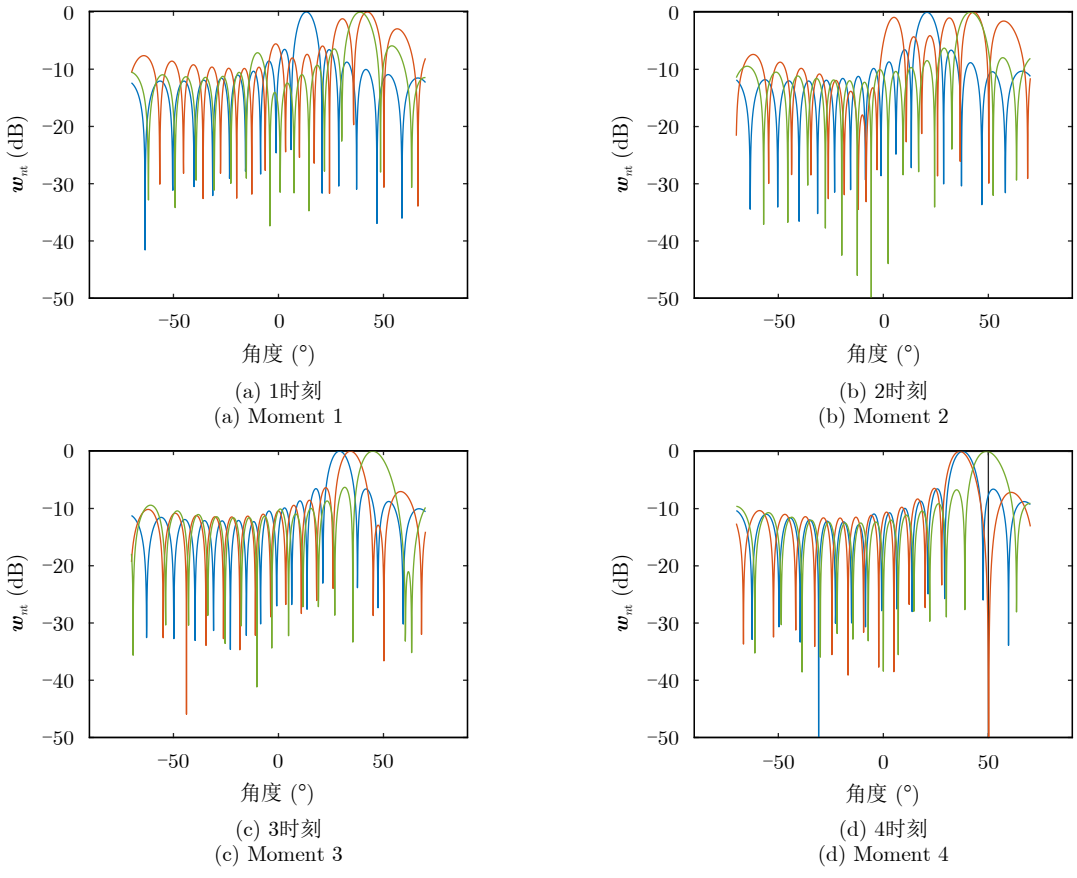

(a) 1时刻
(a) Moment 1

(b) 2时刻
(b) Moment 2

(c) 3时刻
(c) Moment 3

(d) 4时刻
(d) Moment 4

图 7 各时刻干扰机发射波束权矢量(功率归一化)

Fig. 7 Transmit beamforming vectors of jammers at each moment (power normalization)

图6和图7是将每个时刻的干扰机信号功率归一化后在不同角度上的分配情况，主要反映空间域的优化效果。因此，接下来主要说明时间域的波束资源分配。图8、图9是每个时刻对方平台各角度上的接收功率，可见，侦察平台和对方雷达在各时刻都接收来自干扰机方向的较大信号功率，而在其他角度的接收功率相对很小，达到了干信比阈值。

图8、图9表明了每个时刻都能有效干扰对方平台，但接收的干扰信号具体来自哪部干扰机，还不够清晰。图10表示对方平台在干扰机方向的接收功率，由图10(a)，侦察平台1在每个时刻接收的干扰信号都主要来自干扰机2；由图10(b)，侦察平台2在1时刻接收的干扰信号主要来自干扰机2，在2时刻来自干扰机2和干扰机3，后两个时刻主要来自干

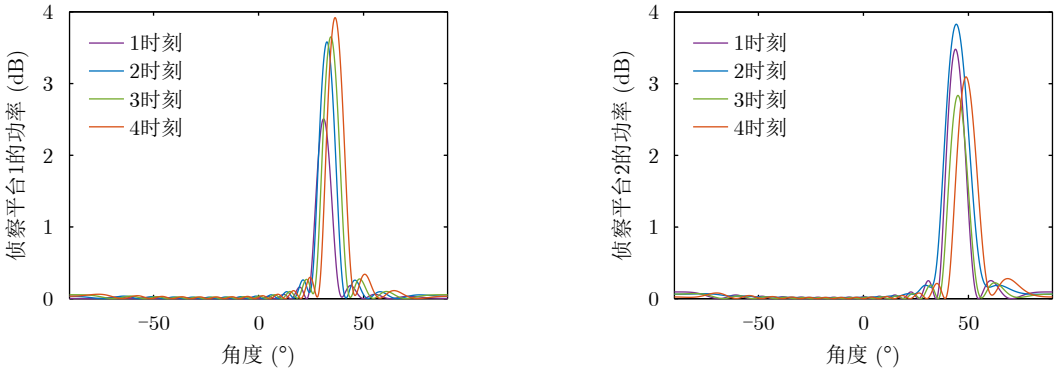

(a) 侦察平台1
(a) The reconnaissance platform 1

(b) 侦察平台2
(b) The reconnaissance platform 2

图 8 侦察平台各角度上的接收功率

Fig. 8 The received power of the reconnaissance platforms at all angles

扰机3；由图10(c)，对方雷达在2时刻接收的干扰信号来自干扰机2，其他时刻主要来自干扰机1。总的来说，侦察平台主要受到干扰机2和干扰机3的干扰，而对方雷达主要受到干扰机1和干扰机2的干扰。这与空间位置分布有关，侦察平台离干扰机2和干扰机3更近，而对方雷达离干扰机1和干扰机2更近，如此分配干扰资源显然效果更优。

综上所述，本文所提方法实现了空间域、时间域的波束资源联合分配，在每个时刻都能有效干扰对方平台，并提高目标探测信干噪比。

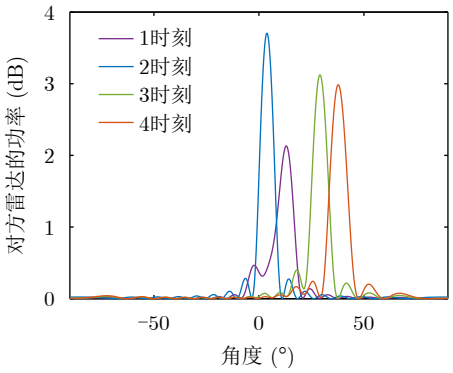

图 9 对方雷达各角度上的接收功率

Fig. 9 The received power of the opposing radars at all angles

由于传统SDR算法在约束多的不定矩阵QCQP问题中很难得到可行解，因此仿真对比取T=1。以图4中初始时刻平台位置分布为例，将本文求解干扰机最优波束权矢量的FPP-SCA算法与SDR和SCA算法进行对比。其中SCA算法以二次曲线近似原问题非凸部分，再逐次迭代直到满足收敛准则，取步长α=1。

图11给出了波束资源联合优化过程中雷达探测目标的信干噪比变化过程。由图中曲线可知，在不同的阵元数下，目标函数均快速收敛，且优化后有明显提升，3种算法都有效。由图11(a)局部放大图可见，相比SDR算法，基于FPP-SCA算法的收敛值更大，这是由于在使用SDR算法的过程中取近似量的误差相对较大。由图11(b)局部放大图可见，相比SCA算法，FPP-SCA算法下优化目标收敛速度更快。

图12是优化后的雷达波束权矢量，其中图12(a)是发射情况，图12(b)是接收情况。可见，3种算法下，优化后雷达发射、接收波束的最大功率都在目标所在角度。

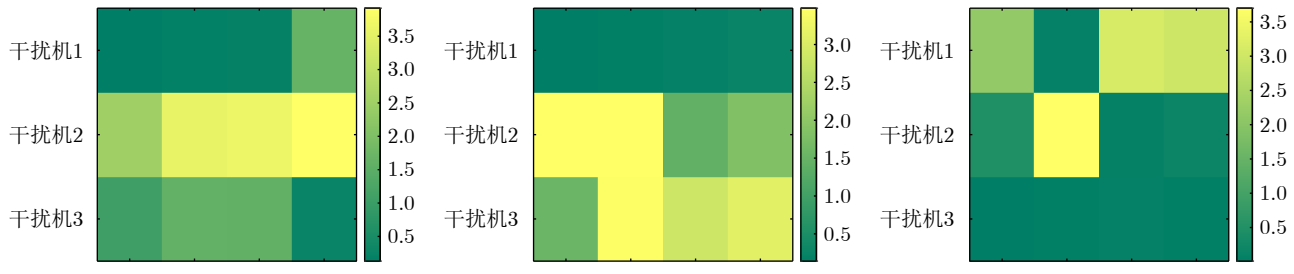

(a) 侦察平台1
(a) The reconnaissance platform 1

(b) 侦察平台2
(b) The reconnaissance platform 2

(c) 对方雷达
(c) The opposing radar

图 10 对方平台在干扰机方向的接收功率

Fig. 10 The received power of the opposing platforms in the direction of the jammers

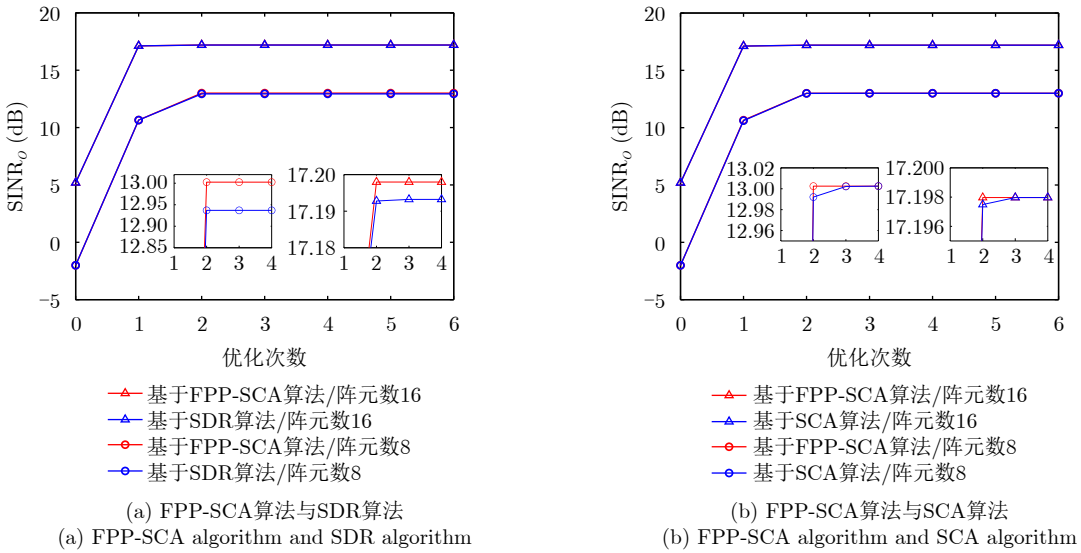

(a) FPP-SCA算法与SDR算法
(a) FPP-SCA algorithm and SDR algorithm

(b) FPP-SCA算法与SCA算法
(b) FPP-SCA algorithm and SCA algorithm

图 11 雷达探测目标的信干噪比

Fig. 11 The signal-to-interference plus noise ratio of the target detected by our radar

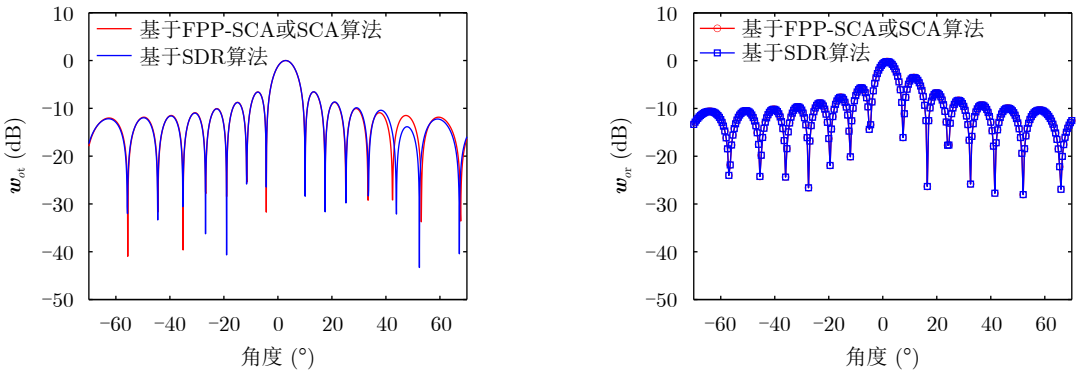

(a) 发射
(a) Transmission

(b) 接收
(b) Receiving

图 12 雷达波束权矢量

Fig. 12 The radar beamforming vectors

图13是优化后对方平台在各角度上的接收功率，其中实线对应FPP-SCA算法，虚线在图13(a)中对应SDR算法，在图13(b)中对应SCA算法。

如图13(a)，两种算法下对方雷达和侦察平台1接收的干扰功率差别不大，但SDR算法下侦察平台2接收的干扰功率远不如FPP-SCA算法，可见FPP-SCA算法的联合分配效果更好。上述差别与算法对干扰机的自动分配有关，以对方雷达为例，由图中横坐标角度可见，FPP-SCA算法下其主要受干扰机1的作用；在SDR算法下，主要受干扰机2和干扰机3的作用。而根据平台位置分布，与干扰机1最近的是对方雷达，将干扰机1的功率主要用于干扰对方雷达，相对具有更优效果。

如图13(b)，两种算法下对方各平台接收的干扰信号来源相同，但FPP-SCA算法下对方每个平台接收的干扰功率都比SCA算法下的高，这是由于FPP-SCA算法对各干扰机功率的分配更准确，造成的资源浪费更少。

综上所述，FPP-SCA算法下的雷达探测信干噪比相对于SDR算法下的更大、相对于SCA算法下的收敛更快；相比SDR和SCA算法，FPP-SCA算法下的协同干扰效果最优。而且，SDR算法复杂度高于FPP-SCA算法[22]，而使用SCA算法要求初始的可行解。因此，FPP-SCA算法最优。

6　结语

本文针对目标探测和协同干扰多任务动态场景，提出了一种雷达与干扰空时协同波束资源联合优化分配的方法，旨在最优化分配有限的波束资源，使其得到最大化利用，以保证多平台对抗体系

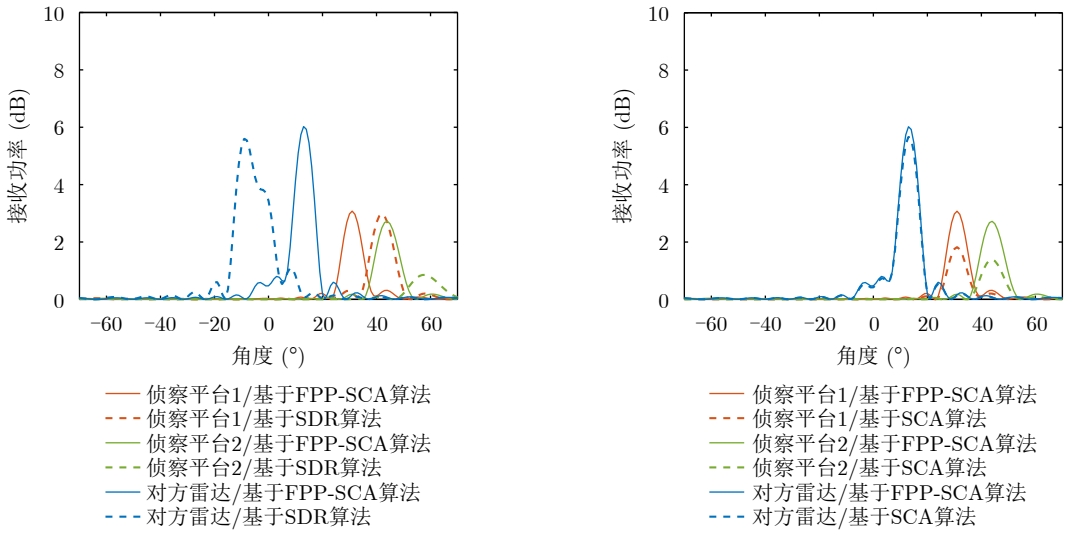

(a) FPP-SCA算法与SDR算法
(a) FPP-SCA algorithm and SDR algorithm

(b) FPP-SCA算法与SCA算法
(b) FPP-SCA algorithm and SCA algorithm

图 13 对方平台在各方向上的接收功率

Fig. 13 The received power of the opposing platforms at all angles

中的低截获探测效果。该方法以雷达探测信干噪比为优化目标，以协同干扰的干信比要求和干扰机能量限制为约束，建立了包含雷达发射、接收、干扰机发射波束权矢量的优化模型。为求解上述模型，本文提出了空时协同波束迭代优化算法，即分别固定两个优化变量，根据场景条件简化问题，求出使目标函数最大化的另一个优化变量，如此迭代直到3个优化变量和目标函数收敛。仿真结果表明，在任意时刻，优化后雷达探测信干噪比均有明显提高，雷达收发波束权矢量主瓣准确指向目标方向、干扰机发射波束权矢量主瓣指向对方各平台方向，且对方所有平台在任意时刻均受到来自干扰机方向的压制干扰。因此，本文所提的雷达与干扰空时协同波束资源联合优化方法有效，且适用于更复杂的对抗场景。

利益冲突 所有作者均声明不存在利益冲突

Conflict of Interests The authors declare that there is no conflict of interests

参 考 文 献

[1] 赵国庆. 雷达对抗原理[M]. 2版. 西安: 西安电子科技大学出版社, 2012: 1–12.
ZHAO Guoqing. Principle of Radar Countermeasure[M]. 2nd ed. Xi'an: Xidian University Press, 2012: 1–12.

[2] 易伟, 袁野, 刘光宏, 等. 多雷达协同探测技术研究进展: 认知跟踪与资源调度算法[J]. 雷达学报, 2023, 12(3): 471–499. doi: 10.12000/JR23036.
YI Wei, YUAN Ye, LIU Guanghong, *et al*. Recent advances in multi-radar collaborative surveillance: Cognitive tracking and resource scheduling algorithms[J]. *Journal of Radars*, 2023, 12(3): 471–499. doi: 10.12000/JR23036.

[3] 王祥丽, 易伟, 孔令讲. 基于多目标跟踪的相控阵雷达波束和驻留时间联合分配方法[J]. 雷达学报, 2017, 6(6): 602–610. doi: 10.12000/JR17045.
WANG Xiangli, YI Wei, and KONG Lingjiang. Joint beam selection and dwell time allocation for multi-target tracking in phased array radar system[J]. *Journal of Radars*, 2017, 6(6): 602–610. doi: 10.12000/JR17045.

[4] HAO Guoqing, FENG Dejun, CHENG Biqin, *et al*. Impact analysis of passive multi-false targets to phased array radar resources[C]. 2023 International Conference on Microwave and Millimeter Wave Technology (ICMMT), Qingdao, China, 2023: 1–3. doi: 10.1109/ICMMT58241.2023.10277047.

[5] TUNCER O and CIRPAN H A. Target priority based optimisation of radar resources for networked air defence systems[J]. *IET Radar, Sonar & Navigation*, 2022, 16(7): 1212–1224. doi: 10.1049/rsn2.12255.

[6] SHI Chenguang, WANG Yijie, SALOUS S, *et al*. Joint transmit resource management and waveform selection strategy for target tracking in distributed phased array radar network[J]. *IEEE Transactions on Aerospace and Electronic Systems*, 2022, 58(4): 2762–2778. doi: 10.1109/TAES.2021.3138869.

[7] 宋晓程, 李陟, 任海伟, 等. 目标动态威胁度驱动的分布式组网相控阵雷达资源优化分配算法[J]. 雷达学报, 2023, 12(3): 629–641. doi: 10.12000/JR22240.
SONG Xiaocheng, LI Zhi, REN Haiwei, *et al*. Threat-driven resource allocation algorithm for distributed netted phased

array radars[J]. *Journal of Radars*, 2023, 12(3): 629–641. doi: 10.12000/JR22240.

[8] 时晨光, 董璟, 周建江. 频谱共存下面向多目标跟踪的组网雷达功率时间联合优化算法[J]. 雷达学报, 2023, 12(3): 590–601. doi: 10.12000/JR22146.
SHI Chenguang, DONG Jing, and ZHOU Jianjiang. Joint transmit power and dwell time allocation for multitarget tracking in radar networks under spectral coexistence[J]. *Journal of Radars*, 2023, 12(3): 590–601. doi: 10.12000/JR22146.

[9] YI Wei, YUAN Ye, HOSEINNEZHAD R, *et al*. Resource scheduling for distributed multi-target tracking in netted colocated MIMO radar systems[J]. *IEEE Transactions on Signal Processing*, 2020, 68: 1602–1617. doi: 10.1109/TSP.2020.2976587.

[10] LI Zhengjie, XIE Junwei, ZHANG Haowei, *et al*. Joint beam selection and power allocation in cognitive collocated MIMO radar for potential guidance application under oppressive jamming[J]. *Digital Signal Processing*, 2022, 127: 103579. doi: 10.1016/j.dsp.2022.103579.

[11] 张大琳, 易伟, 孔令讲. 面向组网雷达干扰任务的多干扰机资源联合优化分配方法[J]. 雷达学报, 2021, 10(4): 595–606. doi: 10.12000/JR21071.
ZHANG Dalin, YI Wei, and KONG Lingjiang. Optimal joint allocation of multijammer resources for jamming netted radar system[J]. *Journal of Radars*, 2021, 10(4): 595–606. doi: 10.12000/JR21071.

[12] YAO Zekun, TANG Chuanbin, WANG Chao, *et al*. Cooperative jamming resource allocation model and algorithm for netted radar[J]. *Electronics Letters*, 2022, 58(22): 834–836. doi: 10.1049/ell2.12611.

[13] WANG Yuedong, LIANG Yan, ZHANG Huixia, *et al*. Domain knowledge-assisted deep reinforcement learning power allocation for MIMO radar detection[J]. *IEEE Sensors Journal*, 2022, 22(23): 23117–23128. doi: 10.1109/JSEN.2022.3211606.

[14] 时晨光, 王奕杰, 代向荣, 等. 面向目标跟踪的机载组网雷达辐射参数与航迹规划联合优化算法[J]. 雷达学报, 2022, 11(5): 778–793. doi: 10.12000/JR22005.
SHI Chenguang, WANG Yijie, DAI Xiangrong, *et al*. Joint transmit resources and trajectory planning for target tracking in airborne radar networks[J]. *Journal of Radars*, 2022, 11(5): 778–793. doi: 10.12000/JR22005.

[15] DURST S, MARQUARDT P, and BRÜGGENWIRTH S. Quality of service based radar resource management for interference mitigation[C]. 2022 IEEE Topical Conference on Wireless Sensors and Sensor Networks (WiSNeT), Las Vegas, USA, 2022: 32–35. doi: 10.1109/WiSNet53095.2022.9721374.

[16] YAN Junkun, JIAO Hao, PU Wenqiang, *et al*. Radar sensor network resource allocation for fused target tracking: A brief review[J]. *Information Fusion*, 2022, 86/87: 104–115. doi: 10.1016/j.inffus.2022.06.009.

[17] GHADIAN M, MOFRAD R F, and ARAND B A. Robust time resource management in cognitive radar using adaptive waveform design[J]. *IETE Journal of Research*, 2023, 69(2): 1070–1080. doi: 10.1080/03772063.2020.1853615.

[18] 王跃东, 顾以静, 梁彦, 等. 伴随压制干扰与组网雷达功率分配的深度博弈研究[J]. 雷达学报, 2023, 12(3): 642–656. doi: 10.12000/JR23023.
WANG Yuedong, GU Yijing, LIANG Yan, *et al*. Deep game of escorting suppressive jamming and networked radar power allocation[J]. *Journal of Radars*, 2023, 12(3): 642–656. doi: 10.12000/JR23023.

[19] DELIGIANNIS A, LAMBOTHARAN S, and CHAMBERS J A. Game theoretic analysis for MIMO radars with multiple targets[J]. *IEEE Transactions on Aerospace and Electronic Systems*, 2016, 52(6): 2760–2774. doi: 10.1109/TAES.2016.150699.

[20] DELIGIANNIS A, PANOUI A, LAMBOTHARAN S, *et al*. Game-theoretic power allocation and the Nash equilibrium analysis for a multistatic MIMO radar network[J]. *IEEE Transactions on Signal Processing*, 2017, 65(24): 6397–6408. doi: 10.1109/TSP.2017.2755591.

[21] 赫彬, 苏洪涛. 认知雷达抗干扰中的博弈论分析综述[J]. 电子与信息学报, 2021, 43(5): 1199–1211. doi: 10.11999/JEIT200843.
HE Bin and SU Hongtao. A review of game theory analysis in cognitive radar anti-jamming[J]. *Journal of Electronics & Information Technology*, 2021, 43(5): 1199–1211. doi: 10.11999/JEIT200843.

[22] MEHANNA O, HUANG Kejun, GOPALAKRISHNAN B, *et al*. Feasible point pursuit and successive approximation of non-convex QCQPs[J]. *IEEE Signal Processing Letters*, 2015, 22(7): 804–808. doi: 10.1109/LSP.2014.2370033.

[23] 任唯祎. 通信侦察信息在组网雷达对抗中的应用[D]. [硕士论文], 电子科技大学, 2021: 1. doi: 10.27005/d.cnki.gdzku.2021.002157.
REN Weiyi. Application of communication reconnaissance information in radar network countermeasures[D]. [Master dissertation], University of Electronic Science and Technology of China, 2021: 1. doi: 10.27005/d.cnki.gdzku.2021.002157.

[24] 宋占福, 赵全习, 范成礼, 等. “信火一体”抗击航空兵编队突防策略分析[J]. 航空兵器, 2022, 29(4): 20–25. doi: 10.12132/ISSN.1673-5048.2021.0196.
SONG Zhanfu, ZHAO Quanxi, FAN Chengli, *et al*. Analysis of information-firepower integration against air force formation penetration[J]. *Aero Weaponry*, 2022, 29(4): 20–25. doi: 10.12132/ISSN.1673-5048.2021.0196.

[25] 戚志刚, 惠新成, 张卫. 天基侦察信息在航母编队信息系统中的应用[J]. 指挥信息系统与技术, 2021, 12(4): 18–22. doi: 10.15908/j.cnki.cist.2021.04.003.
QI Zhigang, HUI Xincheng, and ZHANG Wei. Application of space-based reconnaissance information in aircraft carrier formation information system[J]. *Command Information System and Technology*, 2021, 12(4): 18–22. doi: 10.15908/j.cnki.cist.2021.04.003.

[26] 张鹏程. 基于博弈的空中目标航迹预测及攻防对抗研究[D]. [硕士论文], 浙江大学, 2023: 1–45. doi: 10.27461/d.cnki.gzjdx.2023.000119.
ZHANG Pengcheng. Research on game-based aerial target track prediction and confrontation[D]. [Master dissertation], Zhejiang University, 2023: 1–45. doi: 10.27461/d.cnki.gzjdx.2023.000119.

[27] 王硕, 吴楠, 黄洁, 等. 基于残差修正CNN-BiLSTM的空中目标航迹短期预测算法[J]. 指挥控制与仿真, 2024, 46(1): 55–63. doi: 10.3969/j.issn.1673-3819.2024.01.007.
WANG Shuo, WU Nan, HUANG Jie, *et al*. Short-term prediction algorithm of air target track based on residual correction CNN-BiLSTM[J]. *Command Control & Simulation*, 2024, 46(1): 55–63. doi: 10.3969/j.issn.1673-3819.2024.01.007.

[28] 杨艳洲, 王佳雯, 张玮, 等. 国外天基信息系统装备及技术发展水平研究[J]. 现代信息科技, 2020, 4(6): 53–56, 60. doi: 10.19850/j.cnki.2096-4706.2020.06.019.
YANG Yanzhou, WANG Jiawen, ZHANG Wei, *et al*. Research on the development level of space-based information system equipment and technology abroad[J]. *Modern Information Technology*, 2020, 4(6): 53–56, 60. doi: 10.19850/j.cnki.2096-4706.2020.06.019.

[29] 王帅, 黄富瑜, 李婷, 等. 陆战场红外侦察告警装备作战效能评估[J]. 激光与红外, 2019, 49(3): 341–348. doi: 10.3969/j.issn.1001-5078.2019.03.013.
WANG Shuai, HUANG Fuyu, LI Ting, *et al*. Operational effectiveness evaluation of infrared reconnaissance & warning equipment in warfield[J]. *Laser & Infrared*, 2019, 49(3): 341–348. doi: 10.3969/j.issn.1001-5078.2019.03.013.

[30] 杨艺琼, 吴建新, 梁毅. 机载双基雷达波束域杂波抑制方法[J/OL]. 系统工程与电子技术, 1–11. https://kns.cnki.net/kcms/detail/detail.aspx?dbcode=CAPJ&dbname=CAPJ&filename=XTYD20230905001, 2023.
YANG Yiqiong, WU Jianxin, and LIANG Yi. Airborne bistatic radar beam domain clutter suppression method[J/OL]. *Systems Engineering and Electronics*, 1–11. https://kns.cnki.net/kcms/detail/detail.aspx?dbcode=CAPJ&dbname=CAPJ&filename=XTYD20230905001, 2023.

[31] 董超. 多视角广义特征值最接近支持向量机[D]. [硕士论文], 华东师范大学, 2016: 6.
DONG Chao. Multi-view generalized eigenvalue proximal support vector machines[D]. [Master dissertation], East China Normal University, 2016: 6.

[32] 王奇超, 文再文, 蓝光辉, 等. 优化算法的复杂度分析[J]. 中国科学: 数学, 2020, 50(9): 1271–1336. doi: 10.1360/N012018-00251.
WANG Qichao, WEN Zaiwen, LAN Guanghui, *et al*. Complexity analysis for optimization methods[J]. *Scientia Sinica Mathematica*, 2020, 50(9): 1271–1336. doi: 10.1360/N012018-00251.

[33] LUO Zhiquan, MA W K, SO A M C, *et al*. Semidefinite relaxation of quadratic optimization problems[J]. *IEEE Signal Processing Magazine*, 2010, 27(3): 20–34. doi: 10.1109/MSP.2010.936019.

[34] RAZAVIYAYN M. Successive convex approximation: Analysis and applications[D]. [Ph.D. dissertation], University of Minnesota, 2014: 1–10.

[35] FAN Tao, CUI Guolong, YU Xianxiang, *et al*. Joint design of intra-inter agile pulses and Doppler filter banks for Doppler ambiguous target[J]. *IEEE Transactions on Signal Processing*, 2024, 72: 867–882. doi: 10.1109/TSP.2024.3355768.

作 者 简 介

廖晓容，硕士生，主要研究方向为组网雷达信号处理、资源分配。

孙国皓，博士，副研究员，主要研究方向为认知雷达信号处理、分布式雷达信号处理、机载/星载雷达信号处理、天域态势感知。

钟苏川，博士，副教授，主要研究方向为随机动力系统、随机信号处理等。

余显祥，博士，副教授，主要研究方向为雷达波形设计与处理、最优化理论算法以及阵列信号处理等。

李　明，博士，主要研究方向为机载雷达信号处理、阵列信号处理、干扰抑制技术。

(责任编辑：于青)

Joint Optimization of Radar and Jammer Space-time Cooperative Beamforming for a Multitasking Dynamic Scene

LIAO Xiaorong[①] SUN Guohao[*①②] ZHONG Suchuan[①]
YU Xianxiang[③] LI Ming[④]

[①](*School of Aeronautics and Astronautics*, *Sichuan University*, *Chengdu* 610207, *China*)

[②](*Sichuan Provincial Key Laboratory of Robotics Satellites*, *Chengdu* 610207, *China*)

[③](*School of Information and Communication Engineering*, *University of Electronic Science and Technology of China*, *Chengdu* 611731, *China*)

[④](*Yangtze Delta Region Institute* (*Quzhou*), *University of Electronic Science and Technology of China*, *Quzhou* 324003, *China*)

Abstract: The modern radar confrontation situation is complex and changeable, and inter-system combat has become a basic feature. The overall system performance affects the initiative on the battlefield and even the final victory or defeat. By optimizing the beam resources of radar and jammers in a system, the overall performance can be improved, and the effective low-intercept detection effect can be obtained in the spatial and temporal domains. However, joint optimization of cooperative beamforming in the spatial and temporal domains is a nonconvex problem with complex multiparameter coupling. In this paper, an optimization model is established for a multitasking dynamic scene in the spatial and temporal domains. Radar detection performance is the optimization goal, while the interference performance and energy limitation of jammers are the constraints. To solve the model, a joint design method of space-time cooperative beamforming based on iterative optimization was proposed; that is, iterative optimization of radar transmitting, receiving, and multiple jammers transmitting beamforming vectors was alternately optimized. To solve the Quadratically Constrained Quadratic Programs (QCQP) problem with indefinite matrices for multijammer collaborative optimization, this paper is based on the Feasible Point Pursuit Successive Convex Approximation (FPP-SCA) algorithm. In other words, on the basis of the SCA algorithm, algorithm feasibility is ensured through reasonable relaxation by introducing relaxation variables and a penalty term, which solves the difficulty of obtaining a feasible solution when a problem contains indefinite matrices. Simulation results show that under the constraint of certain jammer energy, the proposed method achieves the effect of multiple jammers interfering with each enemy platform in the spatial and temporal domains to cover our radar detection. This effect is achieved while ensuring high-performance radar detection of the target without interference. Compared with traditional algorithms, the collaborative interference based on the FPP-SCA algorithm exhibits a better performance in the dynamic scene.

Key words: Radar and jammer resources; Space-time beamforming joint optimization; Multiparameter coupling nonconvex problem; Iterative optimization; Feasible Point Pursuit Successive Convex Approximation (FPP-SCA)

CLC index: TN974 **Document code**: A **Article number**: 2095-283X(2024)03-0613-19

DOI: 10.12000/JR23243

Reference format: LIAO Xiaorong, SUN Guohao, ZHONG Suchuan, *et al*. Joint optimization of radar and jammer space-time cooperative beamforming for a multitasking dynamic scene[J]. *Journal of Radars*, 2024, 13(3): 613–631. DOI: 10.12000/JR23243.

Manuscript received December 25, 2023; Revised March 22, 2024; Published online April 23, 2024

*Corresponding Author: SUN Guohao, sghsjw2005@126.com

Foundation Items: The National Natural Science Foundation of China (62201371), Sichuan Provincial Natural Science Foundation (2022NSFSC1952), Municipal Government of Quzhou (2022D013)

Corresponding Editor: YI Wei

©The Author(s) 2024. This is an open access article under the CC-BY 4.0 License
(https://creativecommons.org/licenses/by/4.0/)

1 Introduction

Radar is essential equipment in combat systems for acquiring target information. Damage to the radar not only disrupts this information source but also seriously affects the system's overall combat effectiveness. Active jamming can disrupt the normal operation of an opponent's platform through radiation or electromagnetic wave scattering, thereby preventing it from correctly acquiring information about our radar systems[1]. Therefore, the networking and coordination of radar and jammer systems can achieve the dual goals of reducing the probability of radar signal interception while ensuring target detection performance. Optimal detection performance can be achieved for radar systems in the spatial and temporal domains by networking radar with multiple jammer platforms and jointly allocating time, power, beamforming direction, and other resources across platforms. This approach increases the difficulty for the opponent's reconnaissance and detection platforms to discover radar signals. It also overcomes the limitations of traditional detection platforms that operate independently and one-to-one jamming methods, which are constrained in time, space, and power. However, although jamming platforms offer the advantages of agility and low cost, their resources are severely limited. Therefore, how to reasonably allocate beamforming resources to achieve optimal jamming effects is a key issue in resource optimization for dynamic scenes.

Resource allocation problems adhere to either system resource minimization or task performance optimization criteria. This study primarily explores the latter, which aims to maximize performance by fully utilizing available resources[2]. In recent years, resource allocation problems in radar networks have received widespread attention, with numerous notable studies emerging in this field[3–21]. In Ref. [3], a joint optimization algorithm for beamforming allocation and dwell time is proposed to allocate resources. This approach uses a two-step method to minimize the total beamforming dwell time while ensuring tracking accuracy. However, this method is limited to target-tracking tasks involving a single radar and does not consider joint resource allocation across multiple platforms. Building on this foundation, Ref. [7] addresses multitarget tracking scenes in networked radar systems. Accounting for target threat levels and lower bounds on tracking accuracy, it solves the optimization problem of maximizing the relevant utility function using an iterative descent search method. Similarly, Ref. [8] focuses on multitarget tracking resource allocation problems and examines a scene wherein radar systems share the same operating frequency band with communication base stations. It investigates models for joint optimization of power and time allocation in networked radar systems. Regarding joint allocation of radar beamforming and power resources, Ref. [9] presents a global objective function design based on exponential utility functions for optimal tracking performance criteria. In Ref. [10], the authors reformulate this problem as a convex optimization problem by utilizing a local search method based on the Benefit-Cost Ratio (BCR). In the area of cooperative jamming resource allocation, Ref. [11] optimizes the beamforming and transmission power of multiple jammer platforms to reduce the detection probability of networked radar systems against targets, thereby achieving multitarget penetration. Considering beamforming and power allocation problems under limited jamming resources, Ref. [12] establishes a jamming resource allocation model and solves it using an improved genetic algorithm.

However, these methods primarily address single tasks, such as target tracking or cooperative jamming, without considering resource allocation in a multitasking scene. Furthermore, the optimization of beamforming resources is achieved by traversing and assigning binary values (0 or 1) to variables in the beamforming direction matrix. This method does not achieve continuous optimization at the beamforming weight vector level.

In addition to the aforementioned heuristic algorithm-based research, resource allocation methods based on Deep Reinforcement Learning (DRL) and game theory have been applied to net-

worked resource allocation optimization. DRL algorithms learn optimal mapping strategies from states to actions through agent-environment interactions. Addressing radar resource allocation problems in target detection environments, Ref. [13] treats networked radar as an agent and incorporates domain knowledge into traditional DRL algorithms to enhance the reward mechanism, thereby improving policy network convergence performance and speed. For networked radar power allocation under escort jamming, Ref. [18] models jammers and radars as two separate agents. A Proximal Policy Optimization (PPO) policy network generates radar power allocation vectors, while a hybrid policy network generates beamforming selection and power allocation actions for the jamming agent. Alternating training is then conducted to learn the policy network parameters for both agents. However, DRL requires substantial data for training. Sufficient environmental data in a multitasking confrontation scene are impossible to obtain in advance for agent learning. Moreover, policy networks struggle to converge because of scene complexity. Conversely, game theory-based methods involve both parties selecting strategies that maximize their own benefits under certain constraints. For target detection problems in clutter environments, Ref. [19] optimizes beamforming resource allocation for each radar to minimize transmission power while satisfying specific detection criteria for each target. Ref. [20] presents Nash Equilibrium (NE) analysis for power allocation in multibase distributed multiple input multiple output radar networks, establishing an optimization model that minimizes transmission power under Signal-to-Interference-plus-Noise Ratio (SINR) constraints, combining convex optimization and game theory methods for solution. Additionally, Ref. [21] reviews strategies employed by radar systems for target detection and jamming suppression, including power allocation games, target-jamming games, coding method games, waveform design games, and target detection and tracking games.

However, the optimization models under these game theory approaches typically involve only one or two optimization variables with low coupling. In a multitasking scene, as the number of optimization variables increases and the coupling between variables becomes stronger and more difficult to separate, the solution complexity increases substantially.

Therefore, we address the joint optimization of radar and jammer beamforming resource allocation in a space-time multitasking scene, aiming to achieve an excellent low-intercept detection performance. The key challenges are primarily manifested in two aspects. First, under complex constraints, the simultaneous operation of multiple platforms and joint optimization of multiple tasks result in a nonconvex problem with coupled multiple parameters. Second, the allocation of beamforming and energy resources involves coordinated optimization in the spatial and temporal domains, increasing model complexity and making traditional Semi-Definite Relaxation (SDR) algorithms unsuitable[22]. To address these challenges, we present the main contributions and innovations of our work, which include

(1) A joint design method based on iterative optimization is proposed for a dynamic scene involving multiple optimization tasks, such as transmitting and receiving beamforming of the radar and the coordinated optimization of interference beamforming. This method addresses the issue of coupled multiparameter interference effects in the spatial and temporal domains, with constraints on interference energy.

(2) This study precisely targets beamforming weight vectors in the spatial and temporal domains, achieving flexible allocation of radar and jammer beamforming energy across different time instances and directions.

(3) For the nonconvex optimization problem of Quadratically Constrained Quadratic Programs (QCQP) with indefinite matrices in multijammer cooperative optimization, this study employs the Feasible Point Pursuit Successive Convex Approximation (FPP-SCA) algorithm[22]. This approach resolves the challenge faced by traditional algorithms in obtaining feasible solutions when matrices are indefinite. Compared with SDR

and SCA algorithms, cooperative jamming based on the FPP-SCA algorithm demonstrates superior performance.

2 Modeling the Joint Optimization Problem of Radar and Jammer Beamforming Resources for a Multitasking Dynamic Scene

This section first introduces the dynamic confrontation scene involving radar and jammer cooperation. It then builds a problem model for the scene and finally elaborates the objective function and constraints.

2.1 Radar and jammer scene and parameters

Consider a multitasking dynamic scene: our radar performs target detection, while the opposing side uses L detection radars and K reconnaissance platforms to detect and monitor our radar activities. The opponent's detection radar can obtain information, such as the distance, radial velocity, azimuth, and altitude of our radar relative to the electromagnetic wave emission point, by transmitting electromagnetic waves to illuminate our radar and analyzing the received echoes. The reconnaissance platforms are deployed in a planar formation and are characterized by wide bandwidth and a large field of view. Although the opponent's radar can actively detect our radar, the reconnaissance platforms, which possess high concealment and long operational range, are passively receiving. The combination of airborne detection radars and ground-based reconnaissance platforms employed by the opponent to acquire information about our radar poses a serious threat to our operational security. Therefore, our N jammers collaborate to interfere with the opponent's systems to cover our radar operations. The schematic is shown in Fig. 1.

We assume that the parameters of the opponent's platforms (*e.g.*, position, carrier frequency, beamforming weight vector, noise power) are known. Radar parameters can be obtained through the identification and analysis of electronic reconnaissance systems[23–25]. The movement trajectories of targets and the opponent's radar can be predicted in the short term[26,27]. Information about reconnaissance platforms can be acquired using methods such as satellite and infrared reconnaissance. Numerous high-resolution imaging reconnaissance satellites[28] and infrared reconnaissance warning equipment[29] are currently available for land target surveillance. Ground clutter can be mitigated through appropriate clutter suppression methods[30]. To achieve frequency domain protection, our jamming platforms operate in the same frequency band as our radar. According to the mission requirements of the opponent's reconnaissance platforms, they are configured to collect signals within our radar's frequency band and are directed toward our radar's position. Simultaneously, we assume that an overlapping frequency band exists between the opponent's radar and our platforms.

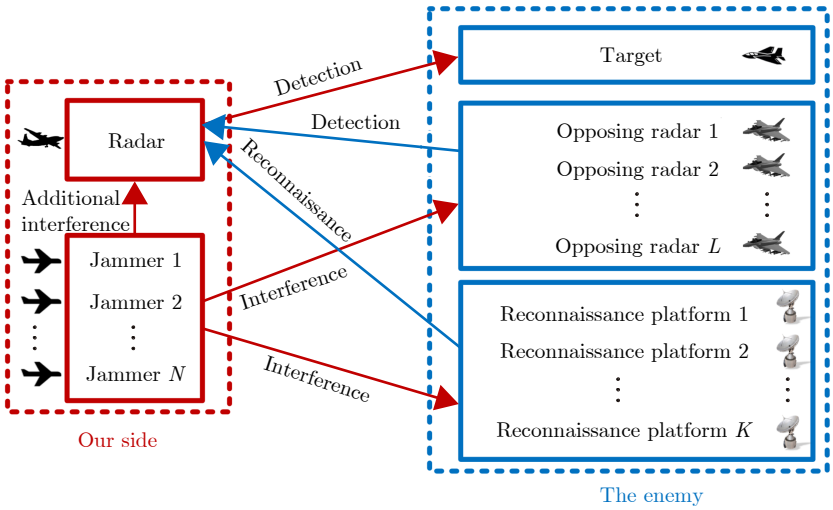

Fig. 1 Schematic of the multitasking scene

To describe the direction of signal transmission and reception, we introduce θ_{12} to represent the angle between the direction of platform 2 and the normal direction of the antenna array of platform 1, where platform 1 serves as the reference point. To characterize the different intensities of transmitting and receiving beamforming across various directions, we introduce the $M \times 1$ transmitting beamforming weight vector $\boldsymbol{w}_{1\mathrm{t}}$ and receiving beamforming weight vector $\boldsymbol{w}_{1\mathrm{r}}$. In this notation, symbols 1 and 2 represent any platform identifiers, where jammers are denoted as $n(n=1,2,\cdots,N)$, radar as o, reconnaissance platforms as $k(k=1,2,\cdots,K)$, opponent's radar as $l(l=1,2,\cdots,L)$, and targets as s. Each platform contains M antennas arranged with equal spacing d, thus allowing the system to transmit or receive up to M beamforming directions simultaneously. Considering the beamforming pointing problem, we introduce $\boldsymbol{a}(\theta_{12})$ and $\boldsymbol{b}(\theta_{12})$ to denote the transmitting and receiving guiding vectors of platform 1 against platform 2, respectively. Additionally, the two general forms of the signal transmission model in this study are defined as $f(1,2,\tau)=\boldsymbol{w}_{1\mathrm{t}}^{\mathrm{H}}(\tau)\boldsymbol{a}\left(\theta_{12}(\tau)\right)$ and $g(1,2,\tau)=\boldsymbol{w}_{1\mathrm{r}}^{\mathrm{H}}(\tau)\cdot\boldsymbol{b}\left(\theta_{12}(\tau)\right)$, representing the transmitted and received signals of platform 1 in the direction of platform 2 at time τ. The notation $[\cdot]^{\mathrm{H}}$ denotes the conjugate transpose operation.

2.2 Joint optimization model for radar and jammer space-time beamforming

To ensure effective target detection and cooperative interference at each time instant, we establish an optimization problem that maximizes the minimum radar detection SINR across all time periods. The optimization is subject to constraints on the jamming-to-signal ratio at reconnaissance platforms and opponent radars, as well as the total energy for each jammer. The model framework is given in Eq. (1).

$$\begin{aligned}&\max\min\ \frac{\text{power of the echo signal detected by the radar}}{\text{power of the interference signal received by the radar + power of noise}}\\&\text{s.t.}\begin{cases}\text{any moment:}\dfrac{\text{power of interference signal received by reconnaissance platform+power of noise}}{\text{power of our radar signal received by reconnaissance platform}}\geq\text{threshold}\\\text{any moment:}\dfrac{\text{power of interference signal received by the opposing radar + power of noise}}{\text{power of our radar signal received by opposing radar}}\geq\text{threshold}\\\text{total power of each jammer}\leq\text{upper limit}\end{cases}\end{aligned}\tag{1}$$

The total time period is discretized into T time instants, with any time instant represented as τ, where $\tau\in[1,T]$. Using P to represent the effective signal power and J to represent the sum of interference and noise power, the problem model corresponding to Eq. (1) is as follows:

$$\begin{aligned}&\max_{\boldsymbol{w}_{or}(\tau),\boldsymbol{w}_{ot}(\tau),\boldsymbol{w}_{nt}(\tau)}\ \min_{\tau\in\{1,2,\cdots,T\}}\frac{P_o(\boldsymbol{w}_{or}(\tau),\boldsymbol{w}_{ot}(\tau))}{J_o(\boldsymbol{w}_{or}(\tau),\boldsymbol{w}_{nt}(\tau))}\\&\text{s.t.}\begin{cases}\dfrac{J_k(\boldsymbol{w}_{nt}(\tau))}{P_k(\boldsymbol{w}_{ot}(\tau))}\geq\gamma_k,\ \ k=1,2,\cdots,K\\\dfrac{J_l(\boldsymbol{w}_{nt}(\tau))}{P_l}\geq\gamma_l,\ \ l=1,2,\cdots,L\\\displaystyle\sum_{\tau=1}^{T}\|\boldsymbol{w}_{nt}(\tau)\|^2\leq\rho_n,\ \ n=1,2,\cdots,N\end{cases}\end{aligned}\tag{2}$$

The optimization variables include the radar transmitting beamforming weight vector $\boldsymbol{w}_{ot}(\tau)$, radar receiving beamforming weight vector $\boldsymbol{w}_{or}(\tau)$, and jammer transmitting beamforming weight vector $\boldsymbol{w}_{nt}(\tau)$. The beamforming weight vectors reflect the energy allocation across antenna array elements. Under fixed system parameters, the effective signal and interference power at each platform are determined by the optimized beamforming weight vectors. Specifically:

(1) The echo signal power $P_o(\boldsymbol{w}_{or}(\tau),\boldsymbol{w}_{ot}(\tau))$ received from the detected target is determined by the radar transmitting and receiving beamforming weight vectors.

(2) The jammers and radar operate in the same frequency band with overlapping spectra, so the radar suffers interference from jammer signals and detection signals from the opponent's radar. Consequently, the total interference and noise power $J_o(\boldsymbol{w}_{or}(\tau),\boldsymbol{w}_{nt}(\tau))$at the radar receiver is determined by the jammer transmitting beamforming weight vector and radar receiving beamforming weight vector.

(3) $J_k(\boldsymbol{w}_{nt}(\tau))$ and $J_l(\boldsymbol{w}_{nt}(\tau))$ represent the interference signal power received by the kth reconnaissance platform and hostile radar l, respectively. These quantities are governed by the jammer beamforming weight vector.

(4) $P_k(\boldsymbol{w}_{ot}(\tau))$ and P_l denote the effective signal power received by the kth reconnaissance platform and opponent's radar l, respectively. For reconnaissance platforms aiming to acquire information from our radar, $P_k(\boldsymbol{w}_{ot}(\tau))$ depends on the radar transmit beamforming weight vector. Conversely, the echo power from the opponent's radar detection of our radar is predominantly influenced by its own parameters.

Additionally, γ_k and γ_l denote the minimum interference-to-signal ratio thresholds required to effectively jam the reconnaissance platform k and opponent's radar l, respectively. ρ_n represents the total energy limit of the nth jammer, and $\|\cdot\|^2$ denotes the vector norm operation.

Therefore, the goal of this space-time cooperative optimization of beam resources is to identify the optimal beam allocation scheme that maximizes target detection performance while satisfying energy constraints and ensuring jamming effectiveness. This optimization process corresponds to solving for the beamforming weight vectors in the proposed model. The following sections provide detailed descriptions of each component in the aforementioned model.

2.2.1 Optimization objective of the problem model

To evaluate the radar target detection performance, this study adopts the SINR as the quantitative metric. Here, SINR is the ratio of the effective signal power received by our radar to the sum of interference power and noise power. The effective signal power corresponds specifically to the echo signal power from the target detected by our radar.

$$P_o(\boldsymbol{w}_{or}(\tau),\boldsymbol{w}_{ot}(\tau))=|g(o,s,\tau)f(o,s,\tau)\Omega_1(\tau)|^2 \quad (3)$$

where $g(o,s,\tau)f(o,s,\tau)\Omega_1(\tau)=\boldsymbol{w}_{or}^{\mathrm{H}}(\tau)\boldsymbol{b}(\theta_{os}(\tau))\,\boldsymbol{w}_{ot}^{\mathrm{H}}(\tau)\cdot\boldsymbol{a}(\theta_{os}(\tau))\,\Omega_1(\tau)$ represents the echo signal from the target detected by our radar. The symbol $\Omega_i(\tau)\,(i=1,2,\cdots,7)$ denotes the amplitude constant of the transmission channel at time τ. Parameter $\Omega_1(\tau)$ primarily depends on the distance between our radar and the target and the target's radar cross section.

In addition, the sum of interference and noise power is expressed as

$$\begin{aligned}&J_o(\boldsymbol{w}_{or}(\tau),\boldsymbol{w}_{nt}(\tau))\\&=\underbrace{\sum_{n=1}^{N}|g(o,n,\tau)f(n,o,\tau)\Omega_2(\tau)|^2}_{\text{(I)}}\\&\quad+\underbrace{\sum_{l=1}^{L}|g(o,l,\tau)f(l,o,\tau)\Omega_3(\tau)|^2}_{\text{(II)}}+\underbrace{\sigma_n^2}_{\text{(III)}}\end{aligned} \quad (4)$$

Eq. (4) can be decomposed into three components:

(I) The aggregate interference power from N jammers to our radar. While collaboratively jamming the opponent's platforms, the signal from the jammer in the direction of our radar is expressed as $g(o,n,\tau)f(n,o,\tau)$, where $\boldsymbol{w}_{or}^{\mathrm{H}}(\tau)\boldsymbol{b}(\theta_{on})\cdot\boldsymbol{w}_{nt}^{\mathrm{H}}(\tau)\boldsymbol{a}(\theta_{no})$. Here, $\Omega_2(\tau)$ denotes the distance between the jammer and our radar.

(II) The total interference power from the opponent's radar L to our radar. The signal from the opponent's radar l in the direction of our radar is given by $g(o,l,\tau)f(l,o,\tau)$, where $\boldsymbol{w}_{or}^{\mathrm{H}}(\tau)\boldsymbol{b}(\theta_{ol}(\tau))\cdot\boldsymbol{w}_{lt}^{\mathrm{H}}(\tau)\boldsymbol{a}(\theta_{lo}(\tau))$. $\Omega_3(\tau)$ represents the distance between the opponent's radar and our radar.

(III) The noise power at the radar receiver.

In summary, the objective function of the proposed model is

$$\begin{aligned}&\mathrm{SINR}_o(\boldsymbol{w}_{or}(\tau),\boldsymbol{w}_{ot}(\tau),\boldsymbol{w}_{nt}(\tau))\\&=\frac{P_o(\boldsymbol{w}_{or}(\tau),\boldsymbol{w}_{ot}(\tau))}{J_o(\boldsymbol{w}_{or}(\tau),\boldsymbol{w}_{nt}(\tau))}\end{aligned} \quad (5)$$

2.2.2 Constraints of the optimization model

The interference received by the opponent's platform includes the coordinated jamming effect of the N jammer and its own noise influence. Therefore, the total interference signal power received by the reconnaissance platform k is

$$J_k(\boldsymbol{w}_{nt}(\tau))=\sum_{n=1}^{N}|g(k,n,\tau)f(n,k,\tau)\Omega_4(\tau)|^2+\sigma_n^2 \quad (6)$$

where $g(k,n,\tau)f(n,k,\tau)$ denotes the interference channel vector from the n jammer to the reconnaissance platform k, equivalently $\boldsymbol{w}_{kr}^{\mathrm{H}}(\tau)$

$\cdot \boldsymbol{b}(\theta_{kn}(\tau))\boldsymbol{w}_{nt}^{\mathrm{H}}(\tau)\boldsymbol{a}(\theta_{nk}(\tau))$. $\Omega_4(\tau)$ is inversely proportional to the squared distance. From the mission requirements of the reconnaissance platform k, the signal from our radar is its effective signal, so the effective signal power received by the reconnaissance platform k is

$$\begin{aligned} P_k(\boldsymbol{w}_{ot}(\tau)) &= \left|g(k,o,\tau)f(o,k,\tau)\Omega_5(\tau)\right|^2 \\ &= \left|\boldsymbol{w}_{kr}^{\mathrm{H}}(\tau)\boldsymbol{b}(\theta_{ko}(\tau))\boldsymbol{w}_{ot}^{\mathrm{H}}(\tau)\right. \\ &\quad \left.\cdot \boldsymbol{a}(\theta_{ok}(\tau))\Omega_5(\tau)\right|^2 \end{aligned} \tag{7}$$

$\Omega_5(\tau)$ is inversely proportional to the square of the distance from our radar to the reconnaissance platform. Any reconnaissance platform needs to satisfy the minimum SINR:

$$\frac{J_k(\boldsymbol{w}_{nt}(\tau))}{P_k(\boldsymbol{w}_{ot}(\tau))} \geq \gamma_k, \quad k = 1, 2, \cdots, K \tag{8}$$

Similarly, the total jamming signal power received by the opponent's radar l is

$$J_l(\boldsymbol{w}_{nt}(\tau)) = \sum_{n=1}^{N} \left|g(l,n,\tau)f(n,l,\tau)\Omega_6(\tau)\right|^2 + \sigma_n^2 \tag{9}$$

where $g(l,n,\tau)f(n,l,\tau)$ represents the jammer n jamming the signal of the opponent's radar l, *i.e.*, $\boldsymbol{w}_{lr}^{\mathrm{H}}(\tau)\boldsymbol{b}(\theta_{ln}(\tau))\boldsymbol{w}_{nt}^{\mathrm{H}}(\tau)\boldsymbol{a}(\theta_{nl}(\tau))$. $\Omega_6(\tau)$ is inversely proportional to the square of the distance between the jammer to the opponent's radar. Similarly, the effective signal power received by the opponent's radar l is

$$\begin{aligned} P_l &= \left|g(l,o,\tau)f(l,o,\tau)\Omega_7(\tau)\right|^2 \\ &= \left|\boldsymbol{w}_{lr}^{\mathrm{H}}(\tau)\boldsymbol{b}(\theta_{lo}(\tau))\boldsymbol{w}_{lt}^{\mathrm{H}}(\tau)\boldsymbol{a}(\theta_{lo}(\tau))\Omega_7(\tau)\right|^2 \end{aligned} \tag{10}$$

Eq. (10) includes the transmit signal $f(l,o,\tau)$, echo signal $g(l,o,\tau)$, and amplitude constant $\Omega_7(\tau)$ of the opponent's radar l in the direction of our radar. Similarly, all radars of the opponent must satisfy the minimum SINR constraints.

$$\frac{J_l(\boldsymbol{w}_{nt}(\tau))}{P_l} \geq \gamma_l, \quad l = 1, 2, \cdots, L \tag{11}$$

In addition, we consider the total energy constraint for each jammer, as shown in Eq. (12).

$$\sum_{\tau=1}^{T} \left\|\boldsymbol{w}_{nt}(\tau)\right\|^2 \leq \rho_n, \quad n = 1, 2, \cdots, N \tag{12}$$

3 Spatial-domain Beamforming Optimization Algorithm Based on Multiparameter Iteration

For illustrative purposes, this section introduces the principles and application of the proposed algorithm in the special case of $T = 1$ and then extends it to the dynamic scene in Section 4.

3.1 Overall framework of spatial-domain beamforming iterative optimization algorithm

This section focuses on the optimization in the spatial domain, with the parameter $T = 1$ in Formula (2). Under this setting, the problem model is obtained, as given in Eq. (13).

$$\begin{aligned} &\max_{\boldsymbol{w}_{ot},\boldsymbol{w}_{or},\boldsymbol{w}_{nt}} \frac{\left|\boldsymbol{w}_{or}^{\mathrm{H}}\boldsymbol{b}(\theta_{os})\boldsymbol{w}_{ot}^{\mathrm{H}}\boldsymbol{a}(\theta_{os})\Omega_1\right|^2}{\sum_{n=1}^{N}\left|\boldsymbol{w}_{or}^{\mathrm{H}}\boldsymbol{b}(\theta_{on})\boldsymbol{w}_{nt}^{\mathrm{H}}\boldsymbol{a}(\theta_{no})\Omega_2\right|^2 + \sum_{l=1}^{L}\left|\boldsymbol{w}_{or}^{\mathrm{H}}\boldsymbol{b}(\theta_{ol})\boldsymbol{w}_{lt}^{\mathrm{H}}\boldsymbol{a}(\theta_{lo})\Omega_3\right|^2 + \sigma_n^2} \\ &\text{s.t.} \begin{cases} \dfrac{\sum_{n=1}^{N}\left|\boldsymbol{w}_{kr}^{\mathrm{H}}\boldsymbol{b}(\theta_{kn})\boldsymbol{w}_{nt}^{\mathrm{H}}\boldsymbol{a}(\theta_{nk})\Omega_4\right|^2 + \sigma_n^2}{\left|\boldsymbol{w}_{kr}^{\mathrm{H}}\boldsymbol{b}(\theta_{ko})\boldsymbol{w}_{ot}^{\mathrm{H}}\boldsymbol{a}(\theta_{ok})\Omega_5\right|^2} \geq \gamma_k, \ k = 1, 2, \cdots, K \\ \dfrac{\sum_{n=1}^{N}\left|\boldsymbol{w}_{lr}^{\mathrm{H}}\boldsymbol{b}(\theta_{ln})\boldsymbol{w}_{nt}^{\mathrm{H}}\boldsymbol{a}(\theta_{nl})\Omega_6\right|^2 + \sigma_n^2}{\left|\boldsymbol{w}_{lr}^{\mathrm{H}}\boldsymbol{b}(\theta_{lo})\boldsymbol{w}_{lt}^{\mathrm{H}}\boldsymbol{a}(\theta_{lo})\Omega_7\right|^2} \geq \gamma_l, \ l = 1, 2, \cdots, L \\ \left\|\boldsymbol{w}_{nt}\right\|^2 \leq \rho_n, \ n = 1, 2, \cdots, N \end{cases} \end{aligned} \tag{13}$$

The model includes three optimization variables and many constraints, making it difficult to solve using traditional methods. Therefore, this study proposes an iterative beamforming joint optimization algorithm, which simplifies the model by treating two of the optimization variables as constants. The model is reduced based on known conditions, and the remaining variable is then optimized to improve the objective function. This iterative process continues until the objective function and optimization variables converge. The overall framework of the algorithm is illustrated in Fig. 2.

3.2 Optimization method of radar receiving beamforming weight vector based on generalized Rayleigh quotient

According to the above algorithm, when the

radar transmitting beamforming weight vector $\boldsymbol{w}_{ot}$ and interference jammer transmitting beamforming weight vector $\boldsymbol{w}_{nt}$ are fixed, the radar receiving beamforming weight vector $\boldsymbol{w}_{or}$ becomes the sole optimization variable. The constraint in Eq. (13) does not involve $\boldsymbol{w}_{or}$, so the model is equivalent to

$$\max_{\boldsymbol{w}_{or}} \frac{\left|\boldsymbol{w}_{or}^{\mathrm{H}}\boldsymbol{b}(\theta_{os})\boldsymbol{w}_{ot}^{\mathrm{H}}\boldsymbol{a}(\theta_{os})\Omega_1\right|^2}{\sum_{n=1}^{N}\left|\boldsymbol{w}_{or}^{\mathrm{H}}\boldsymbol{b}(\theta_{on})\boldsymbol{w}_{nt}^{\mathrm{H}}\boldsymbol{a}(\theta_{no})\Omega_2\right|^2+\sum_{l=1}^{L}\left|\boldsymbol{w}_{or}^{\mathrm{H}}\boldsymbol{b}(\theta_{ol})\boldsymbol{w}_{lt}^{\mathrm{H}}\boldsymbol{a}(\theta_{lo})\Omega_3\right|^2+\sigma_n^2} \tag{14}$$

Let the vectors be defined as $\boldsymbol{a}=\boldsymbol{b}(\theta_{os})\boldsymbol{w}_{ot}^{\mathrm{H}}\cdot\boldsymbol{a}(\theta_{os})\Omega_1$, $\boldsymbol{b}_n=\boldsymbol{b}(\theta_{on})\boldsymbol{w}_{nt}^{\mathrm{H}}\boldsymbol{a}(\theta_{no})\Omega_2$, and $\boldsymbol{c}_l=\boldsymbol{b}(\theta_{ol})\cdot\boldsymbol{w}_{lt}^{\mathrm{H}}\boldsymbol{a}(\theta_{lo})\Omega_3$. Eq. (14) simplifies to

$$\max_{\boldsymbol{w}_{or}} \frac{\boldsymbol{w}_{or}^{\mathrm{H}}\boldsymbol{a}\boldsymbol{a}^{\mathrm{H}}\boldsymbol{w}_{or}}{\sum_{n=1}^{N}\boldsymbol{w}_{or}^{\mathrm{H}}\boldsymbol{b}_n\boldsymbol{b}_n^{\mathrm{H}}\boldsymbol{w}_{or}+\sum_{l=1}^{L}\boldsymbol{w}_{or}^{\mathrm{H}}\boldsymbol{c}_l\boldsymbol{c}_l^{\mathrm{H}}\boldsymbol{w}_{or}+\sigma_n^2} \tag{15}$$

where $\sigma_n^2=\boldsymbol{w}_{or}^{\mathrm{H}}\boldsymbol{I}\sigma_n^2\boldsymbol{w}_{or}/\|\boldsymbol{w}_{or}\|^2$ normalizes the power of the radar receiving beamforming, *i.e.*, $\|\boldsymbol{w}_{or}\|^2=1$, then $\sigma_n^2=\boldsymbol{w}_{or}^{\mathrm{H}}\boldsymbol{I}\sigma_n^2\boldsymbol{w}_{or}$. Let $\boldsymbol{A}=\boldsymbol{a}\boldsymbol{a}^{\mathrm{H}}$ and $\boldsymbol{B}=\sum_{n=1}^{N}\boldsymbol{b}_n\boldsymbol{b}_n^{\mathrm{H}}+\sum_{l=1}^{L}\boldsymbol{c}_l\boldsymbol{c}_l+\boldsymbol{I}\sigma_n^2$. Eq. (15) simplifies to

$$\max_{\boldsymbol{w}_{or}} \frac{\boldsymbol{w}_{or}^{\mathrm{H}}\boldsymbol{A}\boldsymbol{w}_{or}}{\boldsymbol{w}_{or}^{\mathrm{H}}\boldsymbol{B}\boldsymbol{w}_{or}} \tag{16}$$

Where $\boldsymbol{A}$ and $\boldsymbol{B}$ are Hermitian matrices, with $\boldsymbol{B}$ being positive definite. Eq. (16) satisfies the condition of the generalized Rayleigh quotient; thus, the optimal solution of Eq. (16) is[31]

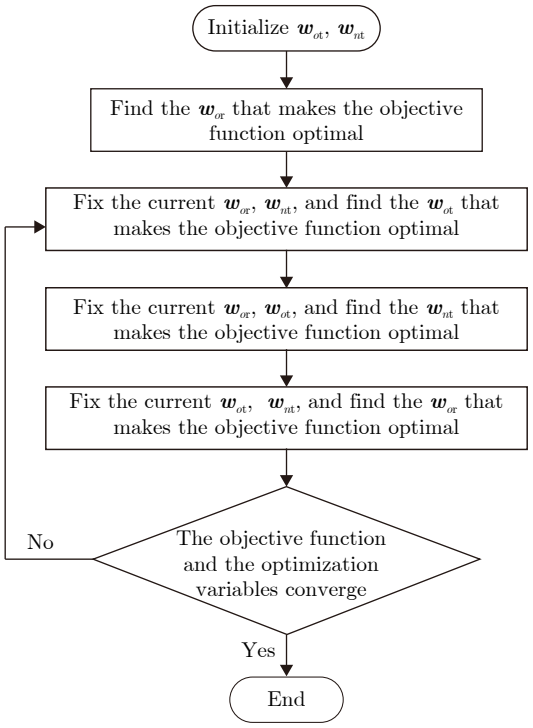

Fig. 2 Overall framework of the joint optimization algorithm of beamforming resources based on iteration

$$\boldsymbol{w}_{or}^{*}=\lambda_{\max}\left(\boldsymbol{B}^{-1}\boldsymbol{A}\right) \tag{17}$$

Where $\lambda_{\max}(\cdot)$ denotes the eigenvector corresponding to the largest eigenvalue of the matrix.

3.3 Optimization of radar transmitting beamforming weight vector based on deflation of semi-negative definite matrix definition

Similarly, when the radar receiving beamforming weight vector $\boldsymbol{w}_{or}$ and jammer transmitting beamforming weight vector $\boldsymbol{w}_{nt}$ are considered constants, Eq. (13) can be simplified as

$$\begin{aligned}&\max_{\boldsymbol{w}_{ot}}\ \left|\boldsymbol{w}_{or}^{\mathrm{H}}\boldsymbol{b}(\theta_{os})\boldsymbol{w}_{ot}^{\mathrm{H}}\boldsymbol{a}(\theta_{os})\Omega_1\right|^2\\&\text{s.t.}\ \frac{\sum_{n=1}^{N}\left|\boldsymbol{w}_{kr}^{\mathrm{H}}\boldsymbol{b}(\theta_{kn})\boldsymbol{w}_{nt}^{\mathrm{H}}\boldsymbol{a}(\theta_{nk})\Omega_4\right|^2+\sigma_n^2}{\left|\boldsymbol{w}_{kr}^{\mathrm{H}}\boldsymbol{b}(\theta_{ko})\boldsymbol{w}_{ot}^{\mathrm{H}}\boldsymbol{a}(\theta_{ok})\Omega_5\right|^2}\geq\gamma_k,\\&\quad k=1,2,\cdots,K\end{aligned} \tag{18}$$

Let the constant $\beta_k=\left(\sum_{n=1}^{N}\left|\boldsymbol{w}_{kr}^{\mathrm{H}}\boldsymbol{b}(\theta_{kn})\boldsymbol{w}_{nt}^{\mathrm{H}}\boldsymbol{a}(\theta_{nk})\Omega_4\right|^2+\sigma_n^2\right)/\gamma_k$, M-dimensional vectors $\boldsymbol{d}=\boldsymbol{w}_{or}^{\mathrm{H}}\boldsymbol{b}(\theta_{os})\boldsymbol{a}(\theta_{os})\Omega_1$, $\boldsymbol{g}_k=\boldsymbol{w}_{kr}^{\mathrm{H}}\boldsymbol{b}(\theta_{ko})\boldsymbol{a}(\theta_{ok})\Omega_5$. It can be obtained as

$$\begin{aligned}&\max_{\boldsymbol{w}_{ot}}\ \left|\boldsymbol{w}_{ot}^{\mathrm{H}}\boldsymbol{d}\right|^2\\&\text{s.t.}\ \left|\boldsymbol{w}_{ot}^{\mathrm{H}}\boldsymbol{g}_k\right|^2\leq\beta_k,\ \forall k\end{aligned} \tag{19}$$

Let the matrix $\boldsymbol{D}=\boldsymbol{d}\boldsymbol{d}^{\mathrm{H}}$, $\boldsymbol{G}_k=\boldsymbol{g}_k\boldsymbol{g}_k^{\mathrm{H}}$, Eq. (19) simplifies to

$$\begin{aligned}&\min_{\boldsymbol{w}_{ot}}\ \boldsymbol{w}_{ot}^{\mathrm{H}}(-\boldsymbol{D})\boldsymbol{w}_{ot}\\&\text{s.t.}\ \boldsymbol{w}_{ot}^{\mathrm{H}}\boldsymbol{G}_k\boldsymbol{w}_{ot}\leq\beta_k,\ \forall k\end{aligned} \tag{20}$$

In Eq. (20), $(-\boldsymbol{D})$ is a semi-negative definite Hermitian matrix, so for any M-dimensional vector $\boldsymbol{z}$, we have[19]

$$\boldsymbol{w}_{ot}^{\mathrm{H}}(-\boldsymbol{D})\boldsymbol{w}_{ot}\leq 2\mathrm{Re}\left\{\boldsymbol{z}^{\mathrm{H}}(-\boldsymbol{D})\boldsymbol{w}_{ot}\right\}-\boldsymbol{z}^{\mathrm{H}}(-\boldsymbol{D})\boldsymbol{z} \tag{21}$$

where $\mathrm{Re}\{\cdot\}$ denotes the real part of the operation. Normalizing the optimization variable $\boldsymbol{w}_{ot}$ power, *i.e.*, $\|\boldsymbol{w}_{ot}\|^2=1$, the optimization problem is finally equivalent to

$$\begin{aligned}&\min_{\boldsymbol{w}_{ot}} \ 2\mathrm{Re}\left\{\boldsymbol{z}^{\mathrm{H}}(-\boldsymbol{D})\boldsymbol{w}_{ot}\right\}-\boldsymbol{z}^{\mathrm{H}}(-\boldsymbol{D})\boldsymbol{z}\\&\text{s.t. } \boldsymbol{w}_{ot}^{\mathrm{H}}\boldsymbol{G}_k\boldsymbol{w}_{ot}\le\beta_k,\ \forall k\\&\quad\boldsymbol{w}_{ot}^{\mathrm{H}}\boldsymbol{w}_{ot}=1\end{aligned}\tag{22}$$

Eq. (22) is a convex optimization problem and can be solved directly.

3.4 Jammer transmitting beamforming vector optimization method based on FPP-SCA algorithm

Prior sections have introduced the methods for optimizing the radar receiving beamforming vector $\boldsymbol{w}_{or}$ and transmitting beamforming vector $\boldsymbol{w}_{ot}$. This section elaborates on the third crucial step of the iterative optimization algorithm that is, treating the interference aircraft transmitting beamforming vector $\boldsymbol{w}_{nt}$ as the sole variable. The model shown in Eq. (13) can be equivalently represented as

$$\begin{aligned}&\min_{\boldsymbol{w}_{nt}} \ \sum_{n=1}^{N}\left|\boldsymbol{w}_{\mathrm{or}}^{\mathrm{H}}\boldsymbol{b}(\theta_{on})\boldsymbol{w}_{nt}^{\mathrm{H}}\boldsymbol{a}(\theta_{no})\Omega_2\right|^2\\&\text{s.t.}\begin{cases}\dfrac{\sum_{n=1}^{N}\left|\boldsymbol{w}_{k\mathrm{r}}^{\mathrm{H}}\boldsymbol{b}(\theta_{kn})\boldsymbol{w}_{nt}^{\mathrm{H}}\boldsymbol{a}(\theta_{nk})\Omega_4\right|^2+\sigma_n^2}{\left|\boldsymbol{w}_{k\mathrm{r}}^{\mathrm{H}}\boldsymbol{b}(\theta_{ko})\boldsymbol{w}_{ot}^{\mathrm{H}}\boldsymbol{a}(\theta_{ok})\Omega_5\right|^2}\ge\gamma_k,\ k=1,2,\cdots,K\\\dfrac{\sum_{n=1}^{N}\left|\boldsymbol{w}_{l\mathrm{r}}^{\mathrm{H}}\boldsymbol{b}(\theta_{ln})\boldsymbol{w}_{nt}^{\mathrm{H}}\boldsymbol{a}(\theta_{nl})\Omega_6\right|^2+\sigma_n^2}{\left|\boldsymbol{w}_{l\mathrm{r}}^{\mathrm{H}}\boldsymbol{b}(\theta_{lo})\boldsymbol{w}_{lt}^{\mathrm{H}}\boldsymbol{a}(\theta_{lo})\Omega_7\right|^2}\ge\gamma_l,\ l=1,2,\cdots,L\\\left\|\boldsymbol{w}_{nt}\right\|^2\le\rho_n,\ n=1,2,\cdots,N\end{cases}\end{aligned}\tag{23}$$

Let vectors $\boldsymbol{h}_n=\boldsymbol{w}_{\mathrm{or}}^{\mathrm{H}}\boldsymbol{b}(\theta_{on})\boldsymbol{a}(\theta_{no})\Omega_2$, $\boldsymbol{p}_{nk}=\boldsymbol{w}_{k\mathrm{r}}^{\mathrm{H}}\cdot\boldsymbol{b}(\theta_{kn})\boldsymbol{a}(\theta_{nk})\Omega_4$, $\boldsymbol{q}_{nl}=\boldsymbol{w}_{l\mathrm{r}}^{\mathrm{H}}\boldsymbol{b}(\theta_{ln})\boldsymbol{a}(\theta_{nl})\Omega_6$ and constants $\beta_k=\left|\boldsymbol{w}_{k\mathrm{r}}^{\mathrm{H}}\boldsymbol{b}(\theta_{ko})\boldsymbol{w}_{ot}^{\mathrm{H}}\boldsymbol{a}(\theta_{ok})\Omega_5\right|^2\gamma_k-\sigma_n^2$, $\beta_l=\left|\boldsymbol{w}_{l\mathrm{r}}^{\mathrm{H}}\boldsymbol{b}(\theta_{lo})\boldsymbol{w}_{lt}^{\mathrm{H}}\boldsymbol{a}(\theta_{lo})\Omega_7\right|^2\gamma_l-\sigma_n^2$. We then obtain

$$\begin{aligned}&\min_{\boldsymbol{w}_{nt}} \ \sum_{n=1}^{N}\left|\boldsymbol{w}_{nt}^{\mathrm{H}}\boldsymbol{h}_n\right|^2\\&\text{s.t.}\begin{cases}\sum_{n=1}^{N}\left|\boldsymbol{w}_{nt}^{\mathrm{H}}\boldsymbol{p}_{nk}\right|^2\ge\beta_k,\ k=1,2,\cdots,K\\\sum_{n=1}^{N}\left|\boldsymbol{w}_{nt}^{\mathrm{H}}\boldsymbol{q}_{nl}\right|^2\ge\beta_l,\ l=1,2,\cdots,L\\\left\|\boldsymbol{w}_{nt}\right\|^2\le\rho_n,\ n=1,2,\cdots,N\end{cases}\end{aligned}\tag{24}$$

Let $\boldsymbol{w}_{\mathrm{t}}=\begin{pmatrix}\boldsymbol{w}_{1\mathrm{t}}^{\mathrm{T}} & \boldsymbol{w}_{2\mathrm{t}}^{\mathrm{T}} & \cdots & \boldsymbol{w}_{N\mathrm{t}}^{\mathrm{T}}\end{pmatrix}^{\mathrm{T}}$ be an MN-dimensional vector, $\boldsymbol{H}=\mathrm{diag}(\boldsymbol{h}_1\boldsymbol{h}_1^{\mathrm{H}},\boldsymbol{h}_2\boldsymbol{h}_2^{\mathrm{H}},\cdots,\boldsymbol{h}_N\boldsymbol{h}_N^{\mathrm{H}})$, $\boldsymbol{P}_k=\mathrm{diag}(\boldsymbol{P}_{1k}\boldsymbol{P}_{1k}^{\mathrm{H}},\boldsymbol{P}_{2k}\boldsymbol{P}_{2k}^{\mathrm{H}},\cdots,\boldsymbol{P}_{\mathrm{N}k}\boldsymbol{P}_{\mathrm{N}k}^{\mathrm{H}})$, and $\boldsymbol{Q}_l=\mathrm{diag}(\boldsymbol{q}_{1l}\boldsymbol{q}_{1l}^{\mathrm{H}},\boldsymbol{q}_{2l}\boldsymbol{q}_{2l}^{\mathrm{H}},\cdots,\boldsymbol{q}_{\mathrm{N}l}\boldsymbol{q}_{\mathrm{N}l}^{\mathrm{H}})$ are MN-order matrix. Let $\boldsymbol{R}_n$ be an MN-dimensional block matrix. The Nth position on the diagonal of $\boldsymbol{R}_n$ is the identity matrix $\boldsymbol{I}$, and the rest is zero matrix $\boldsymbol{0}$, *i.e.*, $\boldsymbol{R}_1=\mathrm{diag}(\boldsymbol{I},\boldsymbol{0},\cdots,\boldsymbol{0})$, $\boldsymbol{R}_2=\mathrm{diag}(\boldsymbol{0},\boldsymbol{I},\boldsymbol{0},\cdots,\boldsymbol{0})$, $\cdots$, $\boldsymbol{R}_N=\mathrm{diag}(\boldsymbol{0},\boldsymbol{0},\cdots,\boldsymbol{0},\boldsymbol{I})$. Simplifying, we obtain

$$\begin{aligned}&\min_{\boldsymbol{w}_{\mathrm{t}}} \ \boldsymbol{w}_{\mathrm{t}}^{\mathrm{H}}\boldsymbol{H}\boldsymbol{w}_{\mathrm{t}}\\&\text{s.t.}\begin{cases}\boldsymbol{w}_{\mathrm{t}}^{\mathrm{H}}(-\boldsymbol{P}_k)\boldsymbol{w}_{\mathrm{t}}\le-\beta_k,\ k=1,2,\cdots,K\\\boldsymbol{w}_{\mathrm{t}}^{\mathrm{H}}(-\boldsymbol{Q}_l)\boldsymbol{w}_{\mathrm{t}}\le-\beta_l,\ l=1,2,\cdots,L\\\boldsymbol{w}_{\mathrm{t}}^{\mathrm{H}}\boldsymbol{R}_n\boldsymbol{w}_{\mathrm{t}}\le\rho_n,\ n=1,2,\cdots,N\end{cases}\end{aligned}\tag{25}$$

In Eq. (25), $\boldsymbol{H}$ is a positive semi-definite matrix. However, $(-\boldsymbol{P}_k)$ and $(-\boldsymbol{Q}_l)$ do not satisfy positive definite or positive semi-definite conditions, so the problem is nonconvex. Therefore, the FPP-SCA algorithm is used for solving[22]. First, we introduce relaxation penalty s_m to ensure the feasibility of the problem and incorporate relaxation parameter μ to balance the original objective function and penalty term, as in Eq. (26). We then track and approximate the feasible points. The specific procedure is shown in Alg. 1.

$$\begin{aligned}&\min_{\boldsymbol{w}_{\mathrm{t}},\boldsymbol{s}} \ \boldsymbol{w}_{\mathrm{t}}^{\mathrm{H}}\boldsymbol{H}\boldsymbol{w}_{\mathrm{t}}+\mu\sum_{m=1}^{(K+L+N)}s_m\\&\text{s.t.}\begin{cases}\boldsymbol{w}_{\mathrm{t}}^{\mathrm{H}}(-\boldsymbol{P}_k)\boldsymbol{w}_{\mathrm{t}}\le-\beta_k+s_k,\ k=1,2,\cdots,K\\\boldsymbol{w}_{\mathrm{t}}^{\mathrm{H}}(-\boldsymbol{Q}_l)\boldsymbol{w}_{\mathrm{t}}\le-\beta_l+s_{K+l},\ l=1,2,\cdots,L\\\boldsymbol{w}_{\mathrm{t}}^{\mathrm{H}}\boldsymbol{R}_n\boldsymbol{w}_{\mathrm{t}}\le\rho_n+s_{K+L+n},\ n=1,2,\cdots,N\\s_m\ge0,\ m=1,2,\cdots,K+L+N\end{cases}\end{aligned}\tag{26}$$

In summary, this section has introduced the joint optimization algorithm of beamforming resources based on iteration in the spatial domain, as shown in Alg. 2.

4 Algorithm for Joint Optimization of Space-Time Beamforming in Dynamic Scene

Section 3 has introduced the principle of the

Alg. 1 Optimization process of jammers' transmitting beamforming vectors based on FFP-SCA algorithm

Step 1 Initialization:

Set the iteration count $q=0$, initialize the M-dimensional vector $\boldsymbol{z}_0$;

Step 2 Iterative execution:

(1) Solve the following convex optimization problem:

$$\min_{\boldsymbol{w}_{\mathrm{t}},\boldsymbol{s}} \ \boldsymbol{w}_{\mathrm{t}}^{\mathrm{H}}\boldsymbol{H}\boldsymbol{w}_{\mathrm{t}}+\mu\sum_{m=1}^{K+L+N}s_m$$

$$\text{s.t.}\begin{cases}2\mathrm{Re}\left\{\boldsymbol{z}_q^{\mathrm{H}}(-\boldsymbol{P}_k)\boldsymbol{w}_{\mathrm{t}}\right\}\le-\beta_k+\boldsymbol{z}_q^{\mathrm{H}}(-\boldsymbol{P}_k)\boldsymbol{z}_q+s_k,\ k=1,2,\cdots,K\\ 2\mathrm{Re}\left\{\boldsymbol{z}_q^{\mathrm{H}}(-\boldsymbol{Q}_l)\boldsymbol{w}_{\mathrm{t}}\right\}\le-\beta_l+\boldsymbol{z}_q^{\mathrm{H}}(-\boldsymbol{Q}_l)\boldsymbol{z}_q+s_{K+l},\ l=1,2,\cdots,L\\ \boldsymbol{w}_{\mathrm{t}}^{\mathrm{H}}\boldsymbol{R}_n\boldsymbol{w}_{\mathrm{t}}\le\rho_n+s_{K+L+n},\ n=1,2,\cdots,N\\ s_m\ge0,\ m=1,2,\cdots,K+L+N\end{cases}$$

Obtain the current optimal solution $\boldsymbol{w}_{\mathrm{t}}^{*}$;

(2) Assign the obtained $\boldsymbol{w}_{\mathrm{t}}^{*}$ from the qth iteration to $\boldsymbol{z}_{q+1}$;

(3) Set $q=q+1$;

The loop continues until the objective function converges, then the iteration ends.

Alg. 2 Joint optimization algorithm of beamforming resources based on iterative optimization in the spatial domain

Step 1 Initialization:

Set up the scenario data (such as platform positions, number of array elements, and inter-element spacing) and provide initial values for $\boldsymbol{w}_{ot}$ and $\boldsymbol{w}_{nt}$;

Step 2 Iterative execution:

Solve Eq. (17) to obtain the current optimal solution $\boldsymbol{w}_{\mathrm{or}}^{*}$: Perform an eigenvalue decomposition on the matrix $\boldsymbol{B}^{-1}\boldsymbol{A}$, where the eigenvector corresponding to the largest eigenvalue is the desired solution $\boldsymbol{w}_{\mathrm{or}}^{*}$;

(2) Solve the convex optimization problem as shown in Eq. (22) to obtain the current optimal solution $\boldsymbol{w}_{\mathrm{ot}}^{*}$;

(3) Obtain the current optimal solution $\boldsymbol{w}_{nt}^{*}$ according to Alg. 1.

The loop ends when the objective function and optimization variables converge.

Step 3 Output results:

The final values of beamforming weight vectors $\boldsymbol{w}_{\mathrm{or}}^{*}$, $\boldsymbol{w}_{\mathrm{ot}}^{*}$, and $\boldsymbol{w}_{nt}^{*}$ represent the optimal result of joint beamforming resource optimization.

joint optimization algorithm of beamforming resources based on iteration in a nondynamic scene with fixed parameters (*e.g.*, $T=1$). In this section, it is generalized to solve the dynamic scene model described in Eq. (2). In this generalized case, the optimization process of radar transmitting and receiving beamforming weight vectors is the same as the previous one. Only the dimension is increased from one to T dimensions. The jammer transmitting beamforming weight vector can also be reduced to the form shown in Eq. (25), which is then solved by the FPP-SCA algorithm. However, owing to the change in the form of the third constraint in the dynamic scene, the simplified process of solving the jammer transmitting beamforming weight vector is no longer consistent. This change is explained below.

Simplifying the objective function gives

$$\tilde{\boldsymbol{w}}_{\mathrm{t}}^{\mathrm{H}}\tilde{\boldsymbol{A}}\tilde{\boldsymbol{w}}_{\mathrm{t}} \tag{27}$$

where $\tilde{\boldsymbol{A}}=\mathrm{diag}(\tilde{\boldsymbol{A}}_1,\tilde{\boldsymbol{A}}_2,\cdots,\tilde{\boldsymbol{A}}_N)$, $\tilde{\boldsymbol{A}}$ and other terms are arranged diagonally across the matrices.

$$\tilde{\boldsymbol{A}}_n=\begin{pmatrix}\tilde{\boldsymbol{a}}_n(1)\tilde{\boldsymbol{a}}_n^{\mathrm{H}}(1) & 0 & \cdots & 0\\ 0 & \tilde{\boldsymbol{a}}_n(2)\tilde{\boldsymbol{a}}_n^{\mathrm{H}}(2) & \cdots & 0\\ \vdots & \vdots & \ddots & \vdots\\ 0 & 0 & \cdots & \tilde{\boldsymbol{a}}_n(T)\tilde{\boldsymbol{a}}_n^{\mathrm{H}}(T)\end{pmatrix} \tag{28}$$

In Eq. (28), $\tilde{\boldsymbol{a}}_n(\tau)=\boldsymbol{w}_{\mathrm{or}}^{\mathrm{H}}(\tau)\boldsymbol{b}(\theta_{on})\boldsymbol{a}(\theta_{no})\Omega_2(\tau)$ and $\tilde{\boldsymbol{w}}_{\mathrm{t}}=\left(\tilde{\boldsymbol{w}}_{1\mathrm{t}}^{\mathrm{H}}\ \tilde{\boldsymbol{w}}_{2\mathrm{t}}^{\mathrm{H}}\cdots\tilde{\boldsymbol{w}}_{nt}^{\mathrm{H}}\ \cdots\ \tilde{\boldsymbol{w}}_{N\mathrm{t}}^{\mathrm{H}}\right)^{\mathrm{H}}$, where $\tilde{\boldsymbol{w}}_{nt}=\left(\boldsymbol{w}_{nt}^{\mathrm{H}}(1)\ \boldsymbol{w}_{nt}^{\mathrm{H}}(2)\ \cdots\ \boldsymbol{w}_{nt}^{\mathrm{H}}(T)\right)^{\mathrm{H}}$.

Simplifying the three constraints, respectively, gives the following:

$$\tilde{\boldsymbol{w}}_{\mathrm{t}}^{\mathrm{H}}\left(-\tilde{\boldsymbol{B}}_k(\tau)\right)\tilde{\boldsymbol{w}}_{\mathrm{t}}\le-\tilde{\beta}_k(\tau),\ k=1,2,\cdots,K;\ \tau=1,2,\cdots,T \tag{29}$$

$$\tilde{\boldsymbol{w}}_{\mathrm{t}}^{\mathrm{H}}\left(-\tilde{\boldsymbol{C}}_l(\tau)\right)\tilde{\boldsymbol{w}}_{\mathrm{t}}\le-\tilde{\beta}_l(\tau),\ l=1,2,\cdots,L;\ \tau=1,2,\cdots,T \tag{30}$$

$$\tilde{\boldsymbol{w}}_{\mathrm{t}}^{\mathrm{H}}\tilde{\boldsymbol{D}}_n\tilde{\boldsymbol{w}}_{\mathrm{t}}\le\rho_n \tag{31}$$

In Eqs. (29) and (30), constant $\tilde{\beta}_k(\tau)=\left|\boldsymbol{w}_{\mathrm{kr}}^{\mathrm{H}}(\tau)\boldsymbol{b}(\theta_{ko}(\tau))\boldsymbol{w}_{\mathrm{ot}}^{\mathrm{H}}(\tau)\boldsymbol{a}(\theta_{ok}(\tau))\Omega_5(\tau)\right|^2\gamma_k-\sigma_n^2$ and $\tilde{\beta}_l(\tau)=\left|\boldsymbol{w}_{lr}^{\mathrm{H}}(\tau)\boldsymbol{b}(\theta_{lo}(\tau))\boldsymbol{w}_{\mathrm{lt}}^{\mathrm{H}}(\tau)\boldsymbol{a}(\theta_{lo}(\tau))\Omega_7(\tau)\right|^2\cdot\gamma_l-\sigma_n^2$, so the NMT-order matrix is expressed as

$$\tilde{\boldsymbol{B}}_k(\tau)=\begin{pmatrix} \boldsymbol{I}_\tau^{\mathrm{H}}\tilde{\boldsymbol{b}}_{1k}(\tau)\tilde{\boldsymbol{b}}_{1k}^{\mathrm{H}}(\tau)\boldsymbol{I}_\tau & \boldsymbol{0} & \cdots & \boldsymbol{0} \\ \boldsymbol{0} & \boldsymbol{I}_\tau^{\mathrm{H}}\tilde{\boldsymbol{b}}_{2k}(\tau)\tilde{\boldsymbol{b}}_{2k}^{\mathrm{H}}(\tau)\boldsymbol{I}_\tau & \cdots & \boldsymbol{0} \\ \vdots & \vdots & \ddots & \vdots \\ \boldsymbol{0} & \boldsymbol{0} & \cdots & \boldsymbol{I}_\tau^{\mathrm{H}}\tilde{\boldsymbol{b}}_{Nk}(\tau)\tilde{\boldsymbol{b}}_{Nk}^{\mathrm{H}}(\tau)\boldsymbol{I}_\tau \end{pmatrix} \tag{32}$$

$$\tilde{\boldsymbol{C}}_l(\tau)=\begin{pmatrix} \boldsymbol{I}_\tau^{\mathrm{H}}\tilde{\boldsymbol{c}}_{1l}(\tau)\tilde{\boldsymbol{c}}_{1l}^{\mathrm{H}}(\tau)\boldsymbol{I}_\tau & \boldsymbol{0} & \cdots & \boldsymbol{0} \\ \boldsymbol{0} & \boldsymbol{I}_\tau^{\mathrm{H}}\tilde{\boldsymbol{c}}_{2l}(\tau)\tilde{\boldsymbol{c}}_{2l}^{\mathrm{H}}(\tau)\boldsymbol{I}_\tau & \cdots & \boldsymbol{0} \\ \vdots & \vdots & \ddots & \vdots \\ \boldsymbol{0} & \boldsymbol{0} & \cdots & \boldsymbol{I}_\tau^{\mathrm{H}}\tilde{\boldsymbol{c}}_{Nl}(\tau)\tilde{\boldsymbol{c}}_{Nl}^{\mathrm{H}}(\tau)\boldsymbol{I}_\tau \end{pmatrix} \tag{33}$$

$\tilde{\boldsymbol{b}}_{nk}(\tau)=\boldsymbol{w}_{kr}^{\mathrm{H}}(\tau)\boldsymbol{b}\left(\theta_{kn}(\tau)\right)\boldsymbol{a}\left(\theta_{nk}(\tau)\right)\Omega_4(\tau)$ in Eq. (32) and $\tilde{\boldsymbol{c}}_{nl}(\tau)=\boldsymbol{w}_{lr}^{\mathrm{H}}(\tau)\boldsymbol{b}(\theta_{ln}(\tau))\boldsymbol{a}(\theta_{nl}(\tau))\Omega_6(\tau)$ in Eq. (33) can be defined as follows. $\boldsymbol{I}_\tau$ denotes the $M\times MT$-dimensional tiling matrix whose τth position is the M-order unit matrix $\boldsymbol{E}_M$. All other positions contain zero matrices:

$$\begin{cases} \boldsymbol{I}_1=\begin{pmatrix}\boldsymbol{E}_M & \boldsymbol{0} & \cdots & \boldsymbol{0}\end{pmatrix} \\ \boldsymbol{I}_2=\begin{pmatrix}\boldsymbol{0} & \boldsymbol{E}_M & \cdots & \boldsymbol{0}\end{pmatrix} \\ \qquad\vdots \\ \boldsymbol{I}_T=\begin{pmatrix}\boldsymbol{0} & \boldsymbol{0} & \cdots & \boldsymbol{E}_M\end{pmatrix} \end{cases} \tag{34}$$

In Eq. (31), $\tilde{\boldsymbol{D}}_n$ denotes the MT-order block matrix. The nth position on the diagonal is an nth-order unit matrix $\boldsymbol{E}_{MT}$, and the rest is the MT-order partition matrix of the NMT-order zero matrix; that is, $\tilde{\boldsymbol{D}}_1=\mathrm{diag}(\boldsymbol{E}_{MT},\boldsymbol{0},\cdots,\boldsymbol{0})$, $\tilde{\boldsymbol{D}}_2=\mathrm{diag}(\boldsymbol{0},\boldsymbol{E}_{MT},\boldsymbol{0},\cdots,\boldsymbol{0})$, $\cdots$, $\tilde{\boldsymbol{D}}_N=\mathrm{diag}(\boldsymbol{0},\cdots,\boldsymbol{0},\boldsymbol{E}_{MT})$.

Thus, the final optimization problem is equivalent to

$$\min_{\tilde{\boldsymbol{w}}_{\mathrm{t}}}\ \tilde{\boldsymbol{w}}_{\mathrm{t}}^{\mathrm{H}}\tilde{\boldsymbol{A}}\tilde{\boldsymbol{w}}_{\mathrm{t}}$$
$$\text{s.t.}\begin{cases} \tilde{\boldsymbol{w}}_{\mathrm{t}}^{\mathrm{H}}\left(-\tilde{\boldsymbol{B}}_k(\tau)\right)\tilde{\boldsymbol{w}}_{\mathrm{t}}\le-\tilde{\beta}_k(\tau),\ k=1,2,\cdots,K \\ \quad \tau=1,2,\cdots,T \\ \tilde{\boldsymbol{w}}_{\mathrm{t}}^{\mathrm{H}}\left(-\tilde{\boldsymbol{C}}_l(\tau)\right)\tilde{\boldsymbol{w}}_{\mathrm{t}}\le-\tilde{\beta}_l(\tau),\ l=1,2,\cdots,L \\ \quad \tau=1,2,\cdots,T \\ \tilde{\boldsymbol{w}}_{\mathrm{t}}^{\mathrm{H}}\tilde{\boldsymbol{D}}_n\tilde{\boldsymbol{w}}_{\mathrm{t}}\le\rho_n,\ n=1,2,\cdots,N \end{cases} \tag{35}$$

Eq. (35) has taken the same form as Eq. (25) and can be solved using Alg. 1.

In summary, the iterative-based joint optimization method of space-time cooperative beamforming resources proposed in this study solves the beamforming resource allocation problem in the space and time domains for multiple platforms, as shown in Alg. 3. In particular, the convex problem is solved based on the original pairwise interior point method, and the overall complexity of the algorithm is $\mathrm{O}\left((MNT+K+L)^{3.5}\right)$ [22,32].

5 Simulation Results and Analysis

In this section, the effectiveness of the space-time cooperative beamforming joint optimization method based on iteration is verified through simulation experiments. Moreover, the FPP-SCA algorithm used for solving the cooperative interference beamforming weight vector is compared with the SDR[33] and SCA algorithms[34,35]. The comparison verifies the better performance of the FPP-SCA algorithm.

5.1 Simulation parameter setting

Assume that our cooperative flight formation has a detection radar and $N=3$ jammers. The opponent has ground reconnaissance platforms $K=2$, airborne detection radar $L=1$, and a tar-

Alg. 3 Joint optimization method of space-time cooperative beamforming resources based on iterative optimization

Step 1 Initialization:

Set the scene data (*e.g.*, platform motion trajectory, number of array elements, and array spacing) and give the $\boldsymbol{w}_{ot}(\tau)$, $\boldsymbol{w}_{nt}(\tau)$ initial value.

Step 2 Execute the loop:

(1) Fix the current $\boldsymbol{w}_{ot}(\tau)$, $\boldsymbol{w}_{nt}(\tau)$, simplify and solve Eq. (2) to get the optimal $\boldsymbol{w}_{or}(\tau)$;

(2) Fix the current $\boldsymbol{w}_{or}(\tau)$, $\boldsymbol{w}_{nt}(\tau)$, simplify and solve Eq. (2) to obtain the optimal $\boldsymbol{w}_{ot}(\tau)$;

(3) Fix the current $\boldsymbol{w}_{or}(\tau)$, $\boldsymbol{w}_{ot}(\tau)$, and solve Eq. (35) using the FPP-SCA algorithm to obtain the optimal $\boldsymbol{w}_{nt}(\tau)$.

Until the objective function and optimization variables converge, the loop ends;

Step 3 Output the results:

The current values of the beamforming weight vectors $\boldsymbol{w}_{or}^*(\tau)$, $\boldsymbol{w}_{ot}^*(\tau)$ and $\boldsymbol{w}_{nt}^*(\tau)$ are the optimal results of the joint optimization of the beamforming resources for the motion platforms.

get detected by our radar. The position of the platforms in relation to the ground and their movement routes are shown in Fig. 3.

Assume that the number of array elements of each platform $M = 16$, and the spacing of array elements d is half wavelength. The typical working frequency band of airborne fire control radar is X-band (8–12 Hz), so we set the carrier frequency of airborne platform signal $f_c = 10$ GHz in this study. The noise power of radar and reconnaissance platforms at the receiving end $\sigma_n^2 = 0$ dB. To cope with different radars, the dry signal ratio required for the effective interference measures varies, generally from a few dB to more than two dozen dB. Therefore, we set the other side of the platforms to be the threshold for effective interference $\gamma = 17$ dB and set the relaxation quantity $\mu = 2$ in the FPP-SCA algorithm. Let the beamforming angle constraint be $(-\pi/2, \pi/2)$. To facilitate the subsequent simulation and analysis, we take our radar as the reference system, and the positions and movement routes of each platform are shown in Fig. 4.

The proposed method pre-allocates the beamforming resources for a short period in the future, setting $T = 4$, and the platform coordinates at each time instance are listed in Tab. 1.

5.2 Algorithm simulation effect

In the joint optimization of radar transmitting and receiving and jammer transmitting beamforming, the change of the objective function in the problem model is shown in Fig. 5. The objective function at each time instance converges quickly under the proposed iterative optimization method, verifying its feasibility. As shown in Fig. 5(a), the SINR values of the radar-detected targets at each time instance after optimization are approximately 16.6, 18.1, 17.7, and 18.0 dB, which are considerably improved compared with those of the initialization state (5.2, 16.0, 10.4, and 10.7 dB). Theoretically, the convergence of the optimization objective can still be maintained even when tracking a large number of time instances. Establishing the objective function optimization process is thus meaningful. The process is shown in Fig. 5(b).

To further illustrate the effect of the joint optimization of beamforming resource allocation, Figs. 6 and 7 depict the beamforming power allocation of our platform in each direction at each time instance after optimization. Fig. 6 presents the results for the radar platform. The target

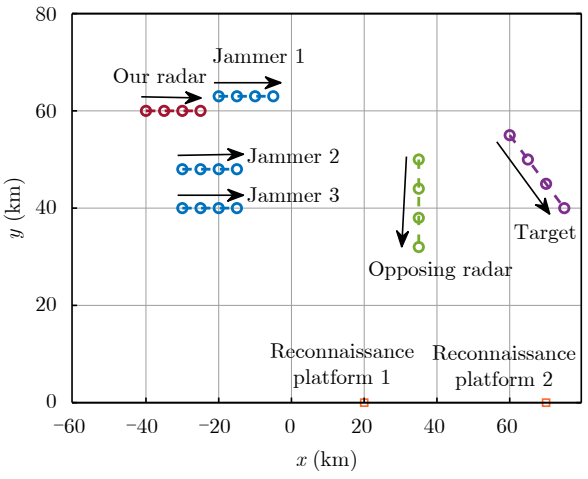

Fig. 3 The position and movement route of each platform relative to the ground

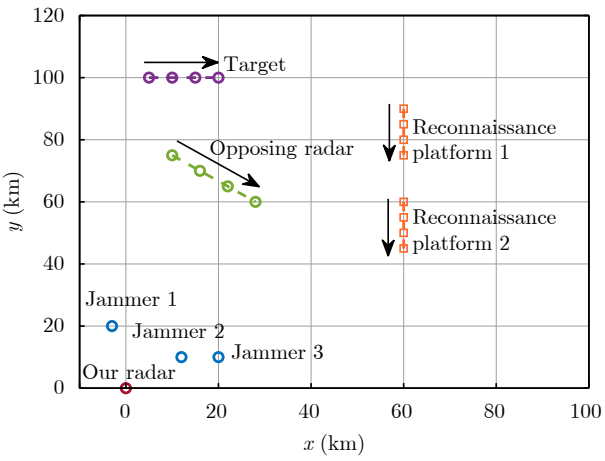

Fig. 4 The position and movement route of each platform relative to the radar

Tab. 1 The coordinates of each platform at each time (km)

Platform	Moment 1	Moment 2	Moment 3	Moment 4
Target	(5, 100)	(10, 100)	(15, 100)	(20, 100)
Opposing radar	(10, 75)	(16, 70)	(22, 65)	(28, 60)
Reconnaissance platform 1	(60, 90)	(60, 85)	(60, 80)	(60, 75)
Reconnaissance platform 2	(60, 60)	(60, 55)	(60, 50)	(60, 45)
Radar	(0, 0)			
Jammer 1	(−3, 20)			
Jammer 2	(12, 10)			
Jammer 3	(20, 10)			

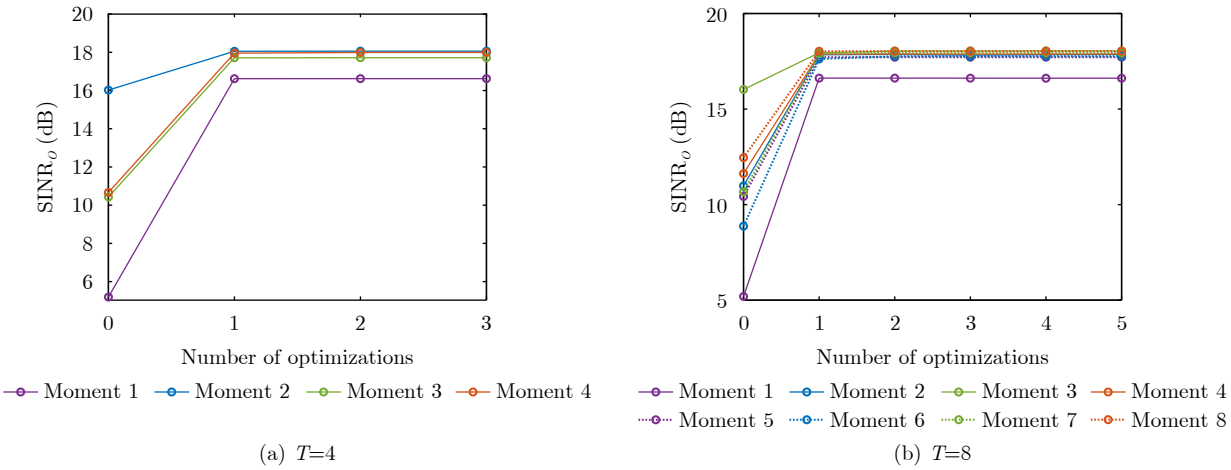

(a) T=4 (b) T=8

Fig. 5 The optimization process of the objective function at each moment

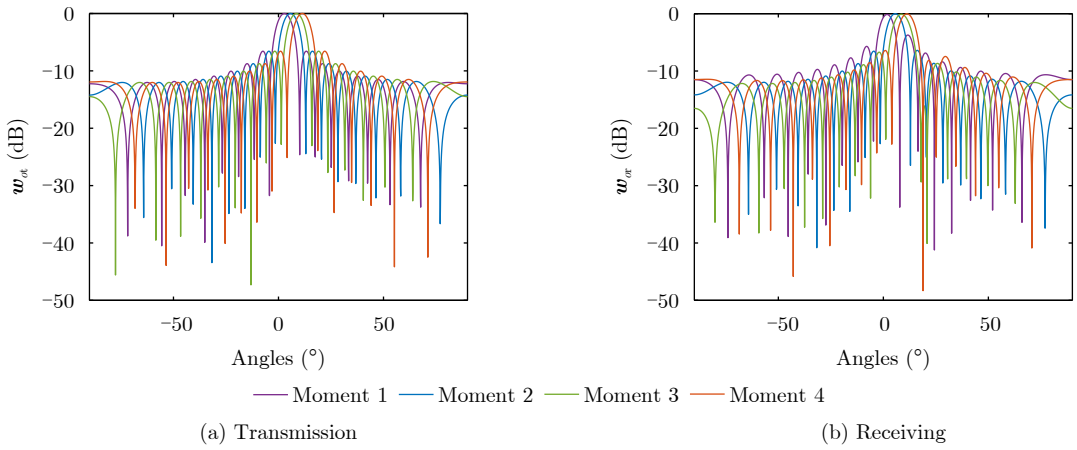

(a) Transmission (b) Receiving

Fig. 6 The beamforming vectors of radar at each moment

moves in the positive direction of the axis relative to the radar, so the angle of the main flap of the radar's transmitting and receiving beamforming in the figure gradually becomes larger over time, which accurately points to the direction of the target. Fig. 7 presents the results for the jammer platform. Each jammer is not fixed to jamming a certain platform. Instead, the system adapts to a more optimal solution according to the scene. The beamforming power is allocated in the angles corresponding to the locations of the opponent's radar or reconnaissance platforms.

Figs. 6 and 7 show the allocation of the jammer signal power at different angles after normalizing it at each time instance. These results mainly reflect the optimization effect in the spatial domain. The next section mainly illustrates the beamforming resource allocation in the time domain. Figs. 8 and 9 show the received power on each angle of the opponent platform at each time instance. The reconnaissance platform and the opponent's radar receive larger signal power from the direction of the jammer at all time instances. By contrast, the received power at the other angles is relatively small and reaches the threshold of the dry signal ratio.

Figs. 8 and 9 show that each time instance can effectively interfere with the other platform, but from which jammer the received jamming signals specifically come remains unclear. Fig. 10 indicates the received power of the other platform in the direction of the jammer. In Fig. 10(a), the jamming signals received by the reconnaissance platform 1 at each time instance mainly come from jammer 2. In Fig. 10(b), the jamming signals received by reconnaissance platform 2 at time instance 1 mainly come from jammer 2. At time instance 2, the signals come from jammer 2 and jammer 3. In the latter two time instances, the jamming signals mainly come from jammer 3.

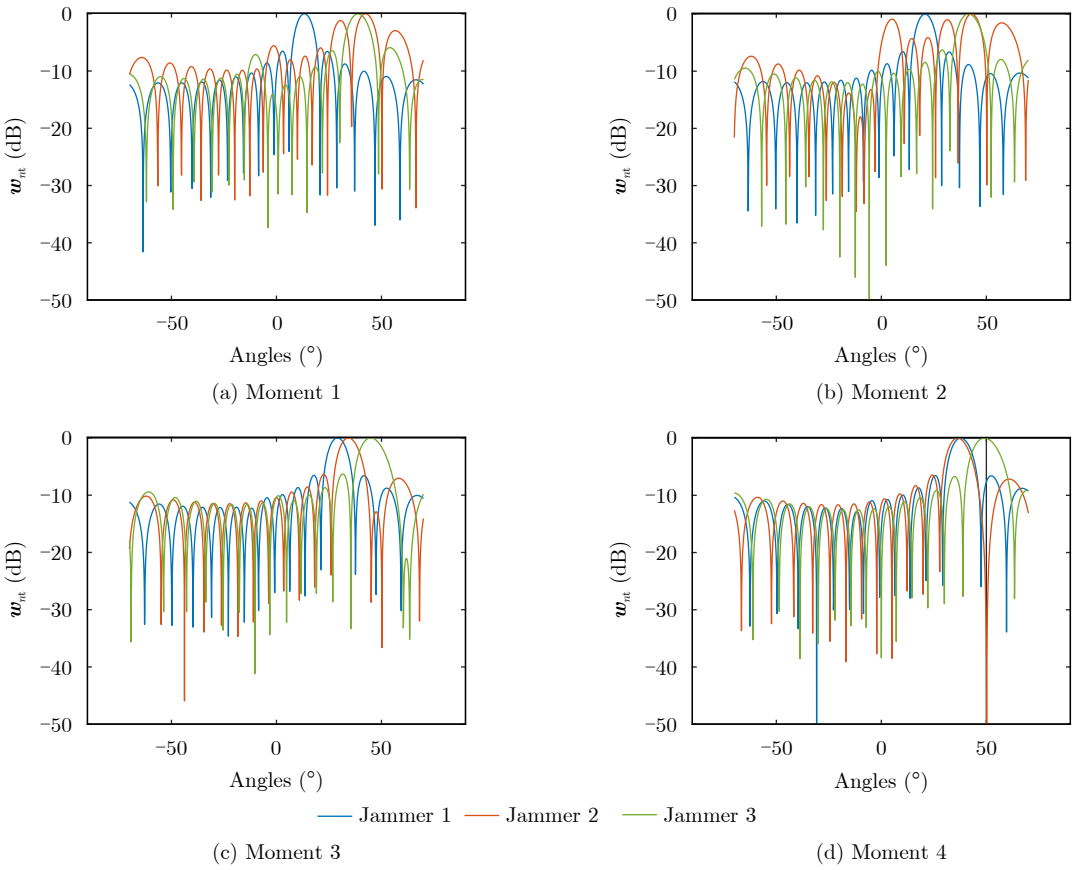

(a) Moment 1 (b) Moment 2

(c) Moment 3 (d) Moment 4

Fig. 7 Transmit beamforming vectors of jammers at each moment (power normalization)

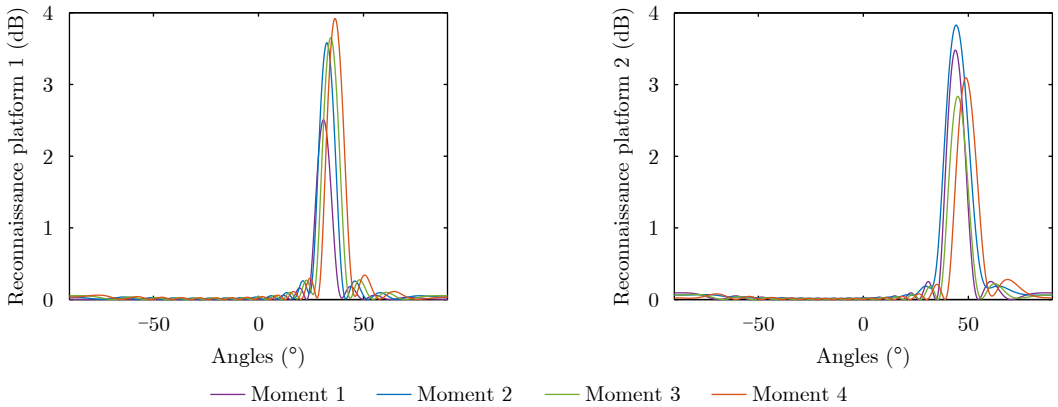

(a) The reconnaissance platform 1 (b) The reconnaissance platform 2

Fig. 8 The received power of the reconnaissance platforms at all angles

In Fig. 10(c), the opponent's radar receives jamming signals from jammer 2 at time instance 2 and from jammer 1 during the other time instances. In general, the reconnaissance platform is mainly jammed by jammer 2 and jammer 3, whereas the opponent's radar is mainly jammed by jammer 1 and jammer 2. This outcome is related to the spatial location distribution. The reconnaissance platform is closer to jammer 2 and jammer 3, whereas the opponent's radar is closer to jammer 1 and jammer 2, so the distribution of jamming resources is more effective.

In summary, the proposed method realizes the joint allocation of beamforming resources in the space and time domains. It effectively interferes with each other's platforms at each time instance and improves the target detection signal-to-noise ratio.

The traditional SDR algorithm struggles to obtain a feasible solution for QCQP problems

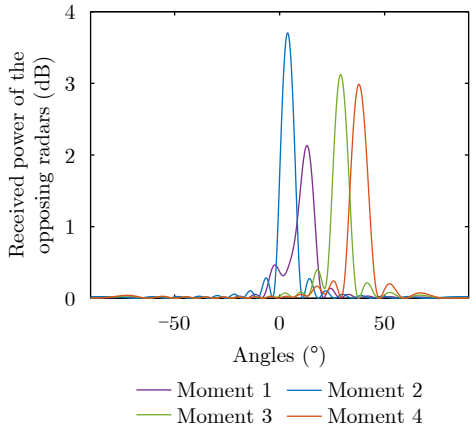

Fig. 9 The received power of the opposing radars at all angles

with indefinite matrices and many constraints, we perform a simulation comparison under the condition $T = 1$. Taking the distribution of the platform position at the initial time instance in Fig. 4 as an example, we compare the FPP-SCA algorithm used for solving the optimal beamforming power vector of the jammer with the SDR and SCA algorithms. The SCA algorithm approximates the nonconvex part of the original problem with a quadratic curve and then iteratively refines the solution until the convergence criterion is satisfied, using the step size $\alpha = 1$.

Fig. 11 illustrates the change in the signal-to-dry noise ratio of the radar-detected target during the joint optimization of beamforming resources. From the curves in the figure, the objective function converges quickly at different numbers of array elements, and improvement after optimization is considerable. All three algorithms are effective. From the local zoom in Fig. 11(a), the convergence value of the FPP-SCA-based algorithm is larger than that of the SDR algorithm due to the relatively large approximation errors inherent in the SDR algorithm. As can be seen from the local zoomed-in graph in Fig. 11(b), the

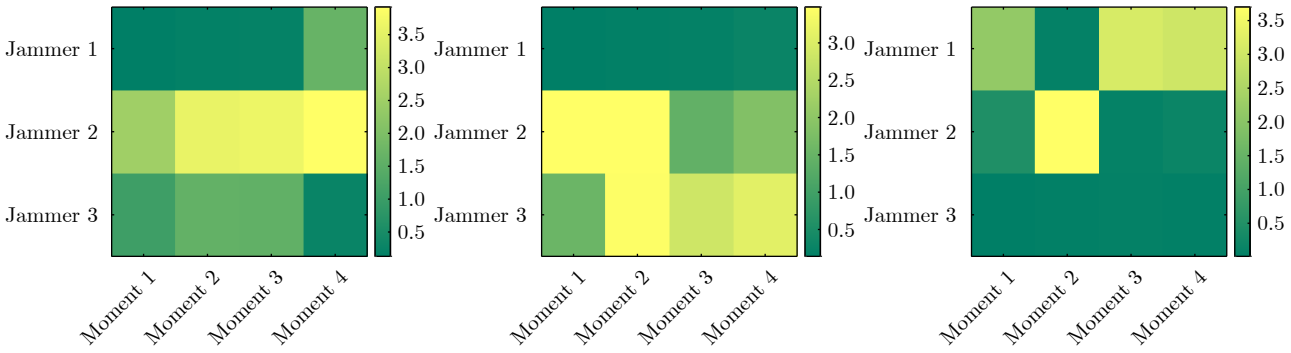

(a) The reconnaissance platform 1 (b) The reconnaissance platform 2 (c) The opposing radar

Fig. 10 The received power of the opposing platforms in the direction of the jammers

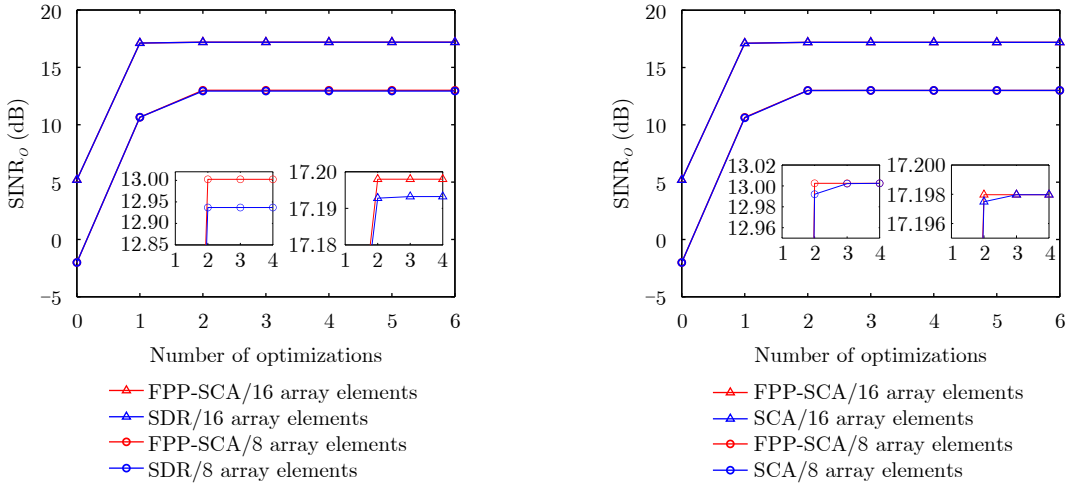

(a) FPP-SCA algorithm and SDR algorithm (b) FPP-SCA algorithm and SCA algorithm

Fig. 11 The signal-to-interference plus noise ratio of the target detected by our radar

optimization objective converges faster under the FPP-SCA algorithm than under the SCA algorithm.

Fig. 12 shows the optimized radar beamforming power vectors, where Fig. 12(a) shows the transmitting case, and Fig. 12(b) shows the receiving case. The maximum power of the optimized radar transmitting and receiving beamforming under the three algorithms is at the angle where the target is located.

Fig. 13 shows the optimized received power of the opponent's platform at various angles. The solid line corresponds to the FPP-SCA algorithm, and the dashed line corresponds to the SDR algorithm in Fig. 13(a) and the SCA algorithm in Fig. 13(b).

As shown in Fig. 13(a), the jamming power received by the opponent's radar and reconnaissance platform 1 is not that different under the two algorithms, but the jamming power received by reconnaissance platform 2 under the SDR algorithm is much less than that of the FPP-SCA algorithm. Hence, the joint allocation of the FPP-SCA algorithm is more effective. The above difference is related to the automatic allocation of the algorithm to the jammer. Taking the opponent's radar as an example, as seen from the horizontal coordinate angle in the figure, it is mainly subject to the role of jammer 1 under the FPP-SCA algorithm. Under the SDR algorithm, it is mainly subject to the role of jammer 2 and jammer 3. Furthermore, according to the platform position distribution, the closest to jammer 1 is the opponent's radar, and the power of jammer 1 is mainly

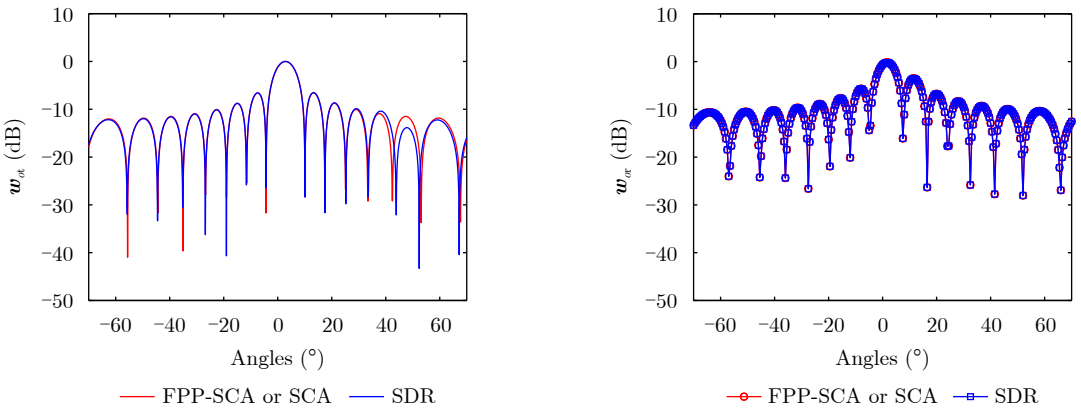

(a) Transmission (b) Receiving

Fig. 12 The radar beamforming vectors

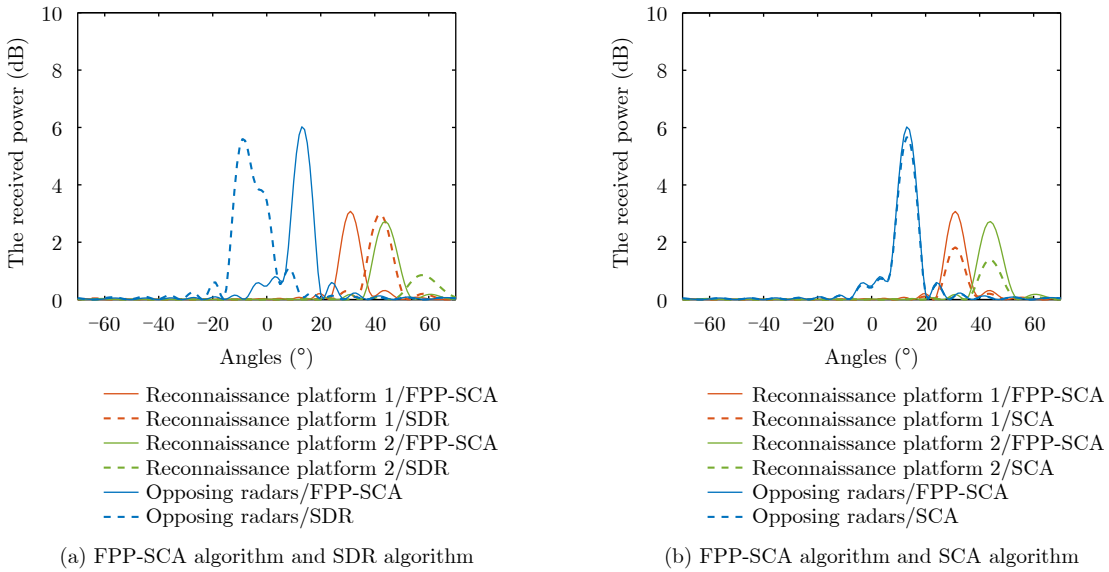

(a) FPP-SCA algorithm and SDR algorithm (b) FPP-SCA algorithm and SCA algorithm

Fig. 13 The received power of the opposing platforms at all angles

used to jam the opponent's radar, which has a relatively more favorable effect.

As shown in Fig. 13(b), the source of the jamming signal received by each platform of the opponent under both algorithms is the same. However, the jamming power received by each platform of the opponent under the FPP-SCA algorithm is higher than that under the SCA algorithm. The reason is the allocation of the power of each jamming machine by the FPP-SCA algorithm is more accurate, reducing resource waste.

In summary, the radar detection SINR under the FPP-SCA algorithm is larger than that under the SDR algorithm, and it converges faster than the SCA algorithm. In addition, the co-interference under the FPP-SCA algorithm is optimal compared with that under the SDR and SCA algorithms. Moreover, the complexity of the SDR algorithm is higher than that of the FPP-SCA algorithm[22], and the use of the SCA algorithm requires an initial feasible solution. Therefore, the FPP-SCA algorithm is optimal.

6 Conclusion

In this study, a method for joint optimal allocation of radar and jammer space-time cooperative beamforming resources is proposed for the multitasking dynamic scene of target detection and cooperative jamming. The method aims to optimally allocate the limited beamforming resources and maximize their utilization to ensure low interception detection in the multi-platform confrontation system. The method takes the radar detection SINR as the optimization objective and takes the dry-to-noise ratio requirement of cooperative jamming and the energy limit of the jammer as the constraints. An optimization model is then established that contains the radar transmitting and receiving and jammer transmitting beamforming power vectors. To solve the above model, an iterative optimization algorithm for space-time cooperative beamforming is proposed. It fixes two optimization variables, simplifies the problem according to the scene conditions, and determines the other optimization variable that maximizes the objective function. It iteratively refines the process until the three optimization variables and the objective function converge. The simulation results show that at any time instance, the optimized radar detection SINR is considerably improved. The main flap of the radar receiving beamforming weight vector accurately points to the target direction, and the main flap of the jammer transmitting beamforming weight vector points to the direction of the other platforms. All the platforms of the opponent are suppressed by the jammer direction at any time instance. Therefore, the joint optimization method of radar and jammer space-time cooperative beamforming resources proposed in this study is effective and applicable to more complex confrontation scenes.

Conflict of Interests The authors declare that there is no conflict of interests

References

[1] ZHAO Guoqing. Principle of Radar Countermeasure[M]. 2nd ed. Xi'an: Xidian University Press, 2012: 1–12.

[2] YI Wei, YUAN Ye, LIU Guanghong, *et al*. Recent advances in multi-radar collaborative surveillance: Cognitive tracking and resource scheduling algorithms[J]. *Journal of Radars*, 2023, 12(3): 471–499. doi: 10.12000/JR23036.

[3] WANG Xiangli, YI Wei, and KONG Lingjiang. Joint beam selection and dwell time allocation for multi-target tracking in phased array radar system[J]. *Journal of Radars*, 2017, 6(6): 602–610. doi: 10.12000/JR17045.

[4] HAO Guoqing, FENG Dejun, CHENG Biqin, *et al*. Impact analysis of passive multi-false targets to phased array radar resources[C]. 2023 International Conference on Microwave and Millimeter Wave Technology (ICMMT), Qingdao, China, 2023: 1–3. doi: 10.1109/ICMMT58241.2023.10277047.

[5] TUNCER O and CIRPAN H A. Target priority based optimisation of radar resources for networked air defence systems[J]. *IET Radar, Sonar & Navigation*, 2022, 16(7): 1212–1224. doi: 10.1049/rsn2.12255.

[6] SHI Chenguang, WANG Yijie, SALOUS S, *et al*. Joint transmit resource management and waveform selection strategy for target tracking in distributed phased array radar network[J]. *IEEE Transactions on Aerospace and Electronic Systems*, 2022, 58(4): 2762–2778. doi: 10.1109/TAES.2021.3138869.

[7] SONG Xiaocheng, LI Zhi, REN Haiwei, *et al*. Threat-driven resource allocation algorithm for distributed netted phased array radars[J]. *Journal of Radars*, 2023, 12(3): 629–641.

doi: 10.12000/JR22240.

[8] SHI Chenguang, DONG Jing, and ZHOU Jianjiang. Joint transmit power and dwell time allocation for multitarget tracking in radar networks under spectral coexistence[J]. *Journal of Radars*, 2023, 12(3): 590–601. doi: 10.12000/JR22146.

[9] YI Wei, YUAN Ye, HOSEINNEZHAD R, *et al*. Resource scheduling for distributed multi-target tracking in netted colocated MIMO radar systems[J]. *IEEE Transactions on Signal Processing*, 2020, 68: 1602–1617. doi: 10.1109/TSP.2020.2976587.

[10] LI Zhengjie, XIE Junwei, ZHANG Haowei, *et al*. Joint beam selection and power allocation in cognitive collocated MIMO radar for potential guidance application under oppressive jamming[J]. *Digital Signal Processing*, 2022, 127: 103579. doi: 10.1016/j.dsp.2022.103579.

[11] ZHANG Dalin, YI Wei, and KONG Lingjiang. Optimal joint allocation of multijammer resources for jamming netted radar system[J]. *Journal of Radars*, 2021, 10(4): 595–606. doi: 10.12000/JR21071.

[12] YAO Zekun, TANG Chuanbin, WANG Chao, *et al*. Cooperative jamming resource allocation model and algorithm for netted radar[J]. *Electronics Letters*, 2022, 58(22): 834–836. doi: 10.1049/ell2.12611.

[13] WANG Yuedong, LIANG Yan, ZHANG Huixia, *et al*. Domain knowledge-assisted deep reinforcement learning power allocation for MIMO radar detection[J]. *IEEE Sensors Journal*, 2022, 22(23): 23117–23128. doi: 10.1109/JSEN.2022.3211606.

[14] SHI Chenguang, WANG Yijie, DAI Xiangrong, *et al*. Joint transmit resources and trajectory planning for target tracking in airborne radar networks[J]. *Journal of Radars*, 2022, 11(5): 778–793. doi: 10.12000/JR22005.

[15] DURST S, MARQUARDT P, and BRÜGGENWIRTH S. Quality of service based radar resource management for interference mitigation[C]. 2022 IEEE Topical Conference on Wireless Sensors and Sensor Networks (WiSNeT), Las Vegas, USA, 2022: 32–35. doi: 10.1109/WiSNet53095.2022.9721374.

[16] YAN Junkun, JIAO Hao, PU Wenqiang, *et al*. Radar sensor network resource allocation for fused target tracking: A brief review[J]. *Information Fusion*, 2022, 86/87: 104–115. doi: 10.1016/j.inffus.2022.06.009.

[17] GHADIAN M, MOFRAD R F, and ARAND B A. Robust time resource management in cognitive radar using adaptive waveform design[J]. *IETE Journal of Research*, 2023, 69(2): 1070–1080. doi: 10.1080/03772063.2020.1853615.

[18] WANG Yuedong, GU Yijing, LIANG Yan, *et al*. Deep game of escorting suppressive jamming and networked radar power allocation[J]. *Journal of Radars*, 2023, 12(3): 642–656. doi: 10.12000/JR23023.

[19] DELIGIANNIS A, LAMBOTHARAN S, and CHAMBERS J A. Game theoretic analysis for MIMO radars with multiple targets[J]. *IEEE Transactions on Aerospace and Electronic Systems*, 2016, 52(6): 2760–2774. doi: 10.1109/TAES.2016.150699.

[20] DELIGIANNIS A, PANOUI A, LAMBOTHARAN S, *et al*. Game-theoretic power allocation and the Nash equilibrium analysis for a multistatic MIMO radar network[J]. *IEEE Transactions on Signal Processing*, 2017, 65(24): 6397–6408. doi: 10.1109/TSP.2017.2755591.

[21] HE Bin and SU Hongtao. A review of game theory analysis in cognitive radar anti-jamming[J]. *Journal of Electronics & Information Technology*, 2021, 43(5): 1199–1211. doi: 10.11999/JEIT200843.

[22] MEHANNA O, HUANG Kejun, GOPALAKRISHNAN B, *et al*. Feasible point pursuit and successive approximation of non-convex QCQPs[J]. *IEEE Signal Processing Letters*, 2015, 22(7): 804–808. doi: 10.1109/LSP.2014.2370033.

[23] REN Weiyi. Application of communication reconnaissance information in radar network countermeasures[D]. [Master dissertation], University of Electronic Science and Technology of China, 2021: 1. doi: 10.27005/d.cnki.gdzku.2021.002157.

[24] SONG Zhanfu, ZHAO Quanxi, FAN Chengli, *et al*. Analysis of information-firepower integration against air force formation penetration[J]. *Aero Weaponry*, 2022, 29(4): 20–25. doi: 10.12132/ISSN.1673-5048.2021.0196.

[25] QI Zhigang, HUI Xincheng, and ZHANG Wei. Application of space-based reconnaissance information in aircraft carrier formation information system[J]. *Command Information System and Technology*, 2021, 12(4): 18–22. doi: 10.15908/j.cnki.cist.2021.04.003.

[26] ZHANG Pengcheng. Research on game-based aerial target track prediction and confrontation[D]. [Master dissertation], Zhejiang University, 2023: 1–45. doi: 10.27461/d.cnki.gzjdx.2023.000119.

[27] WANG Shuo, WU Nan, HUANG Jie, *et al*. Short-term prediction algorithm of air target track based on residual correction CNN-BiLSTM[J]. *Command Control & Simulation*, 2024, 46(1): 55–63. doi: 10.3969/j.issn.1673-3819.2024.01.007.

[28] YANG Yanzhou, WANG Jiawen, ZHANG Wei, *et al*. Research on the development level of space-based information system equipment and technology abroad[J]. *Modern Information Technology*, 2020, 4(6): 53–56, 60. doi: 10.19850/j.cnki.2096-4706.2020.06.019.

[29] WANG Shuai, HUANG Fuyu, LI Ting, *et al*. Operational effectiveness evaluation of infrared reconnaissance &

warning equipment in warfield[J]. *Laser & Infrared*, 2019, 49(3): 341–348. doi: 10.3969/j.issn.1001-5078.2019.03.013.

[30] YANG Yiqiong, WU Jianxin, and LIANG Yi. Airborne bistatic radar beam domain clutter suppression method[J/OL]. *Systems Engineering and Electronics*, 1–11. https://kns.cnki.net/kcms/detail/detail.aspx?dbcode=CAPJ&dbname=CAPJ&filename=XTYD20230905001, 2023.

[31] DONG Chao. Multi-view generalized eigenvalue proximal support vector machines[D]. [Master dissertation], East China Normal University, 2016: 6.

[32] WANG Qichao, WEN Zaiwen, LAN Guanghui, *et al.* Complexity analysis for optimization methods[J]. *Scientia Sinica Mathematica*, 2020, 50(9): 1271–1336. doi: 10.1360/N012018-00251.

[33] LUO Zhiquan, MA W K, SO A M C, *et al.* Semidefinite relaxation of quadratic optimization problems[J]. *IEEE Signal Processing Magazine*, 2010, 27(3): 20–34. doi: 10.1109/MSP.2010.936019.

[34] RAZAVIYAYN M. Successive convex approximation: Analysis and applications[D]. [Ph.D. dissertation], University of Minnesota, 2014: 1–10.

[35] FAN Tao, CUI Guolong, YU Xianxiang, *et al.* Joint design of intra-inter agile pulses and Doppler filter banks for Doppler ambiguous target[J]. *IEEE Transactions on Signal Processing*, 2024, 72: 867–882. doi: 10.1109/TSP.2024.3355768.

LIAO Xiaorong holds a Master's degree and mainly researches networked radar signal processing and resource allocation.

SUN Guohao, Ph.D., is an Associate Researcher, and his main research interests are cognitive radar signal processing, distributed radar signal processing, airborne/spaceborne radar signal processing, and space situational awareness.

ZHONG Suchuan, Ph.D., is an Associate Professor, and his main research interests are stochastic dynamical systems and stochastic signal processing, among others.

YU Xianxiang, Ph.D., is an Associate Professor, and his main research interests are radar waveform design and processing, optimization theory algorithms, and array signal processing.

LI Ming, Ph.D., is mainly engaged in research on airborne radar signal processing, array signal processing, and jamming suppression technology.

(Responsible Editor: YU Qing)